BODLEIAN LIBRARY OXFORD
DEPOSITED
THESIS
15·xi·71

A STUDY OF METASTABLE ATOMIC AND MOLECULAR LEVELS

by

O.M. Williams

Thesis submitted for the degree of
Doctor of Philosophy at the
University of Oxford.

St. Edmund Hall

June 1971

ACKNOWLEDGEMENTS

I wish to thank my supervisor, Dr. A. Corney, particularly for his efforts in securing the necessary experimental equipment. I appreciate also the generosity of Professor G. W. Series, Dr. C. E. Webb and Dr. J. W. Hodby in allowing equipment to be borrowed for long periods. I am very grateful to Messrs. D. G. Saxton, C. W. Goodwin and H. S. Lock for their willing technical assistance and to all those, particularly Dr. C. E. Webb, with whom I have had many fruitful discussions throughout the course of the work. I wish also to thank my wife for typing this thesis.

Financial assistance from the Royal Commission for the Exhibition of 1851 is gratefully acknowledged.

ABSTRACT

In contrast to the large number of measurements which have been made of the transition probabilities of electric dipole allowed spectral lines, there have been very few experimental determinations of the absolute transition probabilities of electric dipole "forbidden" lines. The radiative lifetimes of the metastable states from which forbidden radiation is emitted may be as long as one second or more and in most laboratory spectral lamps such species are destroyed by collision processes before forbidden radiation can be emitted. However, metastable atoms and molecules play important roles in determining the energy balance of the upper atmosphere and many of the prominent spectral features of the aurorae and the airglow are forbidden by the selection rules for electric dipole radiation.

An experimental determination of the radiative lifetime of the $^1S_0$ metastable state of atomic oxygen is presented in this thesis. The principal emission from this state is the electric quadrupole $2^1S_0 - 2^1D_2$ line at 5577Å, which is one of the strongest features of the auroral spectrum. The metastable states of oxygen were populated in a pulsed low current discharge through moderate pressures of either neon or argon which were mixed with a trace concentration (typically 10^{-4} torr) of oxygen. In such a discharge, oxygen molecules are dissociated by collision with metastable inert gas atoms and the oxygen atoms so produced are excited to the

metastable levels by electron exchange collisions. Atomic recombination is slow so that the oxygen is present mainly in the atomic form.

The intensity of the 5577Å forbidden line was recorded as a function of time during the afterglow period which followed a discharge pulse. The light was detected by a photomultiplier tube and the individual photoelectric events were recorded by the multi-channel scaling technique. The channel address cycle was initiated at the end of each discharge pulse and the photopulses were then counted as the channels of the multiscaler were successively addressed during the afterglow period. In this way, the intensity detected from the afterglow was obtained as a function of channel number or time. The statistical scatter on the recorded signal was reduced by adding the intensities detected from many afterglow cycles.

During the late afterglow, the decay of the metastable state population was exponential with decay constant

$$\Gamma = \frac{A'}{p} + \Gamma_o + \alpha' p + \beta' p^2 + \alpha'_o p_o$$

where the terms represent respectively diffusion to the walls of the vessel, the reciprocal Γ_o of the $O(^1S_o)$ radiative lifetime and deactivation of metastable atoms during two and three body collisions with both inert gas atoms and oxygen atoms. Here p and p_o are the partial pressures of the inert gas and of atomic oxygen respectively,

and the coefficients α', β' and α_o' are the rate constants for the different collisional deactivation processes. A large volume discharge vessel and inert gas pressures of typically 10 torr were used in order to reduce the loss of metastable population by diffusion. The spectroscopically pure gases used in the experiments were mixed in a bakeable gas handling system.

The oxygen partial pressure could not be measured directly because of adsorption of atomic oxygen on the walls of the vessel. Instead, the effect of the $O(^1S_0)$ deactivation by atomic oxygen was estimated by correlating the measured decay constants with the observed intensity of the afterglow signal. This intensity decreased as the oxygen was adsorbed. A "reduced" decay constant was determined at each inert gas pressure investigated as the value which would be expected at zero signal intensity or zero oxygen pressure.

Afterglow curves were recorded using both neon and argon at pressures ranging between 1 torr and 40 torr and the radiative lifetime of the $O(^1S_0)$ metastable state was evaluated by correlating the values of the reduced decay constants obtained at different inert gas pressures. The result

$$\tau_{expt}\,[O(^1S_0)] \;=\; 0.76 \pm 0.03 \text{ seconds}$$

is considerably more accurate than the previous experimental determinations and is in good agreement with the best theoretical estimate[1,2) $\tau_{theory}[O(^1S_0)] = 0.80$ seconds.

Furthermore, the result is the first experimental determination of a metastable state radiative lifetime which is sufficiently reliable to be compared to theoretical estimates.

Measurements were also made of the coefficients for diffusion of $O(^1S_0)$ metastable atoms through neon and argon, and the rate constants for deactivating collisions with neon and argon. The products of the inert gas pressure and the diffusion coefficients were determined as

$$416 \pm 12 \text{ torr cm}^2 \text{ s}^{-1} \text{ for neon at } 298^\circ\text{K}$$

and $$208 \pm 8 \text{ torr cm}^2 \text{ s}^{-1} \text{ for argon at } 298^\circ\text{K}$$

in good agreement with previous measurements[3]. These results are consistent with a Lennard-Jones collision diameter of 2.85Å and a force constant $\epsilon/k = 21.7^\circ\text{K}$ for elastic collisions between two $O(^1S_0)$ atoms. Upper limits on the rate constants for two body deactivating collisions between $O(^1S_0)$ atoms and inert gas atoms were determined as

$$4 \times 10^{-19} \text{ cm}^3 \text{ s}^{-1} \text{ for neon}$$

and $$5.5 \times 10^{-18} \text{ cm}^3 \text{ s}^{-1} \text{ for argon.}$$

Deactivation during three body collisions was found to be insignificant compared to the other loss processes.

References

1. O. Sinanoğlu, Comments Atom. Molec. Phys. 2, 79 (1970).

2. T. Yamanouchi and H. Horie, J. Phys. Soc. Japan 7, 52 (1952).

3. E.C. Zipf, Bull. Amer. Phys. Soc. 14, 204 (1969).

CONTENTS

		Page
CHAPTER 1	INTRODUCTION	
1.1.	Metastable States and Forbidden Radiation	1
1.2.	Multipole Radiation Theory and Selection Rules	4
1.3.	Forbidden Lines in Atomic Spectra	7
1.4.	Multipole Transition Probabilities	10
CHAPTER 2	THE METASTABLE STATES OF ATOMIC OXYGEN	
2.1.	The Ground State Configuration of Atomic Oxygen	12
2.2.	Laboratory Studies of the Oxygen Multipole Lines	13
2.3.	Auroral Measurements of Metastable Lifetimes	17
2.4.	The Measurement of Metastable State Radiative Lifetimes	19
2.4a.	Absolute Intensity Measurements	20
2.4b.	The Afterglow Methods	20
CHAPTER 3	THE OXYGEN-INERT GAS DISCHARGES	
3.1.	The Preliminary Experiments	23
3.2.	The Deactivation Processes	25
3.2a.	Solution of the Rate Equation	26
3.2b.	The Diffusion Coefficient	29
3.2c.	The Gas Conditions	30

		Page
3.3.	The Excitation Mechanism	33
3.3a.	Photolytic Dissociation of Oxygen	33
3.3b.	Dissociation and Electron Excitation in a Gas Discharge	35
3.4.	The Spectra of Oxygen-Inert Gas Discharges	37
3.4a.	The Oxygen-Neon Discharge	37
3.4b.	Adsorption of Atomic Oxygen	39
3.4c.	The Oxygen-Argon Discharge	42
3.5.	The Current Dependence of the Forbidden Line Intensity	43
3.6.	The Expected $O(^1S_0)$ Population Density	46
3.7.	Collisional Deactivation by Atomic Oxygen	49
3.8.	Summary	50
CHAPTER 4	THE EXPERIMENTAL SYSTEM	
4.1.	Introduction	52
4.2.	The Vacuum System	53
4.3.	Pressure Measurement and Gas Handling	54
4.4.	The Discharge Tube and Discharge Control System	58
4.4a.	The Discharge Tube	58
4.4b.	The High Voltage Pulse Generator	59
4.4c.	The Spark Generator	60
4.5.	The Light Detection System	62

		Page
	4.5. The Photon Counting System	64
	4.6a. The Photopulse Preamplifier	64
	4.6b. The Discriminator and Pulse Shaper	66
	4.7. The Electronic Timing Sequence	68
	4.8. Data Output	69
	4.9. The Reduction of Dead Time Losses	70
CHAPTER 5	TIME RESOLVED STUDIES OF THE AFTERGLOW	
	5.1. Decay Processes in the Afterglow	75
	5.1a. Decay of the Charged Species	75
	5.1b. Decay of the Inert Gas Metastable Populations	77
	5.2. The Removal of Electrons from the Afterglow	79
	5.3. The Forbidden Line Intensity Decay Rate	82
	5.4. The Exponential Decay Curves	83
	5.5. Temperature Dependence of the Decay Constants	85
	5.6. Analysis of the Decay Curves	86
	5.6a. The Logarithmic Fitting Procedure	86
	5.6b. Data Reduction	87
	5.6c. The Residuals between Experiment and Fit	89
	5.7. The Intensity-Decay Constant Correlation	89
	5.8. Deactivation by Electron Collisions	92
	5.9. The Decay Constant-Pressure Correlation	94

		Page
CHAPTER 6	RESULTS AND DISCUSSION	
6.1.	The Pressure Correlation in Argon	96
6.2.	The Pressure Correlation in Neon	97
6.3.	Three Body Collisional Deactivation	99
6.4.	The Low Pressure Anomalies	102
6.5.	The $O(^1S_0)$ Radiative Decay Constant	102
6.6.	The Diffusion Coefficients	107
6.7.	The Rate Constants for Two Body Deactivation	111
6.8.	Collisional Deactivation by Added Species	113
6.9.	The Red Forbidden Lines of Oxygen	114
6.10.	Summary of Results	115
CHAPTER 7	CONCLUSIONS	
7.1.	The Pulsed Afterglow Method - Extension to Other Systems	117
7.2.	The $O(^1D)$ Radiative Lifetime	119
7.3.	Improvements in the Lifetime Determination	123
APPENDIX 1	THE MEASURED REDUCED DECAY CONSTANTS	125
APPENDIX 2	THE LOW PRESSURE ANOMALIES	
	Incomplete Wall Destruction	126
	Ejection of $O(^1S_0)$ Atoms from the Walls	128
REFERENCES		132

CHAPTER 1

INTRODUCTION

1.1. Metastable States and Forbidden Radiation

Early in the development of atomic spectroscopy it was realized that the reciprocal wavelengths of the observed spectral lines of an atom could be expressed as differences between two numbers called "terms", and that the spectral properties of each atom were characterized by a particular set of terms. It soon became evident that not all the term differences were represented by spectral lines and following the enunciation of Bohr's correspondence principle a number of "selection" rules were derived to account for the absence of certain transitions. Although most transitions appeared to follow these semi-empirical rules, a small number of violations were found and these lead to the formulation of a more general theory of atomic radiation. In this theory the electric and magnetic radiation fields from an atom were expressed as series expansions, the first term of each corresponding exactly to the field from a classical electric dipole oscillator, the second partly from an electric quadrupole and partly from a magnetic dipole oscillator, and the higher terms from higher order electric and magnetic multipoles. The total power radiated from the atom for a particular transition between two terms, or energy states, was deduced in terms of the different electric and magnetic multipole moments, and the probable rate at which a spontaneous emission from

the upper state occurred was thence evaluated as the total radiated power per unit energy of the transition. Although the explicit values of the multipole moments corresponding to a particular transition could not be evaluated by the methods of the old quantum theory, it could be shown that for transitions which did not violate the earlier derived selection rules, the expected electric dipole contribution was several orders of magnitude greater than the expected electric quadrupole and magnetic dipole contributions, and many orders of magnitude greater than those from the higher order multipoles. The origin of most spectral lines was, therefore, explained by electric dipole transitions and the observed violations of the semi-empirical selection rules could often be ascribed to transitions of the electric quadrupole or magnetic dipole type. The validity of the expansion in terms of the multipole moments was later verified by the new quantum theory and it was shown that a different set of selection rules could be derived for each multipole moment. The earlier derived rules were found to correspond exactly to those derived for electric dipole radiation.

An atomic energy state from which all electric dipole transitions to lower lying states are forbidden by one or more of the rigorous selection rules is termed "metastable", and radiation from such a state is termed "forbidden". Radiation which results from a breakdown in the particular coupling model chosen to

represent the atom is not, however, regarded as forbidden. For example, the well-known intercombination lines which result from deviations from pure LS-coupling are regarded as electric dipole transitions. On the other hand, a molecular state is termed "metastable" if all electric dipole transitions to lower energy states are forbidden by any selection rule, whether rigorous or not.

For some metastable states, such as the $2\,^1S_o$ level of helium and its isoelectronic ions, multipole radiation of every order is forbidden. Radiation from such levels can occur, however, by the simultaneous emission of two photons. Forbidden radiation of this type is also emitted from the $2\,^3S_1$ levels and from the $2^2S_{\frac{1}{2}}$ levels of hydrogenic systems since this mode of decay is much more probable than the allowed decay by single photon magnetic dipole radiation. Two photon emissions have been detected from several atomic systems and consist of a wide continuum spread across a range defined by the energy difference between the levels, with a broad maximum intensity at energies close to half that of the single photon transition. References to the study of two photon emission have been given in the recent review article by Corney[1]. Forbidden radiation can also occur as a result of the influence of external fields on an atom, or by the perturbation of the orbital motion of the electrons by a nuclear magnetic moment. This is responsible for the emission of the $6\,^3P_o - 6\,^1S_o$ line in the odd isotopes of

mercury.

The loss of metastable populations in laboratory sources is generally by collision processes. However, in low density sources such as the upper atmosphere or gaseous nebulae where the probability of collisions is low, the main metastable population loss is often by multipole radiation. Over the past few decades there has been a considerable revival of interest in the study of metastable states following the realization of the important roles played by metastable species in the upper atmosphere, in gas discharges and in laser systems. The research described in this thesis is confined, however, almost exclusively to the study of metastable states which emit electric dipole forbidden radiation of atmospheric or astrophysical interest.

1.2. Multipole Radiation Theory and Selection Rules

The basic theory of multipole radiation is given by Condon and Shortley[2]. They derive the formulae for the transition probabilities of the various types of multipole radiation from a consideration of the total rate at which radiation is emitted by the atom and by use of the correspondence principle. For electric dipole radiation the spontaneous transition probability $A_{E1}(A,B)$ between upper level A and lower level B is given by

$$A_{E1}(A,B) = \frac{1}{2J_A + 1} \quad \frac{64\pi^4\nu^3}{3hc^3} \quad S_{E1}(A,B) \qquad (1.1)$$

(in Gaussian units)

where the line strength S_{E1} (A,B) is defined as the sum of the squared matrix elements for the transition.

That is, $$S_{E1}(A,B) = \sum_{a,b} |\langle a| \underline{P} |b\rangle|^2 . \qquad (1.2)$$

Here a,b are sublevels of the upper and lower levels and $\underline{P} = -e \sum_i \underline{r}_i$ is the electric dipole operator. The frequency of the transition is represented by ν and the other symbols have their usual meanings. The magnetic dipole transition probability A_{M1} (A,B) is obtained by simply replacing S_{E1} (A,B) by

$$S_{M1}(A,B) = \sum_{a,b} |\langle a| \underline{M} |b\rangle|^2 \qquad (1.3)$$

where $$\underline{M} = -\frac{e}{2mc} (\underline{L} + 2\underline{S}) \qquad (1.4)$$

is the magnetic dipole operator. The electric quadrupole transition probability is given by

$$A_{E2}(A,B) = \frac{1}{2J_A + 1} \frac{32\pi^6 \nu^5}{5hc^5} S_{E2}(A,B) \qquad (1.5)$$

where the appropriate operator is the quadrupole tensor

$$\underline{N} = -e \sum_i (\underline{r}_i \underline{r}_i - r_i^2 E/3) . \qquad (1.6)$$

Here E is the unit rank two tensor.

It is interesting to examine the above formulae in order to determine the relative importance of the different types of multipole radiation for a given transition. The probability rate for an electric dipole transition between the first excited state and the ground state of atomic hydrogen may be estimated from equation (1.1) as approximately 10^8 s^{-1}. This rate corresponds to a radiative lifetime of 10 ns and is typical of the order of magnitude

encountered for electric dipole transition rates. It is seen from the above formulae that the ratio of the electric quadrupole to the electric dipole transition probability for a given transition is expected to be of the order of $(r/\lambda)^2$ where λ is the wavelength of the emitted radiation. For visible emissions this ratio is of the order of 10^{-8} so that the radiative lifetime of a metastable atom which decays by electric quadrupole emission is expected to be of the order of one second. In a similar manner, the magnetic dipole transition probability may be estimated as being of the order of $(\hbar/2mrc)^2$ or a factor of 10^6 smaller than the electric dipole counterpart. It is clear that higher order multipole radiation is only of importance when the electric dipole contribution is zero. That is, when the electric dipole transition is forbidden by one or more of the rigorous selection rules.

Electric Dipole	Magnetic Dipole	Electric Quadrupole
(1) $\Delta J = 0, \pm 1$	$\Delta J = 0, \pm 1$	$\Delta J = 0, \pm 1, \pm 2$
$(0 \not\leftrightarrow 0)$	$(0 \not\leftrightarrow 0)$	$(0 \not\leftrightarrow 0, \frac{1}{2} \not\leftrightarrow \frac{1}{2}, 0 \not\leftrightarrow 1)$
(2) $\Delta M = 0, \pm 1$	$\Delta M = 0, \pm 1$	$\Delta M = 0, \pm 1, \pm 2$
(3) Parity change	No parity change	No parity change
(4) One electron jump	No electron jump	One or no electron jump
$\Delta l = \pm 1$	$\Delta l = 0, \Delta n = 0$	$\Delta l = 0, \pm 2$
(5) $\Delta S = 0$	$\Delta S = 0$	$\Delta S = 0$
(6) $\Delta L = 0, \pm 1$	$\Delta L = 0$	$\Delta L = 0, \pm 1, \pm 2$
$(0 \not\leftrightarrow 0)$		$(0 \not\leftrightarrow 0, 0 \not\leftrightarrow 1)$

TABLE 1 The Multipole Selection Rules

The selection rules for the different multipole components may be evaluated from the conditions for which nonzero line strengths are obtained and are listed in Table 1. For convenience we have used here the same tabulation as given by Garstang[3]. The notation is standard. The first three selection rules are rigorously obeyed in the absence of nuclear perturbations and two quantum processes. Rule (4), however, holds only when configuration interaction is negligible and rules (5) and (6) hold only for LS-coupling.

1.3. Forbidden Lines in Atomic Spectra

The first forbidden lines to be recognised as such were the $^2D - {}^2S$ series in potassium which were observed by Datta[4] in 1922. The important 5577Å auroral line of atomic oxygen was first observed in the laboratory in 1925 by McLennan and Shrum[5] from discharges through mixtures of an inert gas and oxygen. Later studies by McLennan and his coworkers[6,7,8] revealed that the line corresponded to the OI $2p^4\ {}^1S_0 - 2p^4\ {}^1D_2$ transition and that its wavelength agreed closely with that of the well-known auroral line. Conclusive proof of the electric quadrupole nature of the transition was obtained subsequently by Frerichs and Campbell[9] who showed that the observed Zeeman splitting corresponded to that predicted for electric quadrupole radiation but not to that for electric or magnetic dipole radiation. The $6\ {}^3P_2 - 6\ {}^1S_0$ line of mercury was produced by Rayleigh[10] in 1927 and the $6\ {}^3P_0 - 6\ {}^1S_0$

mercury line by Fukuda[11] in 1926, the latter transition being of interest since it is the result of the perburbation of the orbital motion of the outer electrons by the nuclear magnetic moment.

In 1928 Bowen[12] made the important discovery that many of the strongest lines of the spectra of gaseous nebulae were due to forbidden transitions in OII, OIII and NII. It had earlier been suggested that these lines belonged to a new element named 'nebulium'. It was during the period following Bowen's discovery that the 5577Å oxygen line was identified as a forbidden transition. During the following years a large number of forbidden lines, many of them belonging to highly ionized species, were identified in the spectra of gaseous nebulae and some stars. The red nebular lines at 6300Å and 6364Å were shown by Paschen[13] to belong to atomic oxygen and were later produced in the laboratory by Hopfield[14] from a high current discharge in oxygen which was flowing through a narrow bore tube.

Since the early discoveries of forbidden lines, many of the features of the airglow and auroral spectra have been identified as forbidden atomic or molecular transitions and this has lead to an increasing interest in the study of forbidden radiation. Much of the recent study of the spectral emissions from the upper atmosphere has been directed towards a better understanding of the mechanisms by which energy is transferred from the higher reaches

of the atmosphere to the lower regions, but as yet the situation is far from being completely understood. The recent use of rocket borne experiments coupled with the results of ground based observations and laboratory experiments has, however, substantially increased the knowledge of upper atmospheric physics.

There were few laboratory studies of multipole radiation of astrophysical and atmospheric interest before the recent growth of interest in the study of the collision processes which occur in the upper atmosphere. However, it has now been realized that accurate measurements of many of the rate constants of interest may be made under controlled laboratory conditions. Much of the laboratory work has been performed in flowing afterglow systems in which the reactant species is added to the flowing gas downstream from an excitation or ionization region. The ions of interest are detected further downstream by the use of either a mass spectrometer or electrostatic probes, and the excited atoms are monitored by their emissions. The flowing afterglow technique has been used by chemists for many years as a very convenient method for studying neutral gas reactions, and it is only in the last decade that the technique has been modified for the study of excited state - ground state neutral collisions and ion-neutral collisions. The technique has since been widely used to determine the rate constants for deactivating collisions between metastable atoms of atmospheric interest and various added gas atoms, but it

is only recently that reasonable agreement between the values measured by different experimenters has been obtained. The metastable species are detected in these experiments by their multipole emissions, and the rate constants for collisional deactivation are evaluated from measurements of the decay time or intensity of the emitted radiation as a function of the concentration of the added reactant gas. The principal results have been reviewed recently by Zipf[15] and details of the flowing afterglow technique have been given in a recent review article by Ferguson et al[16].

1.4. Multipole Transition Probabilities

The characteristic long lifetimes of metastable atoms and the high probability that before multipole radiation can occur such an atom will be deactivated by collisions with other atoms or with the walls of a container have presented considerable difficulties in laboratory determinations of absolute transition probabilities for multipole radiation. Although a small number of absolute measurements have been made, the experimental techniques have not been sufficiently advanced to enable the measurement of transition probabilities which are sufficiently reliable to be compared to the available theoretical estimates. Great importance has been attached to these estimates and the lack of reliable laboratory measurements of metastable lifetimes has indicated that a systematic

appraisal of the difficulties involved in the measurements would be valuable. It was considered that the recent advances in ultra-high vacuum technology and signal averaging techniques could be put to advantage in an attempt to measure one of the metastable lifetimes to such an accuracy that a good comparison with theoretical estimates could be made. It was with this motivation that the experiments described in this thesis were performed.

In view of the possible experimental difficulties it is necessary to initially investigate one of the simpler cases. It is also desirable to choose a candidate of astrophysical interest for which theoretical transition probability calculations are available. The choice of the $^1S_0$ metastable state of atomic oxygen was made from the list of metastable species of astrophysical interest and their lifetimes tabulated recently in the review by Zipf[15]. In this thesis a detailed study of the excitation and loss processes involving metastable oxygen atoms in a gas discharge is described. A new determination of 0.76 ± 0.03 seconds for the radiative lifetime of $O(^1S_0)$ metastable atoms is presented.

CHAPTER 2

THE METASTABLE STATES OF ATOMIC OXYGEN

2.1. The Ground State Configuration of Atomic Oxygen

The terms of the $1s^2\ 2s^2\ 2p^4$ ground state configuration of atomic oxygen are shown in figure 1. The levels are identified by their LS-coupling labels although slight departures from the pure coupling scheme occur; these give rise to the finite transition probabilities for the intercombination lines. Only those transitions which have been observed are included in figure 1.

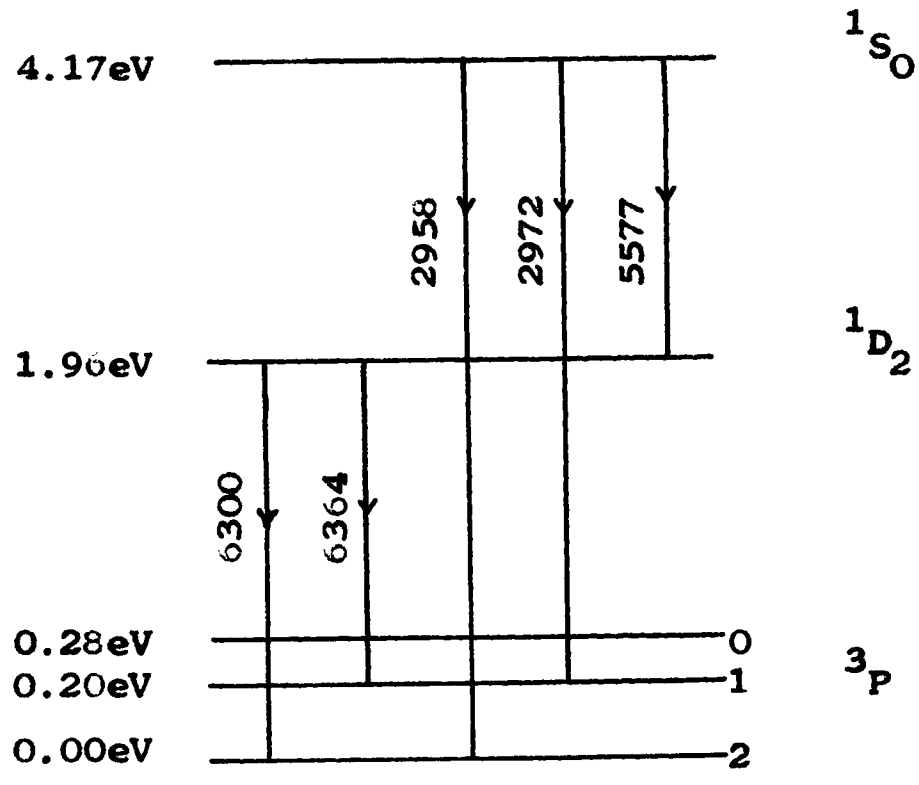


Figure 1 THE OXYGEN GROUND STATE TERMS
(not to scale)

Electric dipole transitions between the terms of the ground state configuration are forbidden by the parity rule. The multipole lines may be conveniently compared by the available theoretical estimates of their transition probabilities. The $^1D_2$ - $^1S_0$ 5577Å transition is an electric quadrupole line of transition probability[17] 1.18 s^{-1} and the $^3P_1$ - $^1S_0$ 2972Å line from the same upper state is a magnetic dipole line but has the lower transition probability[18] of 0.067 s^{-1} since it is an intercombination. The transition probability for the 2958Å electric quadrupole intercombination is even smaller. The two important emissions from the $^1D_2$ metastable state are the nebular lines at 6300Å and 6364Å which have transition probabilities[18] of 5.1×10^{-3} s^{-1} and 1.6×10^{-3} s^{-1} respectively. These lines are magnetic dipole intercombinations with small admixtures of electric quadrupole intercombinations.

2.2. Laboratory Studies of the Oxygen Multipole Lines

The multipole lines of atomic oxygen have been the subject of a large number of experimental investigations both in the laboratory and in the study of atmospheric emissions. The laboratory studies generally fall into one of two classes: the measurement of rate constants for deactivating collisions between metastable atoms and other particles, and measurements of relative or absolute transition probabilities.

The study of the collisional deactivation of oxygen metastable

atoms is of considerable importance for identifying the collision partners which affect the oxygen metastable atom populations of the upper atmosphere. In the laboratory, collisional deactivation has generally been studied by the flowing afterglow technique which we described briefly in §1.3. The oxygen metastable state populations have been usually prepared as reaction products of vacuum ultraviolet photolytic dissociation of either carbon dioxide or nitrous oxide and are monitored by their forbidden emissions. In the latest investigation of the deactivation of $O(^1S_0)$ metastable atoms, Filseth et al[19] used the vacuum ultraviolet emissions from a nitrogen flash lamp to irradiate a mixture of carbon dioxide and the reactant gas of interest, and recorded the time dependence of the decay of the metastable population following each irradiating pulse from the lamp. Flowing gas conditions were used in order to avoid the accumulation of photolysis products in the reaction cell. The rate constant of each deactivating collision investigated was determined as the slope of the linear correlation between the measured decay constants and the concentration of the reactant gas. This type of investigation has revealed that the $O(^1S_0)$ atom population of the upper atmosphere is affected by the presence of oxygen molecules, and that both oxygen molecules and oxygen ground state atoms are particularly effective in deactivating $O(^1S_0)$ metastable atoms in an oxygen discharge lamp. This latter result is particularly relevant to the experiment described in this thesis.

The rate constants for deactivation of $O(^1S_0)$ atoms by either oxygen atoms or molecules are each of the order of 10^4 $torr^{-1}s^{-1}$ [15], so that only small oxygen concentrations may be used if the metastable atom population loss is not to be dominated by collisional deactivation.

There have been several determinations of the relative transition probabilities of the multipole lines of atomic oxygen from measurements of the relative intensities of lines which originate from the same upper level. For such lines, the ratio of the relative photon intensities is simply equal to the ratio of the transition probabilities. Good agreement between the measurements[20] and the theoretical estimates[18] has been obtained for the 6364/6300 transition probability ratio, as might be expected since these lines are each mainly magnetic dipole in character. As can be seen from equations (1.3) and (1.4), the magnetic dipole line strength for LS-coupling is independent of the radial wavefunctions. On the other hand, the electric quadrupole transition probability calculations are strongly dependent on the radial form of the wavefunctions, and are expected to be less reliable than the corresponding magnetic dipole calculations because of the inaccuracies in the chosen wavefunctions. The theoretical methods are discussed in greater detail in §6.5. Satisfactory agreement between experiment[20,21] and theory[17,18] has, however, been obtained for the 5577/2972 transition probability

ratio, a result which gives an important comparison between the magnetic dipole and electric quadrupole calculations.

The only laboratory measurement of the absolute transition probability of the $^1S_0$ - $^1D_2$ 5577Å line of atomic oxygen has been from the simultaneous measurements by McConkey and Kernahan[22] of the number density of $O(^1S_0)$ atoms in an oxygen-helium discharge and of the intensity of the emitted 5577Å line. The 5577Å intensity emitted into unit solid angle is related to the transition probability A(5577) as

$$I(5577) = A(5577)\, N(^1S_0)\, V/4\pi \quad \text{photons per second,}$$

where $N(^1S_0)$ is the number density and V is the emitting volume which is assumed to be uniformly filled with the excited state atoms. The main advantage offered by this method is the independence from the losses of the metastable population by processes other than the emission of radiation. Unfortunately, this advantage is offset by the difficulties of the measurements. McConkey and Kernahan measured the 5577Å intensity to within an accuracy of only 10 percent and found that the determination of the metastable state number density presented formidable experimental problems. They evaluated the number density by recording the intensities of the $3s\ ^1P^o$ - $2p^4\ ^1S_0$ 1218Å OI line emitted from the discharge plasma when the discharge was struck across different lengths of the vessel. The recorded intensity ratios were related to the coefficient for absorption of the 1218Å radiation by the $O(^1S_0)$

atoms present in the discharge, and thence related to the product of $N(^1S_0)$ and the f-value of the 1218Å transition.

Unfortunately, very low 1218Å line intensities of poor signal to noise ratio were recorded, and the background level was found to be difficult to determine because the 1218Å line lay in the wings of the strong Lyman-α impurity line. McConkey and Kernahan used a theoretical estimate of the f-value of the 1218Å transition and evaluated the 5577Å transition probability as 1.0 s^{-1} from a number of separate experimental determinations which showed considerable statistical scatter about the mean value. The claim of only a factor of two accuracy made by the authors emphasises the serious experimental difficulties encountered.

2.3. Auroral Measurements of Metastable Lifetimes

In 1956, Omholt and Harang[23] showed that the lifetime of $O(^1S_0)$ metastable atoms in the upper atmosphere could be determined from a detailed study of fluctuating auroral forms. They considered the rate at which $O(^1S_0)$ atoms were being created and destroyed in the upper atmosphere. During an aurora, the excitation is principally by collisions between oxygen ground state atoms and secondary electrons. The net rate at which the metastable atom population density N changes may be written as

$$\frac{dN}{dt} = R - \Gamma N \qquad (2.1)$$

where R is the excitation rate and Γ is the reciprocal of the lifetime of the metastable atom population. Omholt and Harang assumed that the oxygen metastable states and the upper states of the allowed first negative N_2^+ bands with v' = 0 were populated by the same mechanism, so that the excitation rate R is directly proportional to the intensity I_N of the allowed bands. The band intensity and 5577Å line intensity I_O are then related from equation (2.1) as

$$I_O + \frac{1}{\Gamma}\frac{dI_O}{dt} = KI_N \qquad (2.2)$$

where K is a constant. The forbidden line emission is delayed with respect to the band emission and a determination of the metastable atom lifetime $1/\Gamma$ may be obtained from the above correlation of the observed intensities and the rate at which the forbidden line intensity changes during an auroral fluctuation. Because of the fluctuations in the excitation rate and the statistical fluctuations in the signal intensities, Omholt and Harang were only able to determine the value of the decay constant reliably by use of a sophisticated statistical analysis of the recorded intensity fluctuations.

Omholt[24] has developed improved techniques to analyse the earlier records of the fluctuations in the 5577Å line and 4709Å N_2^+ band intensities and also has presented new observations. The determinations of the $O(^1S_0)$ lifetime from separate records show a wide scatter and are distributed almost symmetrically about

the mean value of 0.7 ± 0.1 seconds. It is not known, however, whether part of this scatter is caused by the effects of collisional deactivation. The rather shorter lifetimes of the order of 0.4 seconds to 0.5 seconds which have been reported from later observations by Paulson and Shepherd[25] have definitely been obtained during atmospheric conditions in which deactivation was of importance. Omholt's mean result is, however, in satisfactory agreement with the theoretical estimate[17,18] of 0.80 seconds, although there is some doubt[24] on the validity of the original assumption that the different excited states are populated by the same mechanism.

Stoffregen and Derblom[26] have made very similar measurements from auroral fluctuations of the 6300Å OI forbidden line intensity. Their results have been reanalysed by Omholt[27] who evaluated the $O(^1D)$ lifetime as lying in the range between 150 and 200 seconds. This value is slightly higher than the theoretical estimate[18] of 135 seconds but must be regarded as satisfactory in view of the extreme longevity of atoms in the $O(^1D)$ metastable state.

2.4. The Measurement of Metastable State Radiative Lifetimes

There have been numerous methods developed for the measurement of excited state lifetimes. These have been reviewed recently by Corney[1]. However, because of the very low multipole transition probability rates, few of the methods may be applied to determine the radiative lifetimes of metastable states.

2.4a. Absolute Intensity Measurements

The determination of the $O(^1S_0)$ lifetime by McConkey and Kernahan[22] has shown that serious experimental difficulties are liable to be encountered in any determination which involves a measurement of the absolute number density of an excited state. However, Shemansky[28] has recently used a similar method in absorption measurements from the $X\ ^1\Sigma_g^+$ ground state of molecular nitrogen to determine the radiative lifetime of the $A\ ^3\Sigma_u^+$ metastable state as 1.36 seconds for $\Sigma = 0$ transitions and 2.70 seconds for $\Sigma = \pm 1$ transitions. The $A\ ^3\Sigma_u^+$ molecule population decays by the well-known Vegard-Kaplan bands. The ground state molecule population was accurately evaluated and the transition probabilities for many of the rotational components of each band were determined to an accuracy better than 5 percent. However, the radiative decay constant, which is obtained as the summation of the individual transition probabilities, could be evaluated to within only 20 percent because of inaccuracies in the transition probability measurements of some of the rotational components.

2.4b. The Afterglow Methods

The only alternative methods at present available for the determination of the radiative lifetime of the $O(^1S_0)$ metastable state involve time-resolved measurements in either a flowing afterglow or a pulsed static afterglow. Noxon[29] has used the

flowing afterglow method to determine the lifetime of the $A\,^3\Sigma_u^+$ state of nitrogen as approximately one second. The metastable molecules were produced by discharge through nitrogen at a pressure of the order of one atmosphere, and time-resolved measurements of the Vegard-Kaplan band intensities were recorded by varying the speed of the gas flow which was typically 1 m/s. Noxon did not, however, fully investigate the losses of the metastable molecules by diffusion or by collisional deactivation. Phillips[30] has used a similar slow speed flowing gas system to determine the N_2 ($A\,^3\Sigma_u^+$) lifetime as 1.1 $\pm$ 0.4 seconds, but he also did not fully investigate the losses by diffusion and collisional deactivation.

There have been two measurements of the N_2 ($A\,^3\Sigma_u^+$) lifetime by the pulsed afterglow method. In this technique, the metastable states are populated during a discharge pulse and the time dependence of the decay of the forbidden line or band intensity is recorded during the subsequent afterglow. The technique has the disadvantage that the recorded lifetime is not determined solely by radiation losses but also by the losses due to diffusion and collisional deactivation. Only in rare cases can these be eliminated and it is more usual that the radiative lifetime is evaluated from a set of decay time measurements which cover a wide range of gas conditions. Zipf[31] has used the method to measure the N_2 ($A\,^3\Sigma_u^+$) radiative lifetime as 0.9 seconds in good

accordance with the results obtained by the other methods. However, no assessment of the reliability of the result is given. The later determination of 10 seconds by Bromer and Spiewick[32] who used the same experimental method cannot be regarded as reliable since the pressure correlation of their individual experimental measurements shows considerable statistical scatter and insufficient measurements were made.

In view of the experimental facilities available, it was decided to attempt to determine the radiative lifetime of the $O(^1S_0)$ state by the pulsed afterglow method. It was considered that higher gas purity levels could be maintained in a bakeable static gas system than in a flowing system, so that the difficulties caused by collisional deactivation of metastable atoms by impurity gas atoms could possibly be more easily avoided. It was considered further that the use of signal averaging techniques would enable the $O(^1S_0)$ lifetime to be determined to an accuracy of better than 10 percent by the pulsed afterglow method. In chapter 3 we examine in detail the processes by which oxygen metastable atoms may be created and are destroyed in a laboratory vessel. The experimental system is described in chapter 4 and the details of the pulsed afterglow method and the results of the investigation are discussed in chapters 5 and 6 respectively.

CHAPTER 3

THE OXYGEN - INERT GAS DISCHARGES

3.1. The Preliminary Experiments

The initial experimental work was based on the much earlier research by McLennan and his collaborators[5-8] and was aimed at producing high intensities of 5577Å radiation in an oxygen-inert gas discharge. Once this had been accomplished it was hoped that the decay of the metastable population in the afterglow of the discharge would be readily observable. McLennan et al[8] noted that the intensity of the forbidden radiation increased the heavier the inert gas used, argon producing intensities which were some fifty times stronger than those obtained when helium was used under similar conditions. Later workers[33-35] showed, however, that molecular-like bands associated with the forbidden line were always present when argon was used as the inert buffer gas. These bands have been attributed to radiation from an unstable argon-oxygen molecule and in order to avoid possible complications it was decided to initially study helium-oxygen discharges.

The first investigations were made of a 100 mA d.c. glow discharge through a gas mixture containing 10 torr of helium and 2 torr of oxygen. This mixture had been reported by McLennan et al[8]

as producing the highest intensity of the forbidden line. The gases were mixed in a grease-tap high vacuum system pumped by a mercury diffusion pump. The discharge tube design was similar to that of McLennan et al[8] and consisted of a 4 cm diameter pyrex glass tube of 30 cm length with nickel electrodes housed in side arms at each end of the tube. Light from the discharge was viewed along the axis of the tube and photographed by a prism spectrograph of 100 A/mm linear dispersion. The photographs showed a barely discernible line at 5577Å after an exposure time of one hour and it quickly became evident that a superior means of excitation would be required if quantitative measurements were to be made.

Much higher intensities were obtained when a high current pulsed discharge was employed. In these experiments a 1 μF capacitor shunted across the discharge tube was slowly charged through a 50 kilohm ballast resistor. Following the gas breakdown when the striking potential was reached, the capacitor discharged rapidly through the low impedance path offered by the ionized gas. Peak discharge currents of 30 amperes were obtained. The discharge was pulsed at a rate of typically 10 Hz which was determined by the recharge time of the capacitor and a clearly visible line was recorded at 5577Å after an exposure time of a few minutes. An attempt was made to record the afterglow by monitoring the forbidden radiation by means of an EMI type 9558 QB photomultiplier

tube positioned behind a slit in the focal plane of the spectrograph. The photocurrent was amplified and displayed on an oscilloscope trace triggered at the start of the discharge pulse. However, no afterglow could be detected. It was later realised that this result was caused by the rapid collisional deactivation of the oxygen metastable atoms by the high partial pressures of oxygen used in the gas mixture, although at the time the absence of a detectable afterglow was ascribed to severe electron quenching of the metastable atoms during the early afterglow. As a result of this failure it was decided to transfer the investigation to argon discharges containing trace concentrations of oxygen. These were soon found to produce high intensities of the forbidden line and an observable afterglow.

3.2. The Deactivation Processes

Following the failure of the early experiments, a more systematic appraisal of the investigation was made in order to evaluate the best conditions under which the experiment should be performed. In this chapter, we examine in detail the processes by which oxygen metastable atoms are created and destroyed in a laboratory vessel. The excited and ionic species present within the volume are identified from the observed spectra. However, we defer until chapter 5 the discussion of the decay of the populations of the inert gas metastable atoms and of the charged

species in the afterglow which follows a pulse of excitation.

3.2a. Solution of the Rate Equation

Most of the experimental conditions required for a laboratory determination of the radiative lifetime of the $O(^1S_0)$ metastable state may be evaluated from the development of the rate equation which governs the formation and destruction of the metastable atoms. The overall rate of growth of the metastable population density n may be written as

$$\frac{dn}{dt} = \left(\frac{dn}{dt}\right)_{exc} + \left(\frac{dn}{dt}\right)_{rad} + \left(\frac{dn}{dt}\right)_{coll} + \left(\frac{dn}{dt}\right)_{diff} \qquad (3.1)$$

where the terms correspond respectively to the excitation rate (which will be unspecified at present) and the loss rates due to spontaneous emission, atomic collision processes occurring within the volume and diffusion of metastable atoms to the walls of the vessel. The loss rates may be written immediately as

$$\left(\frac{dn}{dt}\right)_{rad} = -\Gamma_0 n \ , \qquad (3.2)$$

$$\left(\frac{dn}{dt}\right)_{coll} = -\sum_i \alpha_i N_i n - \sum_{i,j} \beta_{ij} N_i N_j n \qquad (3.3)$$

and

$$\left(\frac{dn}{dt}\right)_{diff} = D\nabla^2 n \ . \qquad (3.4)$$

Here Γ_0 is the reciprocal of the radiative lifetime of the

metastable atom population and α_i and β_{ij} are respectively the rate constants for two and three body deactivation collisions between the metastable atoms of interest and particles of the different species present in the volume. Equation (3.4) takes the form of the well-known time dependent diffusion equation (see, for example, McDaniel,[36] p.495) where we have assumed that the diffusion coefficient D is independent of position within the vessel.

We wish to evaluate the time dependence of the decay of the metastable population after the source of excitation is abruptly turned off at time t = 0. Equation (3.1) then becomes simply

$$\frac{d}{dt}\left(ne^{\Gamma_1 t} \right) = D\nabla^2\left(ne^{\Gamma_1 t} \right) \qquad (3.5)$$

where we have defined

$$\Gamma_1 = \Gamma_0 + \sum_i \alpha_i N_i + \sum_{i,j} \beta_{ij} N_i N_j . \qquad (3.6)$$

The solution of the diffusion equation (3.5) depends on the geometry of the container and on the boundary conditions and is given by McDaniel[36] for the interesting case of a cylindrical vessel of radius r_0 and height H. It is assumed that all the metastable atoms which strike the walls are destroyed. Using McDaniel's solution (McDaniel[36], §10.8), we have that the instantaneous number density of metastable atoms in the afterglow

is given by

$$n(r,z,t) = e^{-\Gamma_1 t} \sum_{j,k} G_{jk} J_0(\mu_j r) \cos[\frac{(2k-1)\pi z}{H}] \exp[-\Gamma_d^{jk} t] \quad (3.7)$$

where the centre of symmetry is chosen as the origin of the cylindrical coordinate system and where the diffusion decay constant Γ_d^{jk} is defined by the relation

$$\frac{1}{\Lambda_{jk}^2} = \Gamma_d^{jk} / D = \mu_j^2 + [(2k-1)\pi/H]^2 . \quad (3.8)$$

Here Λ_{jk} is the characteristic diffusion length of the jk mode, $\mu_j r_0$ is the j-th root of the zero order Bessel function $J_0(\mu_j r)$ and the G_{jk} are coefficients which are determined only by the spatial distribution of metastables at the time that the source of excitation is removed. We notice that the decay of population during the afterglow consists of only a single exponential when the first order diffusion mode dominates. In that case

$$n(r,z,t) = e^{-\Gamma t} G_{11} J_0(\frac{2.405r}{r_0}) \cos(\pi z/H) \quad (3.9)$$

$$\text{where} \quad \frac{1}{\Lambda_{11}^2} = \Gamma_d^{11} / D = (2.405r/r_0)^2 + (\pi/H)^2 \quad (3.10)$$

and where we have defined the decay constant

$$\Gamma = \Gamma_1 + \Gamma_d^{11} . \quad (3.11)$$

Equation (3.9) is satisfied throughout the afterglow period only when the initial spatial distribution is entirely that of the first

order mode. However, it is evident from equation (3.8) that the decay rates for the different diffusion modes increase rapidly with increasing order, so that after a time of the order of $1/\Gamma_d^{11}$ the loss of metastable population will approximate closely to a single exponential decay, particularly if the initial spatial distribution resembled that of the first order mode.

3.2b. The Diffusion Coefficient

The form of the mutual diffusion coefficient is given as

$$D = \frac{3}{8}\left(\frac{\pi kT}{2M_r}\right)^{\frac{1}{2}} (N\pi d_{12}^2)^{-1} \qquad (3.12)$$

in the first approximation of the Chapman-Enskog[36] theory for the special case of elastic sphere collisions. Here M_r is the reduced collision mass, d_{12} is the classical collision diameter and N is the total number density. The higher order corrections in the theory are small and are usually ignored. The use of an elastic sphere coefficient is particularly relevant to the case of diffusion of $O(^1S_0)$ metastables through a buffer gas of $^1S_0$ atoms since the electron charge distributions of both species are closely spherically symmetric. The atoms consequently have low polarizabilities and collisions between them are likely to approximate closely to elastic sphere impacts. It is evident from equation (3.12) that in order to minimize diffusion losses, an experiment should be performed in high pressure conditions in

a large volume vessel. The actual conditions chosen are usually determined by the practical aspects of the experiment.

3.2c. The Gas Conditions

We have established for the simplest case of first order diffusion that the overall rate of growth of the metastable atom population is determined by the relation

$$\frac{dn}{dt} = \left(\frac{dn}{dt}\right)_{exc} - \Gamma n \qquad (3.13)$$

where the rate constant Γ, which is defined by

$$\Gamma = DN/(\Lambda_{11}^2 N) + \Gamma_0 + \sum_i \alpha_i N_i + \sum_{i,j} \beta_{ij} N_i N_j \qquad (3.14)$$

governs both the loss of the metastable atom population in the late afterglow and the rate of growth of the population at times greater than $1/\Gamma^{11}$ following a step of excitation applied at time t = 0. It is instructive to evaluate the orders of magnitude of the terms of equation (3.14) with a view to determining the most suitable gas conditions for an experimental determination of the radiative decay constant Γ_0. It is evident that the conditions should be chosen so that the radiation loss, the extent of which may be estimated from the theoretical value[17,18] of 1.25 s^{-1} for Γ_0, is maximized with respect to the losses by diffusion and collisional deactivation.

The importance of the collisional deactivation terms of

Collision	Ref.	Rate Constant $cm^3\ s^{-1}$	Rate Constant $torr^{-1}\ s^{-1}$ at 20^oC
$O(^1S) - O(^3P)$	15	2×10^{-13}	6.4×10^3
$O(^1S) - O_2$	15	4×10^{-13}	1.3×10^4
$O(^1S)$ - inert gas	19	$<3 \times 10^{-16}$	<10
$O(^1S) - H_2O$	19	7×10^{-11}	2.2×10^6

TABLE 2 Rate Constants for collisional deactivation of $O(^1S_0)$ atoms.

equation (3.14) may be evaluated from a knowledge of the rate constants for two and three body collisions. The two body rate constants have been measured by a number of investigators and their results have been reviewed recently by Zipf[15]. These investigations have also shown no evidence that $O(^1S_0)$ metastable atoms are deactivated during three body collisions and explicit values of the three body rate constants are not available. We have, however, listed in table 2 the values of the two body rate constants of interest. It is immediately evident that both oxygen molecules and oxygen ground state atoms are particularly effective in deactivating $O(^1S_0)$ metastable atoms by collision, so that oxygen concentrations of less than 10^{-4} torr must be used in the experiment in order to ensure that the collisional deactivation loss does not dominate the radiation loss. The signal intensity

is consequently expected to be low. The very large rate constant for collisional deactivation by water molecules serves as a useful indication that the experiment should be performed in the clean conditions of a bakeable gas handling system.

The diffusion term of equation (3.14) may be determined from the values of the diffusion length Λ_{11} and the diffusion coefficient D. A diffusion length of 2.2 cm is evaluated from equation (3.10) for the cylindrical vessel of 11 cm diameter and 27 cm average length which was used throughout the experimental work. Evidently, the diffusion loss could be decreased by use of a larger vessel. Zipf[37] has used the pulsed afterglow method to study the diffusion of $O(^1S_0)$ metastable atoms in argon and in neon, and has measured the respective diffusion coefficients as $257/p$ cm^2 s^{-1} and $405/p$ cm^2 s^{-1} by recording the observed decay rates of the emitted 5577Å intensity as a function of the inert gas pressure p in torr at 25°C. The corresponding values of the decay constants for the diffusion losses encountered in the vessel used in the experiments described here are $53/p$ s^{-1} for argon and $84/p$ s^{-1} for neon, so that total gas pressures of the order of 50 torr must be used if the diffusion loss is to be reduced to the same order as the radiation loss of metastable population. On the other hand, it seems from table 2 that the rate constant for collisional deactivation of metastable atoms by inert gas atoms is of sufficient magnitude that at such pressures the metastable atom population

loss would be dominated by collisional deactivation. However, it is probable that in previous measurements the deactivation has been caused by impurities in the inert gases used and it is considered that significantly lower values of the rate constants should be obtained under clean static gas conditions.

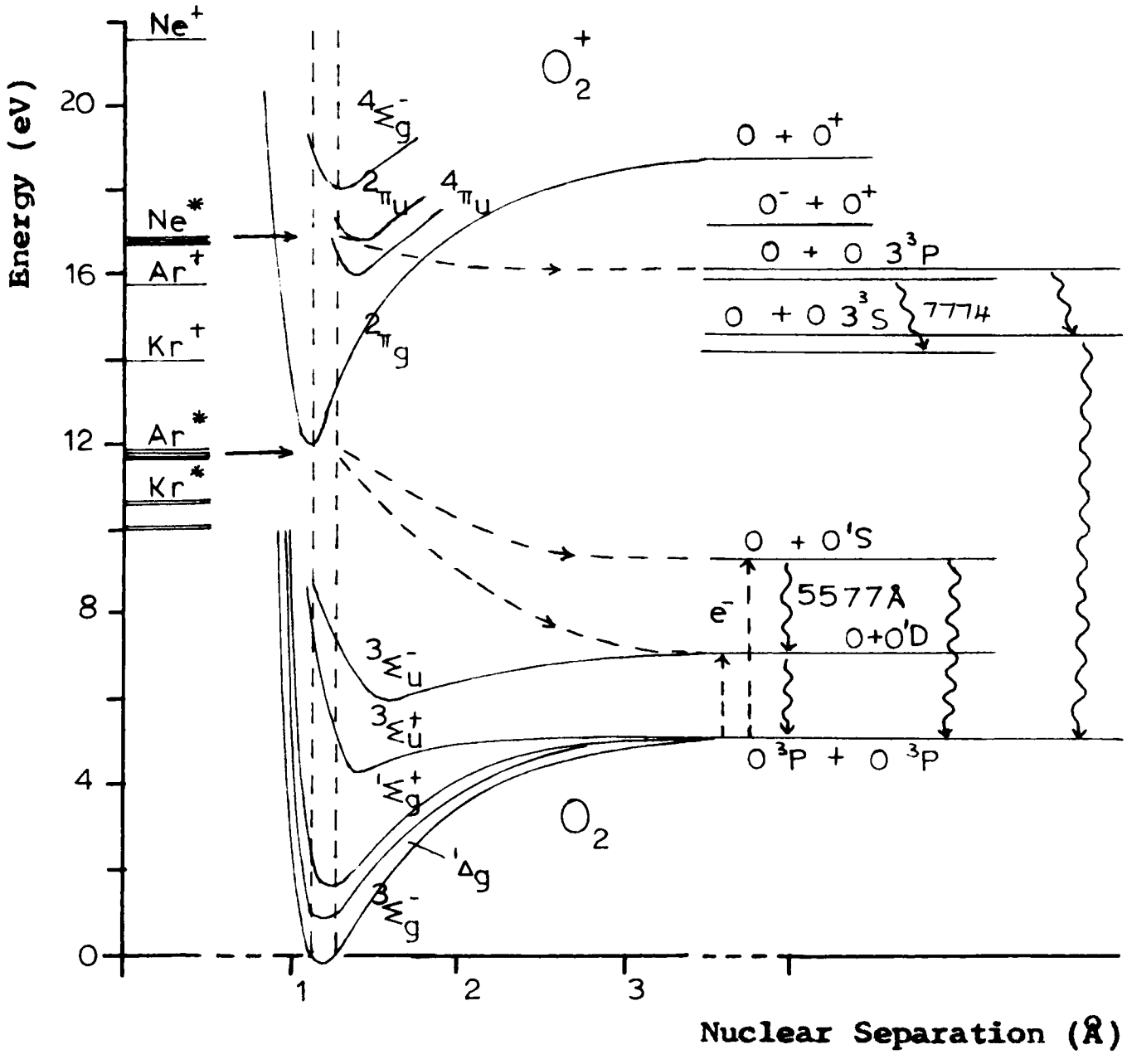
It is evident from the above discussion that the experiment is most suitably conducted in a vessel of large volume in which trace concentrations of oxygen are mixed with moderate pressures of an inert buffer gas. In the low pressure region the diffusion loss is expected to determine the level of the metastable atom population, and at high gas pressures collisional deactivation is expected to be of importance.

3.3. The Excitation Mechanism

Two alternative methods of populating the metastable states of oxygen were considered at the outset of this work, being photolytic dissociation and electron excitation in a gas discharge. These may be compared by reference to the relevant potential energy curves of molecular oxygen shown in figure 2 which have been drawn from the data of Gilmore.[38)]

3.3a. Photolytic Dissociation of Oxygen

At first sight, photolytic dissociation may appear to be a very convenient means of excitation, particularly since it is



THE ENERGY LEVELS OF OXYGEN

Figure 2

possible to produce the metastable atoms in the absence of ionization or the production of highly excited atoms. It is well-known that excitation from the lowest vibrational level of the ground state of a molecule occurs with a high probability in the Franck-Condon region, being that included between the two vertical lines shown in figure 2. For the case of photolytic absorption, the transition must be optically allowed and must terminate on one of the molecular potential energy levels. In order that the required process

$$O_2\,(^3\Sigma_g^-) \quad + \quad h\nu \rightarrow (O_2^*)_{\text{unstable}} \longrightarrow O(^3P) + O(^1S) \qquad (3.15)$$

can occur, at least one energy curve which leads to the desired dissociation products must cross the Franck-Condon region at an energy in excess of the total potential energy of the dissociation products. For $O(^1S_0)$ production, this energy corresponds to vacuum ultraviolet wavelengths shorter than 1350Å. Filseth and Welge[39] have recently reported the production of 5577Å radiation by the vacuum ultraviolet photolysis of oxygen. They used the emissions from a nitrogen flash lamp to irradiate a flowing gas mixture of oxygen and either argon, krypton or xenon. The emissions were transmitted through a lithium fluoride window to the reaction vessel.

Although photolytic dissociation may be successfully employed to produce 5577Å radiation, a fundamental difficulty precludes its

use as a population mechanisn in an experiment designed to determine the metastable lifetime in a static gas system. The use of trace concentrations of oxygen in the proposed experiment considerably lowers the probability of the recombination

$$O + O + M \longrightarrow O_2 + M \quad , \qquad (3.1\text{b})$$

a reaction which requires the collision between and hence the close proximity of two oxygen atoms. Furthermore, the photolytic absorption process can occur only if oxygen molecules are present since absorption from the ground state of atomic oxygen is forbidden. The measurements of the rate constant for the above recombination process have been reviewed recently by Schiff[40], the accepted value being of the order of 10^{-33} cm^6 s^{-1}. This leads to a very slow volume recombination rate unless very high pressures of oxygen are used. Of course, wall recombination will be a much more important process although recombination there depends also on the close proximity of two oxygen atoms. The problems of wall recombination and the adsorption of oxygen atoms on the walls are discussed in §3.4b.

3.3b. Dissociation and Electron Excitation in a Gas Discharge

An alternative means of populating the $O(^1S_0)$ level is by dissociation of the oxygen molecules and subsequent electron excitation of the atomic oxygen which is produced. A guide to

the means of dissociation is obtained from the research of Bennett et al[41,42] on the mechanisms of the oxygen-neon and oxygen-argon lasers. In their experiments, the metastable and resonance levels of the inert gas were populated in a gas discharge. Oxygen molecules were dissociated in collisions with inert gas metastable and resonance atoms. That is, by the process

$$X_m^* + O_2(^3\Sigma_g^-) \longrightarrow (O_2^*)_{\text{unstable}} + X(^1S_0)$$
$$(O_2^*)_{\text{unstable}} \longrightarrow O(^3P) + O(^3P, ^1D, ^1S) . \qquad (3.17)$$

The dissociation occurs via the dotted repulsive potential energy curves of figure 2 which have been estimated by Bennett et al[41]. Close energy resonance is not required here since the three product atoms are available to share the excess energy and satisfy the additional requirement of momentum conservation. This fact is reflected in the relatively large rate constant measured as typically 10^{-10} cm^3 s^{-1} by Bennett et al[42] for the dissociation (3.17). The average lifetime of an oxygen molecule in the discharge is then typically $10^{10}/[X_m^*]$ seconds. Since metastable atoms are generally in plentiful supply in an inert gas discharge, it is likely that this lifetime will be much shorter than the recombination lifetime of an oxygen atom. The equilibrium concentration of oxygen molecules will then be very small compared to the concentration of oxygen atoms. The basic assumption we have used here that inert gas metastable atoms are in plentiful supply is discussed further

in §3.5b in context with the observed spectral features of the experiment.

Following the dissociation process, the oxygen metastable levels are populated by electron collisional excitation principally from the ground state. That is, by the process

$$O(^3P) + e \longrightarrow O(^1D, ^1S) + e \qquad (3.18)$$

in which the incident electron is captured by the atom and an atomic electron of opposite spin is ejected. Such an excitation is only expected to be effective for close encounters. The rate of excitation by the collision process (3.18) is discussed in detail in §3.5.

3.4. The Spectra of Oxygen - Inert Gas Discharges

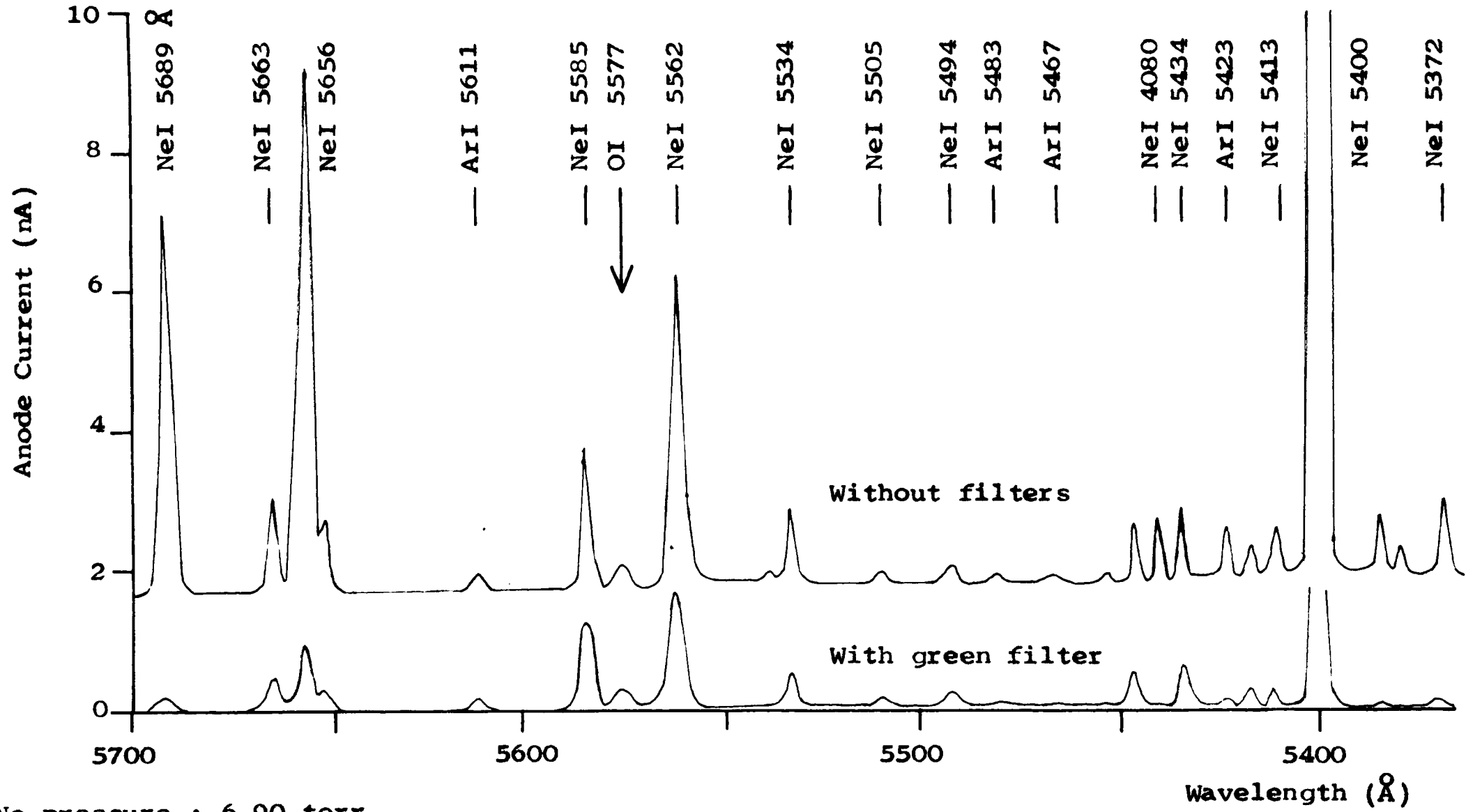
Light from oxygen-neon and oxygen-argon low current discharges was monitored by a grating monochromator used at a resolution of approximately 2Å. Full details of this instrument are given in §4.5. The light was passed from the monochromator to an EMI type 9558 QB photomultiplier tube and the resulting photocurrent was measured by a d.c. electrometer amplifier. A cylindrical d.c. discharge tube of 11 cm diameter and 27 cm average length was employed. This tube is described in detail in §4.4a.

3.4a. The Oxygen - Neon Discharge

A typical oxygen-neon discharge spectrum in the neighbourhood

of the forbidden green oxygen line is shown in figure 3. Only trace amounts ($\sim$ 0.01 mtorr) of oxygen were present in the volume. Separate intensity readings were recorded for different positions of the micrometer screw used to rotate the grating table. Apart from the 5577Å line of atomic oxygen and the four argon lines, all the recorded features correspond to the characteristic lines of NeI, although full classification is not included for the sake of clarity. The appearance of the ArI lines was probably caused by the extensive previous use of the tube for the study of argon-oxygen discharges. Argon would then possibly be desorbed from the walls during the neon discharge. The monochromator was blazed so that the green region of the visible spectrum appeared in third order. The background continuum from excited molecular neon present in the discharge volume occurred mainly in the blue region of the spectrum (fourth order diffraction) and was severely attenuated by the use of a 200Å bandpass interference filter centred close to 5577Å.

The O_2^+ first negative bands which would be prominent in the spectrum of figure 3 if O_2^+ ($^4\Sigma_g^-$) was an important excited species in the discharge volume were never observed, even though a wide range of discharge parameters was investigated. Either O_2^+ ions are not present in the discharge in any great quantity or the O_2^+ ($^4\Pi_g$) state is not significantly populated. It is interesting to note also from figure 3 the absence of the 5461Å HgI line which



Ne pressure : 6.90 torr

Slit : 0.7 mm x 20 mm

Discharge Current : 1.2 mA

Figure 3

PARTIAL SPECTRUM OF THE NEON-OXYGEN DISCHARGE

shows that the trapping of mercury vapour in the gas handling system is efficient.

The only spectral features of oxygen revealed from further studies of the visible and near infrared emissions from the oxygen-neon discharge were the 5577Å forbidden line and under certain conditions, the allowed $3\ ^5P - 3\ ^5S$ line at 7774Å. The intensity of each line depended markedly on the partial pressure of oxygen, as is discussed below in §3.4b.

It is interesting to evaluate the forbidden line intensity shown in the typical spectrum of figure 3 as a 'photon' detection rate. For a typical photomultiplier tube gain of 2×10^6, the 0.2 nA peak current of the 5577Å line corresponds to a photon count rate of approximately 0.6 KHz, or for the time-resolved afterglow experiments described in chapter 5 where apertures larger by a factor of ten were used, to a count rate of 6 KHz. Decay times of typically 0.1 seconds were recorded in the afterglow experiments, so that the forbidden line intensity of figure 3 corresponds to a total afterglow count of only 600, It is evident then that in order that quantitative measurements of the decay time may be made, signal averaging techniques should be employed over a number of afterglow cycles.

3.4b. Adsorption of Atomic Oxygen

Several earlier investigators[8,35] have reported that the

forbidden line intensities in oxygen-inert gas discharges are not developed fully when the discharge is initially struck but increase slowly over a period of perhaps up to one hour. This effect was consistently noticed in the experiments described here and is a direct consequence of the difference in the ionization potentials of oxygen (12.2 eV) and neon (21.6 eV).

When the oxygen-neon discharge is initially struck, the positive column appears transparent although the characteristic red colour of neon is observed in the anode and cathode fall regions. In this regime it appears that O_2^+ acts as the main positive ion and that few neon ions or metastable atoms are produced. As a consequence, the dissociation of oxygen molecules by the reaction (3.17) is inhibited. Oxygen atoms are produced, however, by the dissociative recombinations

$$\begin{aligned} O_2^+ + e &\longrightarrow O + O \\ O_2^+ + O_2^- &\longrightarrow O_2 + O + O \end{aligned} \qquad (3.19)$$

where the products are generally excited. Atomic oxygen is strongly adsorbed on the walls of a vessel so that the partial pressure of oxygen slowly decreases. Eventually, insufficient numbers of O_2^+ ions are available to balance the electron density within the positive column. At this time more neon atoms are ionized and the metastable neon population is increased. The

importance of the dissociation (3.17) is increased and further oxygen atoms are adsorbed. During this period, the diffuse blue neon molecular continuum develops and the OI 7774Å line can be detected. This line is produced[42] by the dissociation

$$Ne(^3P_0, ^3P_1) + O_2 \longrightarrow O(3^3P, 3^5P) + O(2^3P) + Ne(^1S_0) \quad (3.20)$$

and by subsequent radiation from the excited $O(3^5P)$ level.

As the discharge develops further, the principal positive ion gradually changes from O_2^+ to Ne^+ and the diffuse blue background of the positive column is complemented by a characteristic red glow caused by the allowed lines of NeI. Although the 5577Å intensity is still quite strong in this regime, the 7774Å intensity falls rapidly. At this stage the dissociation (3.20) is of little importance since the oxygen is present mainly in the atomic form.

The oxygen partial pressure continues to fall for some time although eventually an equilibrium situation is reached when the number of atoms adsorbed per unit time equals the rate at which oxygen is desorbed from the walls. The desorption process is probably caused by atomic recombination on the walls and the subsequent escape of the more loosely held oxygen molecules into the volume. Such molecules would then be rapidly dissociated in collisions with neon metastable atoms. Oxygen adsorption causes difficulties in estimating the effect of the deactivation of $O(^1S_0)$ atoms by ground state oxygen atoms. Obviously the instantaneous partial pressure of oxygen atoms bears little relation to the initial pressure and an estimate of the collisional deactivation

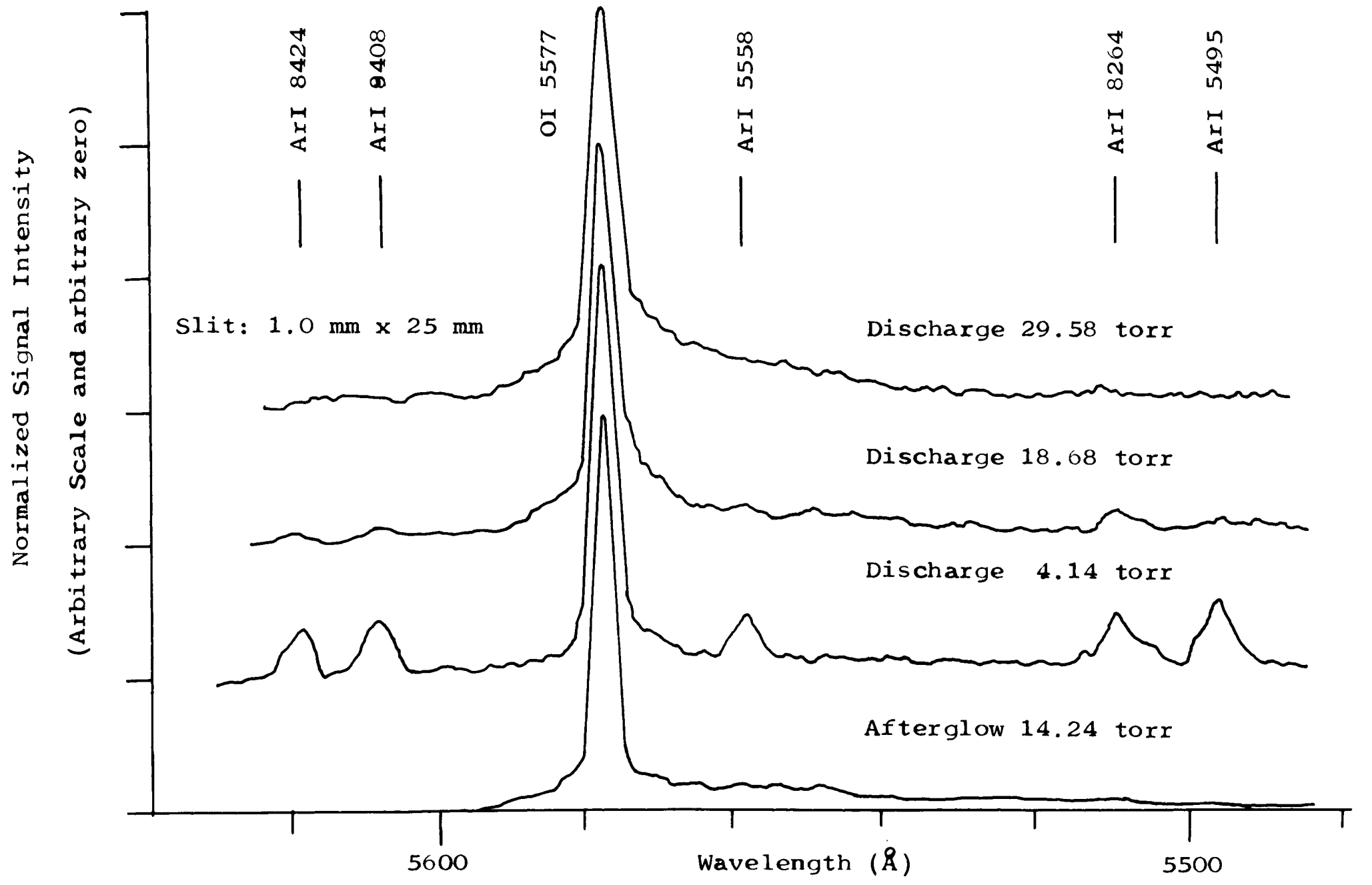
must be made from a correlation between the measured decay constant and the observed forbidden line intensity. Details of this correlation procedure are discussed in §3.7.

3.4c. The Oxygen-Argon Discharge

Several typical oxygen-argon discharge spectra which were recorded in the neighbourhood of the forbidden green line at different argon pressures are shown in figure 4. The spectra were traced by an X-T recorder during an automatic wavelength scan and have been normalized here to equal forbidden line intensities. The background levels, which were larger than the corresponding levels observed in the neon-oxygen discharge spectra, are not shown except for that of the lowest trace which was recorded during the discharge afterglow. The decay of the detected afterglow intensity was recorded at different wavelengths by use of the signal averaging techniques which are described in chapter 4. The intensities of both the forbidden line and the accompanying diffuse structure decayed at the same rate during the late afterglow, so that the intensities at the different wavelengths could be directly compared from the relative afterglow intensities. It is interesting to note that the afterglow method acts as an efficient discriminant against all features not associated with the forbidden lines of oxygen.

The colour of the positive column was governed by the molecular argon continuum and changed gradually as the oxygen was adsorbed on

Figure 4 OXYGEN-ARGON DISCHARGE SPECTRA NEAR 5577Å



the walls from a pale diffuse blue to an off-white. The forbidden line emission was the only line feature sufficiently strong to be observed by means of a pocket spectroscope. Lines from both the green (third order diffraction) and the infrared (second order diffraction) regions appear in the spectrum of figure 4. These lines were distinguished by use of colour glass filters.

The forbidden green line was always accompanied by a diffuse structure to short wavelengths. This structure has been investigated by a number of experimenters[33-35]. It is apparent from figure 4 that the intensity increases approximately linearly with argon pressure, relative to the forbidden line intensity. Further evidence from the afterglow measurements, which is discussed in § 6.7, shows that the dependence is closely linear. The short wavelength continuum has been attributed to radiation from an unstable excited argon-oxygen molecule which is formed during the collision of an $O(^1S_0)$ atom with a ground state argon atom. Discrete band heads have previously been reported[34] but these are not apparent from the spectra of figure 4.

3.5. The Current Dependence of the Forbidden Line Intensity

In an oxygen-inert gas discharge in which the oxygen is totally dissociated, the $O(^1S_0)$ state is populated by electron collisions of the type (3.18). The metastable atoms are destroyed by the emission of radiation, by diffusion to the walls of the

containing vessel and by deactivation during collisions with both atoms and electrons present in the discharge volume. At equilibrium, the excitation and deactivation rates balance so that the population density in the j-th excited state may be evaluated as

$$n_j = \frac{\sum_i s_{ij} N_e n_i}{\Gamma_j + \sum_i s_{ji} N_e} \qquad (3.21)$$

where the i-th term of the numerator equals the rate at which oxygen atoms in the i-th level are excited (or deactivated) by electron collisions to the j-th level. N_e is the mean electron density and the rate constants s_{ij} and s_{ji} define respectively the electron excitation and electron deactivation processes to and from the j-th level. The observed intensity I_{jk} of an emission from the j-th level to the lower k-th level may be evaluated from the population density n_j as

$$I_{jk} = G S_{jk} A_{jk} n_j \qquad (3.22)$$

where G is a constant geometrical factor and S_{jk} is the instrumental sensitivity which depends on the wavelength of the emission. A_{jk} is the transition probability rate.

It is evident from equations (3.21) and (3.22) that an investigation of the current dependence of the forbidden line intensity may be used to determine the relative importance of electron quenching compared to the other forms of deactivation during

the discharge. It is assumed here that the electron density scales linearly with discharge current. The 5577Å intensity detected from an oxygen-neon discharge (gas conditions as for figure 3) is shown in figure 5 as a function of discharge current. Similar tests were conducted over a wide range of gas conditions in both oxygen-neon and oxygen-argon discharges and showed there is little deviation from a linear current dependence. The slight deviations from linearity may be attributed to a weak dependence of the electron temperature, and hence of the excitation rate constants of equation (3.21), on discharge current. Such a dependence was found in later measurements of the current dependence of the discharge running voltage. It is shown further in figure 5 that the intensities of the 5577Å forbidden line, the neighbouring 5585Å allowed line of NeI and the molecular background emissions all scale in a similar manner with increasing discharge current. To a good approximation then, the population density n_j may be written from equation (3.21) as

$$n_j = \frac{1}{\Gamma_j} \sum_i s_{ij} N_e n_i \cdot \qquad (3.23)$$

It is evident from equation (3.21), however, that the excited population densities eventually saturate at high electron number densities when electron deactivation is of considerable importance.

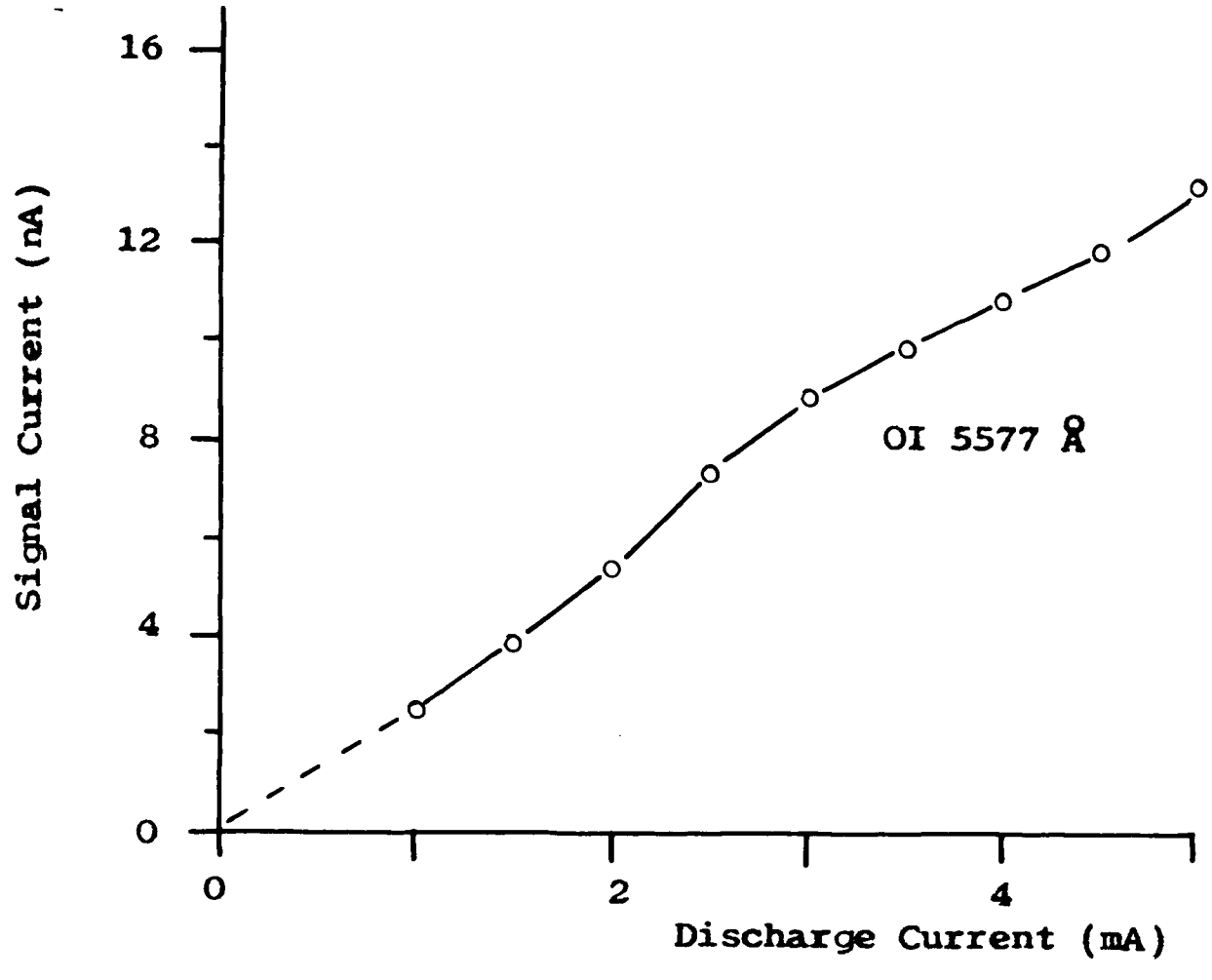


Figure 5 THE INTENSITY VARIATION WITH DISCHARGE CURRENT IN NEON-OXYGEN

3.6. The Expected $O(^1S_0)$ Population Density

It is interesting to evaluate approximately from equation (3.23) the population density of the $O(^1S_0)$ state which may be expected in the proposed experiments. We examine here the properties of a 5 mA oxygen-neon discharge at a pressure of 10 torr in a cylindrical vessel of 11 cm diameter.

The expected value of the decay constant Γ_2 may be estimated as 10 s^{-1} from the discussion of §3.2c. The electron number density is estimated as 4×10^8 cm^{-3} from the well-known expression for current density, namely

$$J = N_e e v_d . \qquad (3.24)$$

Here v_d is the electron drift velocity which may be evaluated from the measured properties of the positive column of an inert gas discharge. (See, for example, von Engel[43], figures 61, 125). The mean electron energy may be evaluated as 2.0 eV from the theoretical relationship between electron temperature and the reduced tube radius Rp. (See, for example, von Engel[43], figure 124.)

Seaton[44] has calculated rate constants for deactivation of oxygen metastable atoms during collisions with electrons, and these may be related to the excitation coefficients by use of the well-known Klein-Rosseland connection between the respective collision cross sections. For the case of a Maxwell distribution of electron energies, the excitation and deactivation rate

constants are related simply as

$$s_{ij} = \frac{g_j}{g_i} s_{ji} \exp[-(E_j-E_i)/kT_e] \qquad (3.25)$$

where g_i and E_i are respectively the statistical weight and energy of the i-th level. This equation is used to evaluate the rate constant for electron excitation from the $O(^3P)$ ground state to the $O(^1S_0)$ state as 8×10^{-11} cm^3 s^{-1} for electrons of 2.0 eV mean energy. We have used here Seaton's value[44] of 6×10^{-9} cm^3 s^{-1} for the rate constant for deactivation.

The above estimates are used to evaluate the contribution n_{20} to the $O(^1S_0)$ population density by electron excitation from the ground state as

$$n_{20} \sim 3 \times 10^{-3} n_0 \qquad (3.26)$$

where n_0 is the ground state population. It may readily be shown by a similar use of Seaton's rate constant values[44] for deactivation that the ground state population is expected to be much greater than each of the excited and metastable state populations, so that n_{20} is the dominant contribution to the $O(^1S_0)$ population density. We may use this result to reduce equation (3.23) to the simplified form

$$n_j = \frac{1}{\Gamma_j} s_{0j} N_e n_0 \qquad (3.27)$$

to the first order approximation.

Equation (3.26) is expected to be accurate only to within an

order of magnitude since none of the estimated values of the parameters of equation (3.23) are expected to be very reliable. In particular, there has been no experimental verification of Seaton's values for the deactivation rate constants. Using the values quoted above, we obtain

$$S_{20}\, n_e \backsim 2.4\ s^{-1}$$

which is certainly not negligible compared to the 10 s^{-1} value assumed for the other forms of deactivation. Evidently, it seems that Seaton's estimate is too high, so that the coefficient of equation (3.26) would be expected to be too large. A reliable experimental estimate of the rate constant for deactivation can only be obtained, however, if the electron density is measured. A possible method for measuring the deactivation rate constants is discussed in §5.8.

The expected forbidden line intensities are related to the metastable population densities by equation (3.22). It is convenient here to evaluate from equations (3.22) and (3.27) the intensity ratio

$$\frac{I_{jk}}{I_{1m}} = \frac{S_{jk}}{S_{1m}} \cdot \frac{A_{jk}}{A_{1m}} \cdot \frac{s_{0j}}{s_{01}} \cdot \frac{\Gamma_1}{\Gamma_j} \,. \tag{3.28}$$

A measurement of the relative line intensities and the relative decay constants leads to a relationship between the transition probabilities and excitation rates. The implications of this

equation are discussed in §7.2 with reference to a proposed experiment designed to determine the absolute radiative lifetime of $O(^1D)$ atoms.

3.7. Collisional Deactivation by Atomic Oxygen

As mentioned earlier in §3.4b, one of the difficulties of a pulsed afterglow determination of the $O(^1S_0)$ radiative lifetime is caused by oxygen adsorption on the discharge tube walls, which leads to an uncalibrated concentration of oxygen atoms in the discharge volume. The effects of collisional deactivation of the oxygen metastable atoms by oxygen ground state atoms must be estimated by a correlation between the forbidden line intensity and the measured decay constant. We proceed to evaluate the form of this correlation from equations (3.22) and (3.27). We have that

$$n_0 \propto I_{jk} \Gamma_j \tag{3.29}$$

at constant discharge current and constant electron temperature. Further, from equation (3.14) we may write the measured decay constant Γ_j as

$$\Gamma_j = \Gamma_{j0} + \alpha_0 n_0 \tag{3.30}$$

where Γ_{j0} represents the decay constant obtained in the absence of oxygen atom quenching. By combining equations(3.29) and (3.30)

we obtain the proportionality

$$\Gamma_j - \Gamma_{j0} \propto I_{jk} \Gamma_j \qquad (3.31)$$

so that the reduced decay constant Γ_{j0} may be evaluated as the intercept of the linear graph of $I_{jk} \Gamma_j$ against Γ_j. Deviations from linearity do in fact occur if the oxygen is not fully dissociated or if the electron temperature and hence the excitation rate change during the course of the discharge. In practice, such a nonlinearity is easily noticeable when the results are plotted according to the proportionality (3.31).

3.8. Summary

It has been established in this chapter that trace amounts of oxygen are almost completely dissociated in an oxygen-neon or oxygen-argon discharge. The $O(^1S_0)$ state is populated by electron excitation from the ground state and a moderate 5577Å forbidden line intensity is emitted from the discharge volume provided that the radiation loss of the metastable population is not negligible compared to the diffusion and collisional deactivation losses. The radiation loss is maximized in a large volume discharge tube in which moderate pressures of spectroscopically pure inert gases are used.

The decay constant for $O(^1S_0)$ atoms may be measured by recording the exponential decay of the forbidden line intensity

during the late afterglow of a pulsed discharge. By correlating the measurement of decay constant with the gas pressure measurements and the signal intensities observed, it is expected that an estimation of the radiative lifetime of the metastable state may be obtained. We describe in chapter 4 the experimental system for producing a pulsed discharge and for monitoring the afterglow signal. Since the signal intensities are expected to be small, signal averaging techniques are employed.

CHAPTER 4

THE EXPERIMENTAL SYSTEM

4.1. Introduction

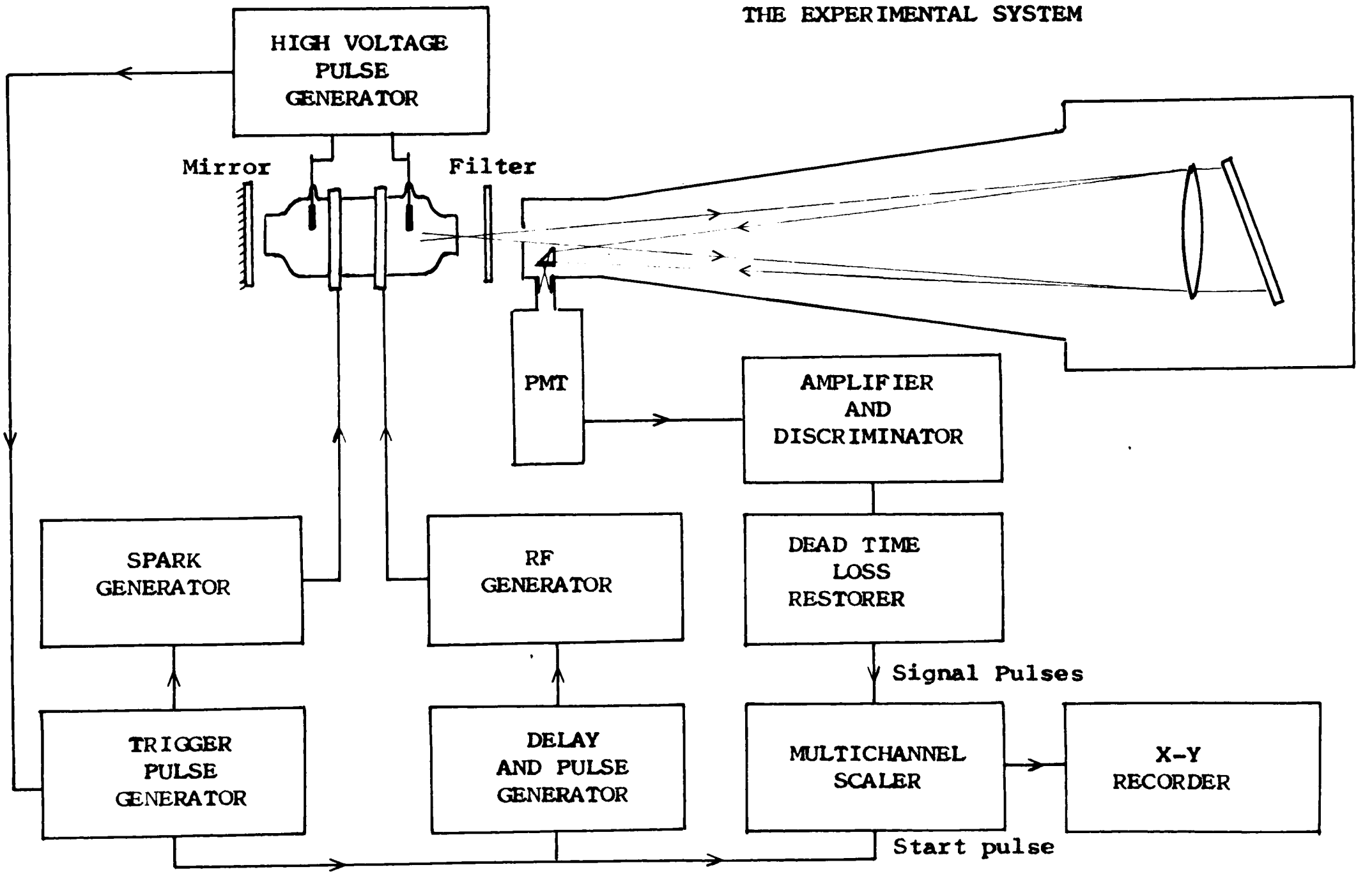
A block diagram of the experimental system which was developed for the pulsed afterglow studies of oxygen-inert gas discharges is shown in figure 6. A 2.5 litre d.c. discharge tube of pyrex glass was filled with spectroscopically pure gases from a bakeable gas handling system. The discharge voltage was pulsed at the desired rate by use of a high voltage pulse generator. For some gas conditions it was found necessary to facilitate the gas breakdown at the start of the discharge period by the application of a high voltage (5 kV) transient to a strip of aluminium foil wound about the circumference of the discharge tube.

Light emitted from the discharge was collected by a Littrow mounted grating monochromator and the radiation which was dispersed in a 30Å bandpass centred about 5577Å was detected by a photo-multiplier tube. Individual photoelectric events were amplified and shaped into standard pulses.

The time dependence of the intensity of the detected afterglow radiation was recorded by the multichannel scaling technique in which the channel address cycle was initiated at the end of each discharge pulse. The photopulses were then counted as the channels of the multiscaler were successively addressed during the afterglow

Figure 6

THE EXPERIMENTAL SYSTEM



period. In this way, the intensity of the light detected from the afterglow was obtained as a function of channel number or time. The statistical scatter on the recorded signal was reduced by adding the intensities detected from many afterglow cycles and at the end of each experiment the memory contents of the multiscaler were read by use of an X-Y recorder.

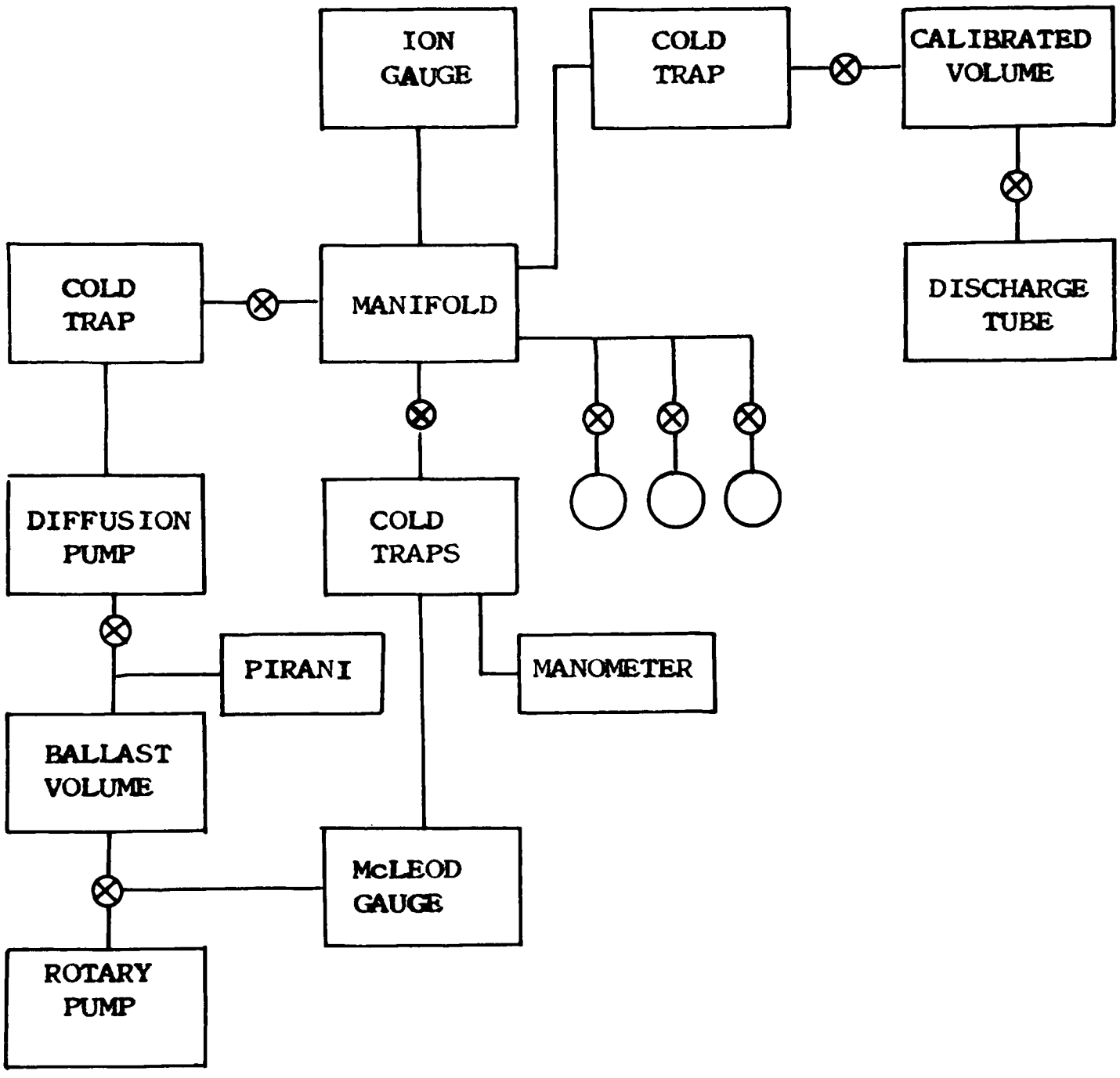
It was necessary to reduce the intensity of the allowed spectral lines emitted from the excited atoms which are produced during the afterglow by the dissociative recombination of electrons and molecular ions. This was achieved by increasing the electron diffusion rate during the early stages of the afterglow by coupling radiofrequency power to the electrons within the volume, so that the electrons were removed rapidly to the walls of the vessel.

4.2. The Vacuum System

A block diagram of the bakeable vacuum system used throughout the experiments is shown in figure 7. The system was pumped by an Edwards model E02 oil diffusion pump backed by an Edwards model ES35 rotary pump. The diffusion pump could be isolated from the high vacuum side of the system by closing the Mullard type VTB14 bakeable valve mounted on top of a Speedivac vapour trap. The high vacuum region was built in pyrex glass and the different sections interconnected by Hoke 411 series bakeable valves. Ultimate pumping pressure in the manifold was monitored by a Mullard

Figure 7

THE VACUUM SYSTEM



type IOG-12 ionization gauge operated by a model WPS-3 control unit. The system was thoroughly outgassed by baking the glassware and main valve at 250°C and the Hoke valves at 80°C by means of heating tapes wound about the components. After some twenty hours of baking at these temperatures an ultimate pressure of typically 4×10^{-9} torr was recorded when the system was cool, although it should be realized that in this pressure region the ionization gauge filament was operating as the main pumping element. The outgassing rate from the system after bakeout was recorded consistently in the region of 10^{-7} torr litre/minute. Since the Speedivac trap required servicing every twelve hours the main valve was closed overnight. This procedure proved quite satisfactory in that no deterioration in the vacuum was noticed over a long period, and it also enabled any vapours frozen in the trap during the day to be pumped through the backing region overnight. The total volume of the high vacuum region was approximately 5 litres.

4.3. Pressure Measurement and Gas Handling

The gases used in the experiments were of X-grade spectroscopic quality and were supplied by the British Oxygen Company in two litre soda glass bottles. Gas pressures in the range from 10 millitorr to 4 torr were measured by a calibrated mercury McLeod gauge and pressures in excess of 4 torr by a closed arm mercury manometer. The pressure measuring region was isolated from the main manifold

by a single vapour trap. Liquid nitrogen was used to keep this trap cold throughout the complete set of experiments. The mercury levels were monitored by a laboratory built cathetometer which was permanently mounted in front of the gauges. The cathetometer vertical and horizontal traverse were 40 cm and 20 cm respectively and a microscope of focal length 12 cm allowed adequate depth of focus to be obtained. The vertical position of the microscope could be recorded to within 0.01 mm by measurement from a precision steel rule mounted on the vacuum table and vernier attached to the microscope mount.

The McLeod gauge design enabled pressures as low as 20 mtorr to be recorded with an uncertainty of typically 1% and higher accuracy to be obtained for higher pressure measurements. The gauge volume was measured before the capillary arm was closed by weighing the volume of mercury required to fill the capillary and bulb. The cross-sectional area was also measured at this time by using a travelling microscope to record the length of tube occupied by a bead of mercury of known weight. No noticeable change in length occurred when the bead was displaced to different positions along the tube, indicating that the cross section was uniform along the length. The calibration constant for the gauge calculated from these measurements was

$$\text{cross sectional area/volume, } A/V = (4.16 \pm 0.01) \times 10^{-4}\ \text{cm}^{-1}$$

where the quoted error is a single standard deviation from the

mean. The pressure p corresponding to the length h of trapped gas in the capillary is deduced from the McLeod gauge formula

$$p = (A/V)h^2 + (A/V)ph$$

where the second term here is often neglected since the pressure to be measured is small in comparison with that of the trapped gas. No correction was necessary for the Ishii[45] effect. This is caused by the pressure difference between the McLeod gauge and the vacuum system which is established as a result of the flow of mercury vapour towards the cold trap. The effect is negligible at pressures greater than a few mtorr.

In order to facilitate the pressure readings, the manometer was built from $\frac{1}{2}$" diameter glass tubing so that a flat region of the meniscus could be monitored. Reading accuracy was determined by the reproducibility of successive measurements and all readings were repeated until consistency was obtained. The individual readings were reproducible to within 0.05 mm for the McLeod gauge and to within 0.01 mm for the mercury manometer.

For some experiments it was necessary to add to the discharge region an accurately recorded amount of oxygen at a pressure of a few tenths of a mtorr. This addition must be made with care since in this pressure region a finite quantity of the oxygen may be adsorbed on the clean glass wall. If a portion of inert gas at a few torr is then added to the discharge vessel, the adsorbed

oxygen will be displaced into the volume. The resultant partial pressure of the oxygen will then be very different from that initially measured. In order to overcome this problem the inert gas was added to the discharge volume and oxygen at a pressure of a few tens of mtorr was added to a neighbouring calibration volume. At this pressure the fraction of oxygen adsorbed on the walls may be neglected. The required conditions were then obtained by mixing the gases and the partial pressures were evaluated from the measured pressures and the known ratio of volumes.

The volume of the discharge region was determined as 2471 $\pm$ 10ml by weighing the volume of distilled water required to fill the vessel and associated pumping line. The calibration volume consisted of a spiral of 3/8" diameter glass tubing connecting two of the Hoke valves, a design which reduced the risk of mechanical strain being placed on the metal to glass seals during bakeout. The volume here was determined as 27.3 $\pm$ 0.1 ml by evacuating the region between the valves and then filling the volume with distilled water from a calibrated burette. This procedure ensured that no air bubbles were trapped in the volume during the measurement.

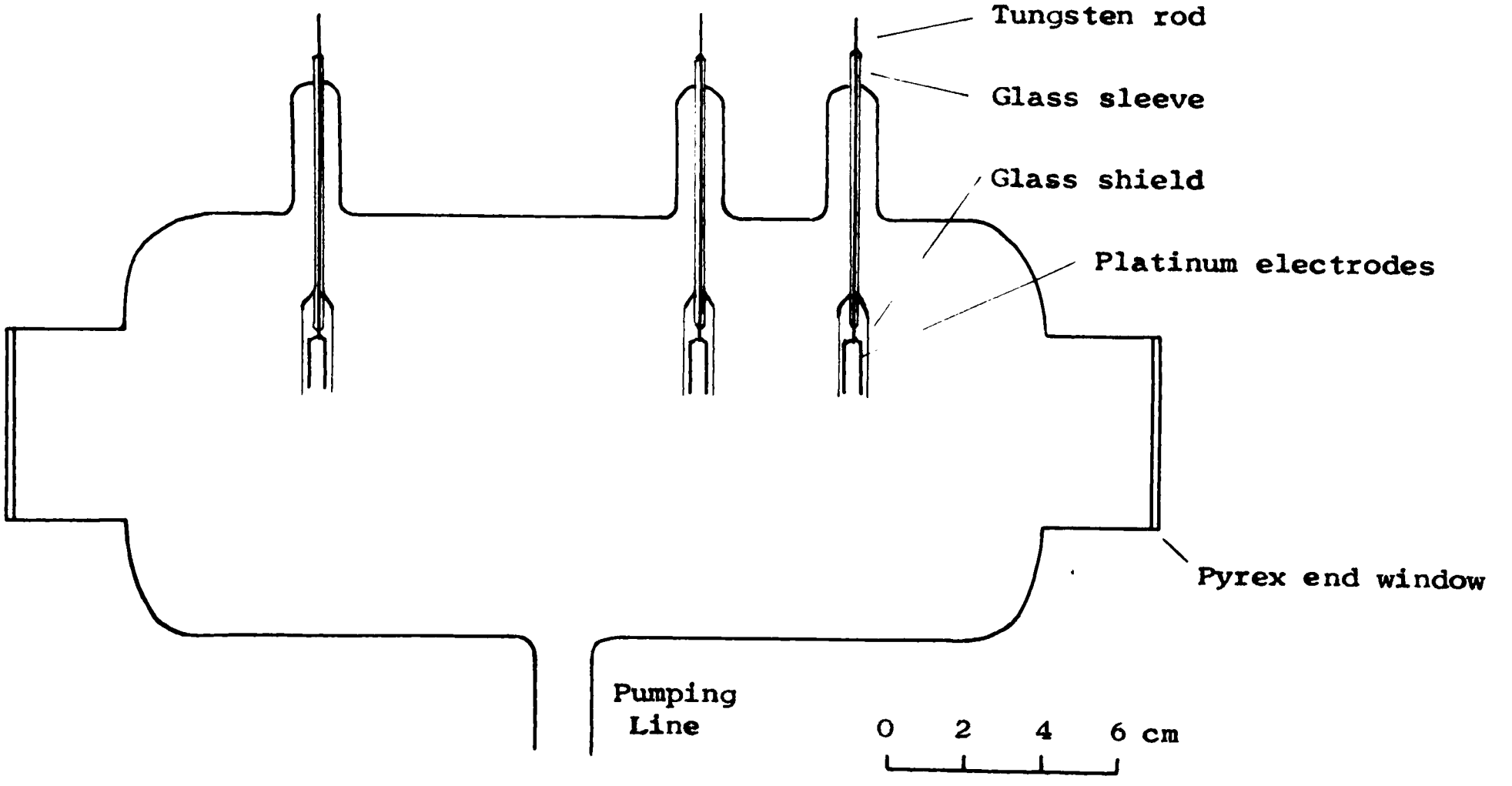
A consistent method of gas admission to the discharge tube was devised in order to reduce the risk of contamination to a minimum. The discharge tube, calibration volume and neighbouring vapour trap were baked initially for a period of twenty minutes. The vapour trap was then immersed in liquid nitrogen and a few tenths of a mtorr of oxygen were added to the discharge volume.

After the excess oxygen in the manifold had been exhausted, the inert gas was slowly seeped through the vapour trap into the discharge region over a period of some fifteen minutes. This technique served to remove any condensable impurities which may have been admitted to the gas by outgassing from the valve mounted above the gas bottle. The pressure measurement was delayed for a further twenty minutes to ensure that the gas in the discharge region had attained thermal equilibrium with the walls of the vessel and the surroundings. Room temperature was also recorded at this stage.

4.4. The Discharge Tube and Discharge Control System

4.4a. The Discharge Tube

A low current d.c. glow discharge through oxygen-inert gas mixtures was employed as a source of oxygen metastable atoms. A scale diagram of the discharge tube used is drawn in figure 8. The vessel consisted of an 11 cm diameter pyrex tube which was reduced to 5 cm diameter at each end. The tube was 30 cm long and the ends were sealed by pyrex glass optical flats which were fused to the main body. The electrodes consisted of platinum foil wound into small cylinders of 1.2 cm length, each of which was spot welded to a tungsten lead. Apart from the vicinity of weld, the full length of each of these leads was enshrouded in glass ensuring that only a small area of tungsten was exposed to the gas in the



SCALE DIAGRAM OF DISCHARGE TUBE

Figure 8

vessel. Platinum was chosen as the electrode material because of the convenient properties of low oxygen adsorption and low tendency to sputter under discharge conditions. (See Kohl[46] pp 241-256.)

4.4b The High Voltage Pulse Generator

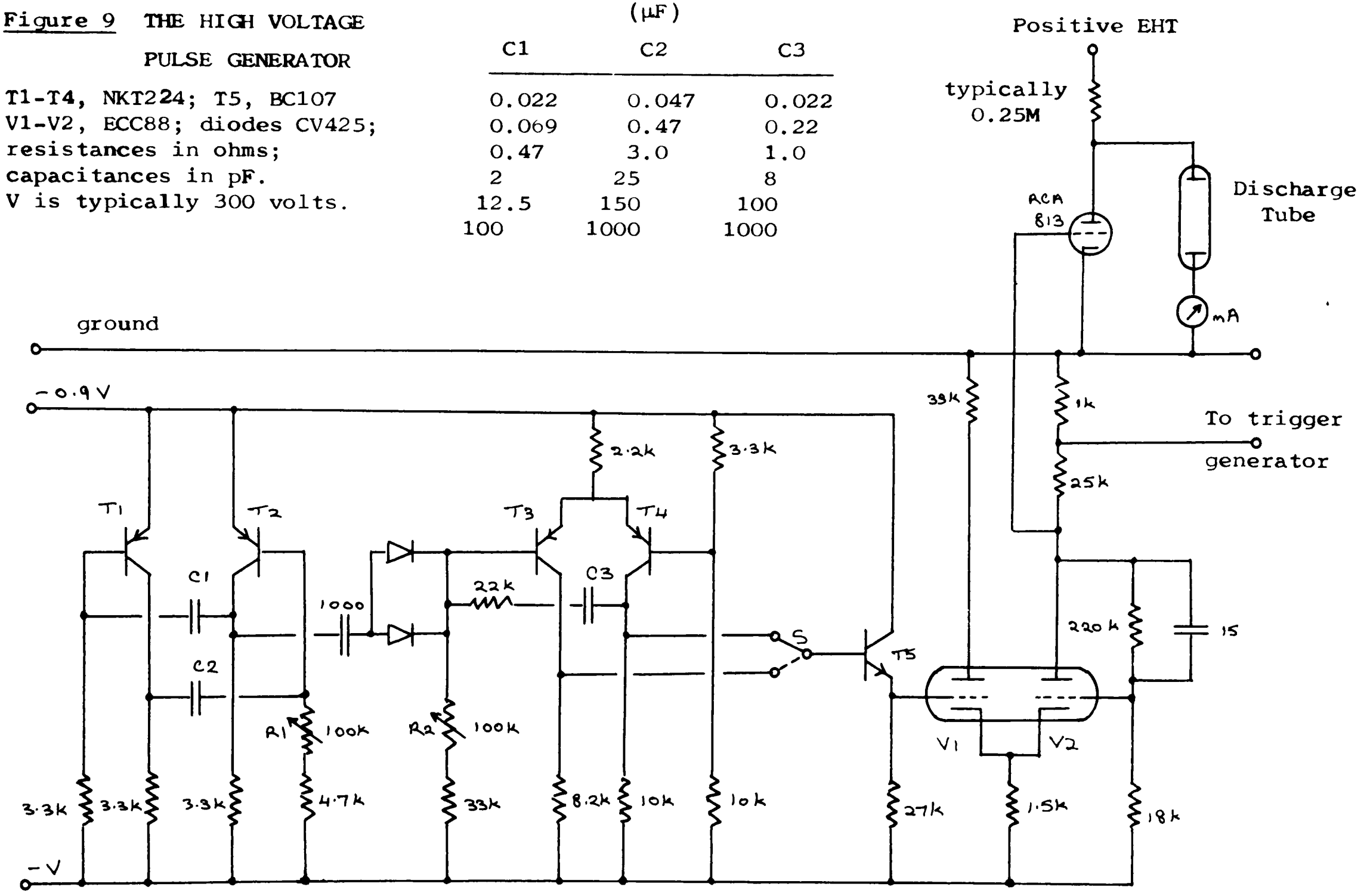
The discharge current was supplied by a Labgear type D4140 high voltage supply or when currents in excess of 5 mA were required, by a Fluke model 405B supply. The discharge was operated by a positive voltage and was stabilized by a ballast resistor of typically 0.25 megohms. As no commercial device capable of pulsing the high voltage supply was readily available, it was necessary to build a high voltage pulse generator; the circuit diagram of this device is shown in figure 9.

The discharge voltage was controlled by the negative bias applied to the grid of an RCA-813 power triode which was connected as a shunt across the discharge tube. Current was drawn by the valve when zero bias voltage was applied to the grid and in this mode of operation the voltage appearing across the discharge tube was held below that required to operate the discharge. However, when the triode was driven hard into cutoff by a negative bias of typically 250 volts, the tube voltage rose quickly towards the applied supply voltage. A discharge then struck if this voltage exceeded the breakdown potential of the gas.

Figure 9 THE HIGH VOLTAGE PULSE GENERATOR

T1-T4, NKT224; T5, BC107
V1-V2, ECC88; diodes CV425;
resistances in ohms;
capacitances in pF.
V is typically 300 volts.

(μF)		
C1	C2	C3
0.022	0.047	0.022
0.069	0.47	0.22
0.47	3.0	1.0
2	25	8
12.5	150	100
100	1000	1000



The bias control circuitry shown in figure 8 was of standard design. The switching frequency was controlled by an astable multivibrator (T1, T2) which produced rectangular pulses of mark-space ratio equal to 0.1. These pulses were differentiated and used to trigger a monostable circuit (T3, T4) which generated pulses of the required duration. The variable controls in these two circuits enabled the pulse width and repetition period to be chosen in the range 0.1 ms to 10 s. The output from the monostable was connected to the input of a valve Schmitt trigger circuit (V1, V2) which operated both as a fast switch and as a voltage amplifier. Negative voltage pulses of 250 volt amplitude were generated here when a 300 volt supply voltage was used These pulses were used as the bias control for the main power triode. The pulse rise and fall times were each 2 μs.

A small fraction of each pulse was applied to the input of a trigger generator circuit which was used to produce separate timing pulses in synchronism with each change of bias voltage. The circuit diagram is shown in figure 10a. Each input pulse is differentiated to produce two 5 volt timing pulses of 5 μs duration which appear at separate outputs, one pulse in coincidence with the rise of the discharge tube voltage and the other in coincidence with the fall.

4.4c. The Spark Generator

On some occasions, particularly when high pressures of argon

were used, the applied voltage was insufficient to break down the gas in the tube. In order to overcome this problem a spark generator was designed, the basic principle employed in the device being the discharge of a capacitor across the primary windings of a step-up pulse transformer. A high voltage transient then occurs across the secondary windings and this was applied to a strip of aluminium foil wound about the circumference of the discharge tube. A transient amplitude in excess of 5 kV was found to be sufficient to break down the gas over the complete range of pressures employed.

The circuit diagram of the spark generator is shown in figure 10b. The control rheostat RV adjusts the bias applied to, and hence the current drawn by the transistor T. This current determines the level to which the capacitor C is charged as being in the range from 30 V to 180 V for the full range of adjustment of RV. A silicon controlled rectifier S shunts the series combination of C and the primary windings of the pulse transformer. In the quiescent conditions S is passive. However, when the voltage is applied to the discharge tube S is triggered by the timing pulse that is generated. C then rapidly discharges through the low impedance path presented by S and the primary windings of the transformer and the characteristic LRC type of oscillation appears across the secondary windings; this oscillation is heavily damped by the resistor R. The amplitude of the initial positive excursion

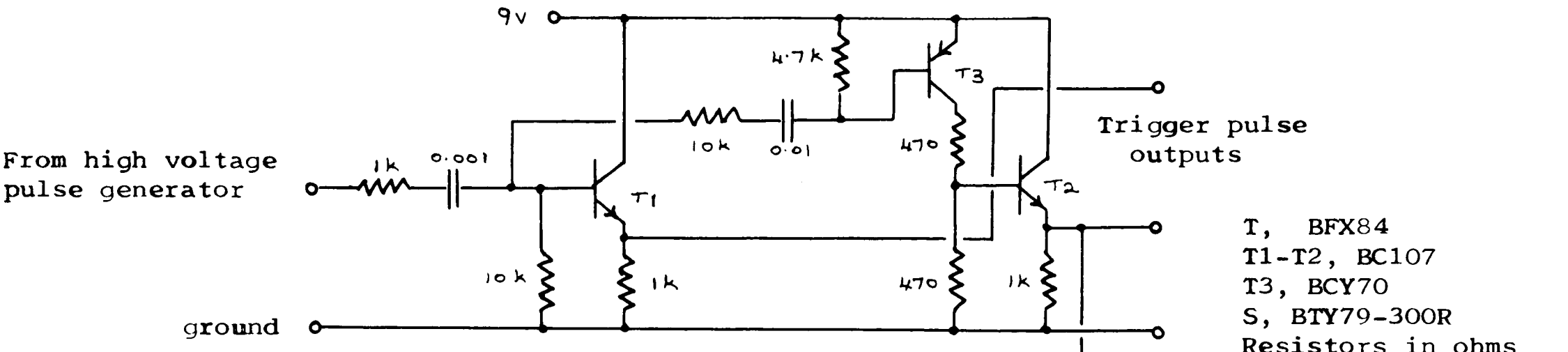


Figure 10a THE TRIGGER GENERATOR CIRCUIT

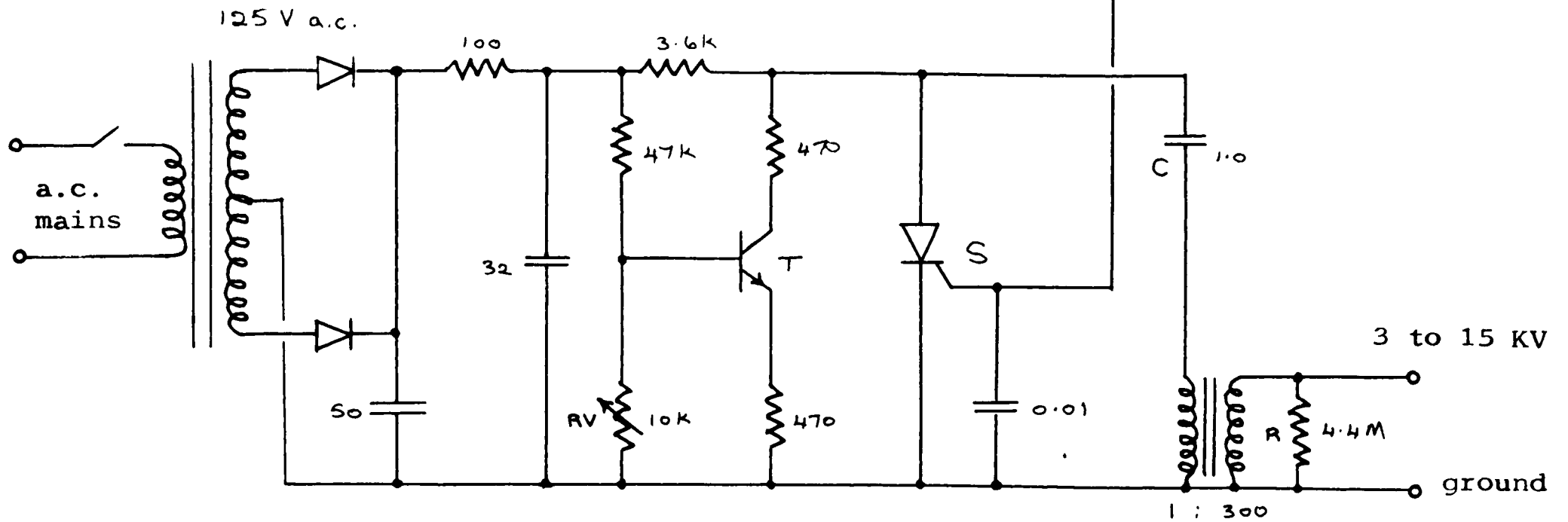


Figure 10b THE SPARK GENERATOR CIRCUIT

may be adjusted between 3 kV and 16 kV. S is switched off by the first negative oxcillation. The transient lasts for approximately 1 ms and the maximum repetition frequency is limited at 200 Hz by the peak power dissipation level of the mains transformer used.

4.5. The Light Detection System

Light emitted from the positive column of the glow discharge was dispersed by a Littrow mounted grating monochromator which was positioned along the axis of the discharge tube. The entrance slit of the monochromator was situated close to one end of the tube in order to obtain maximum input light flux. An aluminium mirror placed directly behind the far end of the tube also served to increase the collection efficiency.

The collection efficiency is not increased by use of a condensing lens system since the light is then collected from a much smaller volume of the discharge tube. For the same reason, the light collected by the combination of a collimating lens and a narrow band interference filter would not greatly exceed that collected by the monochromator, particularly if a wide entrance slit is used. The monochromator is, of course, considerably more versatile than an interference filter.

A sketch of the monochromator is shown in the block diagram, figure 5. A 12.8 cm x 10.2 cm Bausch and Lomb grating ruled 600 lines/mm was used as the dispersive element of the system.

The grating was blazed at 1.6 microns in first order and was generally used at 5577Å in third order. Light from the other orders was severely attenuated by use of the combination of a green interference filter and a green glass filter in conjunction with the monochromator. The 200Å bandpass of this combination was centred about 5577Å at which the transmission coefficient was 65%. The collected light was collimated by a 12 cm diameter lens of 180 cm focal length and the exit beam was deviated towards the exit slit by a right angled prism placed close to the entrance slit. The linear dispersion at the exit slit was then 3Å/mm. The wavelength of the light observed here was calibrated in terms of the position of a motor driven micrometer screw used to rotate the grating table. Details of the table construction are given by Webb[47]. Each aperture was constructed from razor blade edges and could be adjusted in width. The maximum aperture size was limited at 2.5 cm x 1 cm by the difficulty of separating the input and exit beams. The majority of the afterglow measurements were recorded with the apertures at maximum width.

Light from the monochromator was detected by an EMI type 9558 QB photomultiplier tube. Metal oxide 110 kilohm resistors were used in the standard dynode chain (total resistance = 1.65 megohms) and were connected to the pins of the tube by hyperboloidal contacts. The tube was held horizontally inside a cylindrical brass housing by means of electrically insulated

brass spring clips. A 5" length of open ended brass tubing was soldered directly to the main housing and could be filled with powdered solid carbon dioxide. Thermal conduction then enabled the interior of the housing to cool to near -70°C. At this temperature the dark current from the photocathode was reduced to less than 10 picoamperes. The housing was connected to the monochromator exit port by a length of 3" diameter stainless steel which served to reduce the conduction of heat towards the housing. The interior was also thermally isolated from the monochromator by means of a 10 cm long evacuated glass cylinder of 6 cm diameter. Dry air was continuously blown on the monochromator end of this cylinder in order to prevent the condensation of water vapour on the face.

The dynode chain current was supplied by a Brandenburg model 470 stabilized high voltage supply which was operated generally at 1200 V, the corresponding tube gain being greater than 10^6. The anode voltage was developed across a 4.7 kilohm resistor and the photoelectric pulses were coupled through a short length of 75 ohm coaxial cable to the matched input of the photopulse amplifier described below.

4.6. The Photon Counting System

4.6a. The Photopulse Preamplifier

Since the anode to ground stray capacitance of the

photomultiplier tube and the associated output cable capacitance add to approximately 50 pF, it is necessary to use an a.c. anode load of typically 100 ohms in order to avoid integration of the individual photopulses. At a tube gain of 10^6 an average photopulse develops a peak voltage of the order of one millivolt across a 100 ohm anode load. This voltage is not sufficiently large to operate conventional electronic switching circuitry so that each pulse must be initially amplified by a high frequency preamplifier. The circuit diagram of the amplifier designed for this purpose is drawn in figure 11.

The preamplifier is of simple design, consisting of two cascaded integrated circuit stages followed by an inverter stage and emitter-follower current amplifier. The active components of the circuit are built into a block of dural which acts as the earth plane. This design reduces the effects of stray capacitance. Stray inductance is reduced by interconnecting the active components by the passive elements and by ensuring that all leads are cut to as short a length as is practical. The overall voltage gain is 400 and the frequency response is flat to 70 MHz. Saturation occurs at the inverter stage when the height of the output pulses reaches 1.0 volts but below this level the shape is undistorted apart from a 5% overshoot; this is caused by the finite recharge time of the coupling capacitors following the transmission of a pulse through the amplifier.

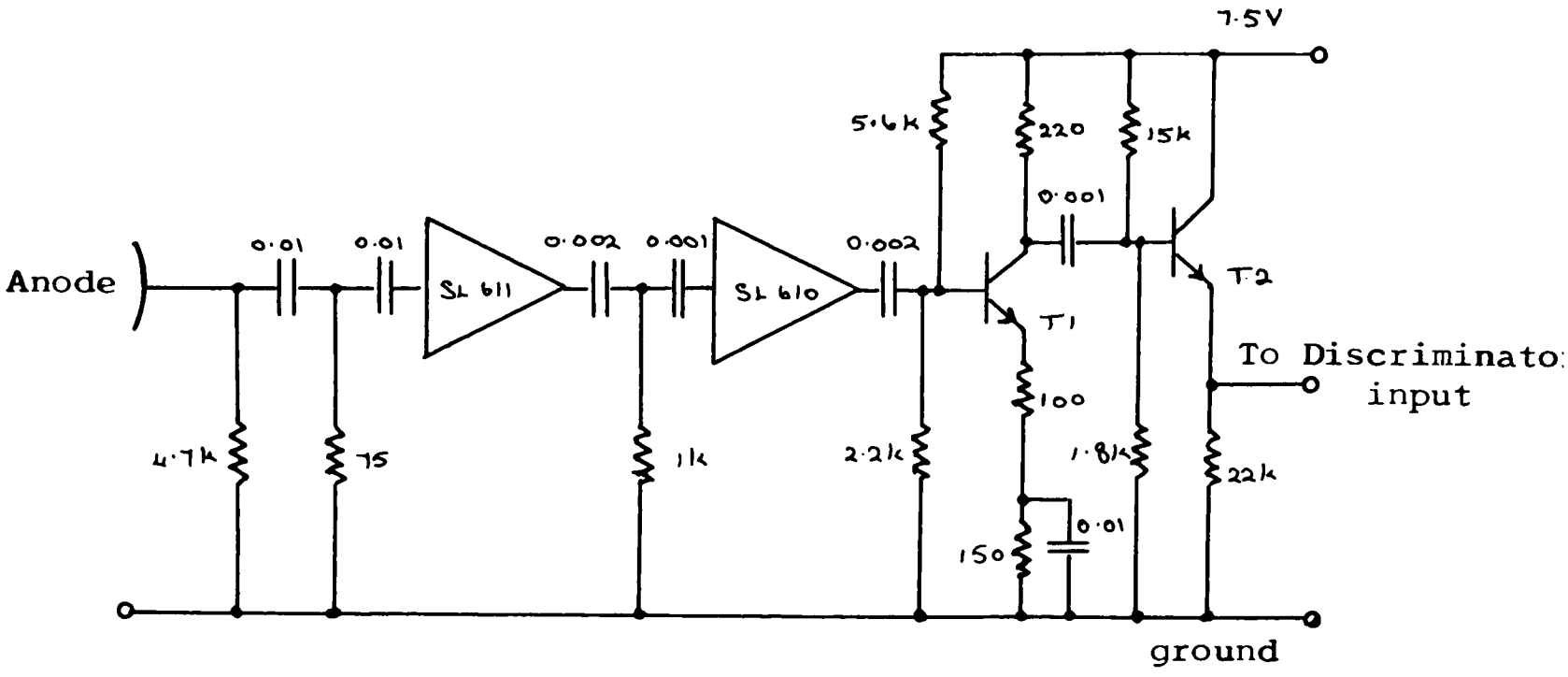


Figure 11 THE PHOTOPULSE PREAMPLIFIER

T1-T2, BFY90; Resistances in ohms, Capacitances in μF

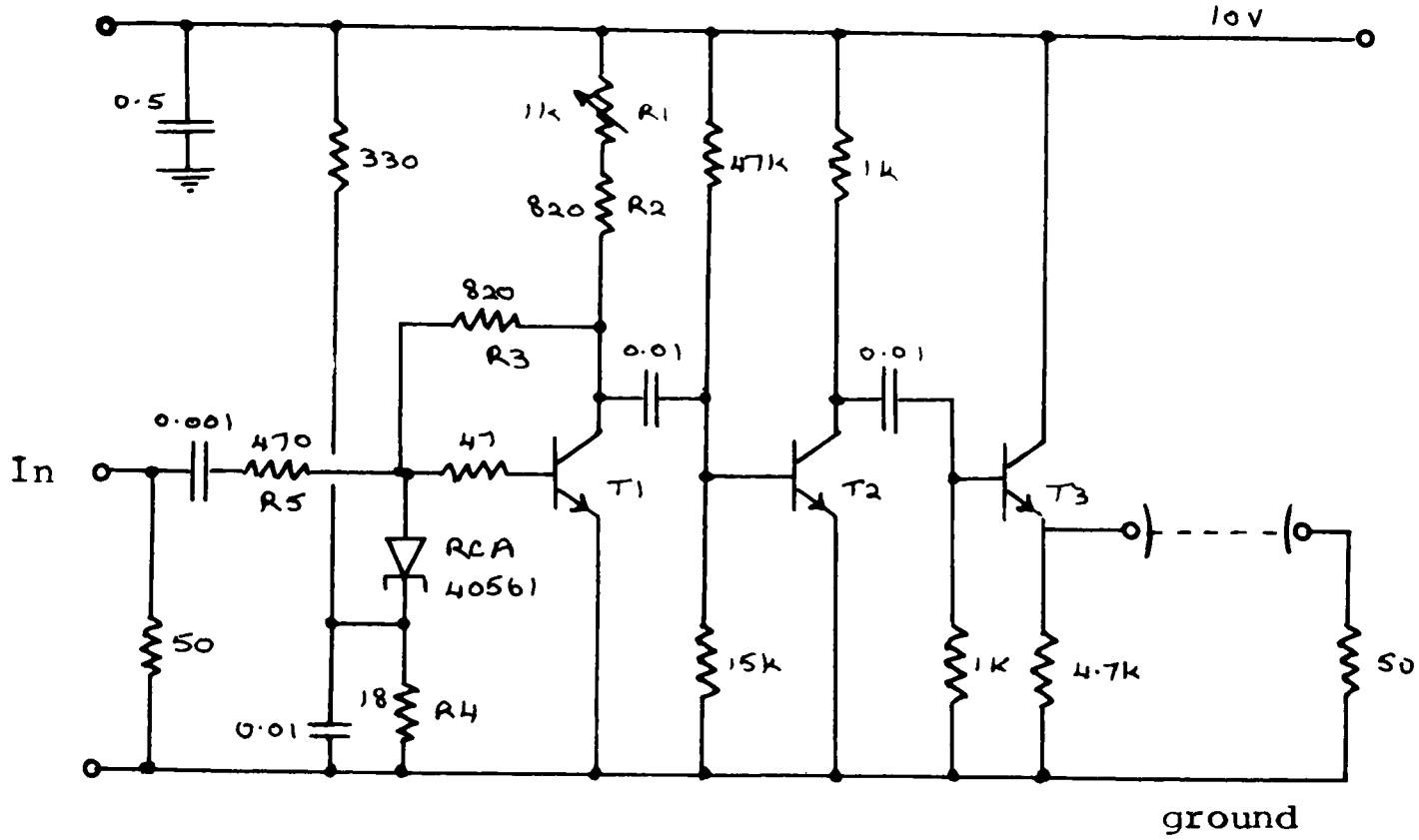


Figure 13 THE DISCRIMINATOR AND PULSE SHAPER

T1, BC107; T2-T3, BFX20;
Resistances in ohms,
Capacitances in μF

4.6b. The Discriminator and Pulse Shaper

Each 20 ns positive preamplifier pulse is transmitted along 50 ohm coaxial cable to the matched input of a discriminator and shaper circuit. The operation of this device is twofold. Firstly, it must be capable of accepting all pulses above a preselected voltage level and secondly, identical output pulses must be generated over a wide range of input pulse characteristics. The dead time of the circuit will then be independent of the input pulse shape and size. The discriminator must also be free from long term drifts and able to be triggered by input pulse amplitudes as small as 50 mV.

The discriminator used throughout the experiments utilized the very convenient negative resistance properties of a tunnel diode. A plot of the current-voltage characteristics of the RCA type 40561 tunnel diode used in the discriminator circuit is shown in figure 12. The existence of the unstable intermediate voltage region causes very rapid switching between the upper and lower stable regions independently of the form of the triggering voltage. The device is consequently very useful as a discriminator, particularly when used in conjunction with a switching transistor which acts as a voltage amplifier.

A diagram of the discriminator circuit is drawn in figure 13. In the quiescent conditions the tunnel diode operating point is

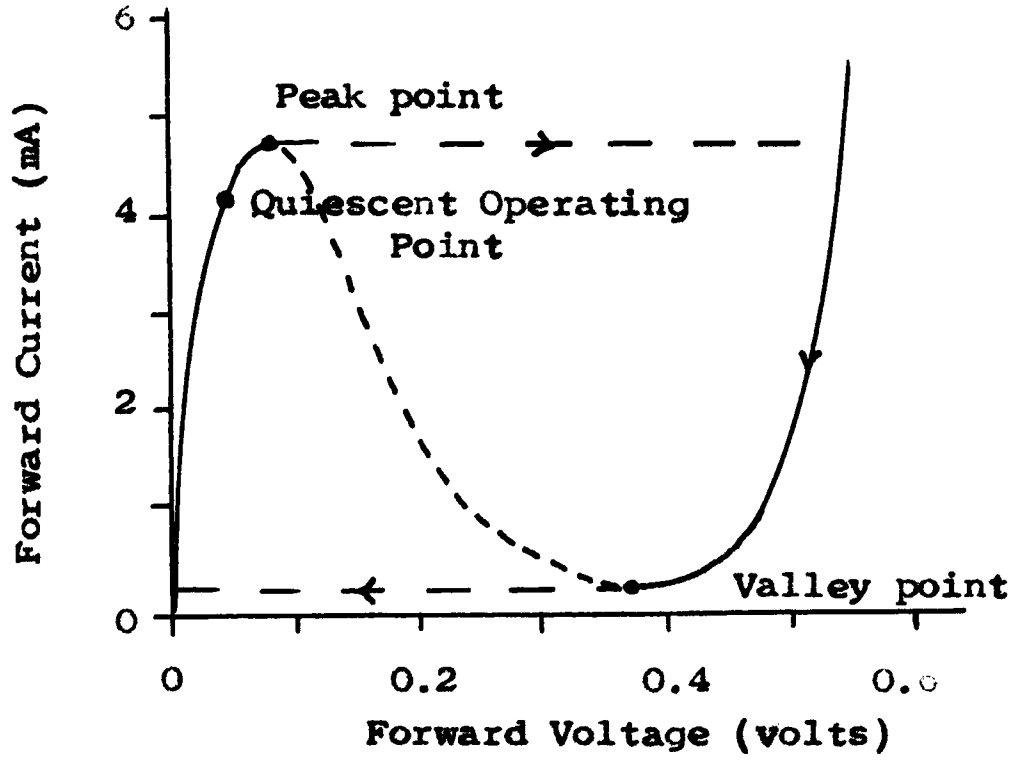


Figure 12 CHARACTERICS OF THE RCA 40561 TUNNEL DIODE

held close to the characteristic "peak point" (figure 12) by means of the current supplied through the resistors R1, R2 and R3. Additional current supplied to the resistor R4 maintains the transistor T1 on the verge of the active region of operation. The transient voltage of a pulse arriving at the input terminals is divided between the a.c. resistance of the tunnel diode and the series resistor R5. If the increment appearing across the tunnel diode is sufficient to lift the operating point to the peak point of the characteristics, the device is triggered very rapidly to the higher stable state. T1 is driven hard into saturation by the accompanying positive 0.4 volt step and the current supply to the tunnel diode is reduced towards zero as the transistor internal and stray capacitances discharge. As this occurs, the tunnel diode operating point moves towards the "valley point" of the

characteristics and rapidly returns to the lower stable region. T1 is then switched off and the quiescent conditions once more assumed.

Each time the discriminator circuit is triggered, a 3 volt negative pulse is generated at the output of T1. This pulse is used to drive the switching transistor T2 into cutoff and the resulting 70 ns positive pulse is current amplified by T3. Each 2.5 volt output pulse is of standard shape and of duration determined principally by the time required to discharge the capacitances associated with T1. The discriminator level is set by the potentiometer R1 and may be adjusted so that input pulse amplitudes as low as 50 mV trigger the circuit. With this sensitivity, most of the preamplifier pulses generated from photoelectric pulses will trigger the discriminator circuit. The circuit was found to be free from long term drifts in the constant temperature environment in which the experiments were conducted. The output pulses were coupled to the input of a "dead time loss restorer" which was used to modify slightly the interval distribution of the pulses. Discussion of this device is deferred until §4.9.

4.7. The Electronic Timing Sequence

The high voltage pulse generator acts as the basic timing device of the electronic system shown in figure 6. The first timing pulse from the trigger generator in synchronism with the

application of the discharge tube voltage is used to produce a high voltage transient if this is necessary to strike the discharge. After a preselected period the discharge high voltage is removed and the second timing pulse is generated. This pulse "starts" the sweep of the Nuclear Data series 1100 multichannel scaler and signal pulses from the photon counting system are counted for a preset period into the first channel. At the end of this period the channel address is advanced by one and counts are accumulated for the same period into the second channel. The channel address again advances by one and the sequence is continued until the final channel is reached. At the end of the counting period here, the multiscaler returns to the quiescent state and awaits the next triggering pulse to initiate the channel address cycle. On each sweep then, the intensity of light detected from the afterglow is obtained as a function of channel number or time. The timing sequence is repeated at a rate determined by the requirements for the discharge and afterglow periods and the whole experiment is continued until the statistical scatter on the accumulated signal has been reduced to a tolerable level. The multichannel scaler thus acts as a signal averager.

4.8. Data Output

Counts were accumulated into 256 channels each of width determined to crystal accuracy by the 100 KHz multiscaler internal

clock. At the end of each experiment the memory contents were plotted by a Bryans model 21001 X-Y recorder. Data from each plot was read on a point-to-point basis in order to overcome the need to rely on the linearity of the plotter, and in order to obtain a digital output.

The analogue Y-signal to the plotter is derived internally from only two digits of the memory content of a particular multi-scaler channel. Significant rounding errors can occur, particularly when the number defined by the two digits is close to zero, as often occurred for the late afterglow signal. This difficulty was avoided, however, by ensuring that three digit numbers were always obtained from the memory contents of the channels. The analogue signal corresponding to the second and third most significant digits of each channel content was plotted, and the value of the most significant digit was easily inferred from the known monotonic decreasing form of the decay curve. The rounding errors were then always significantly smaller than the uncertainty caused by statistical scatter. The range of the plot was set to cover 100 mm of the Y-axis of the recorder in order to facilitate the transfer from the analogue signal to a set of three digit numbers. These numbers were used directly in the computer analysis of the signal.

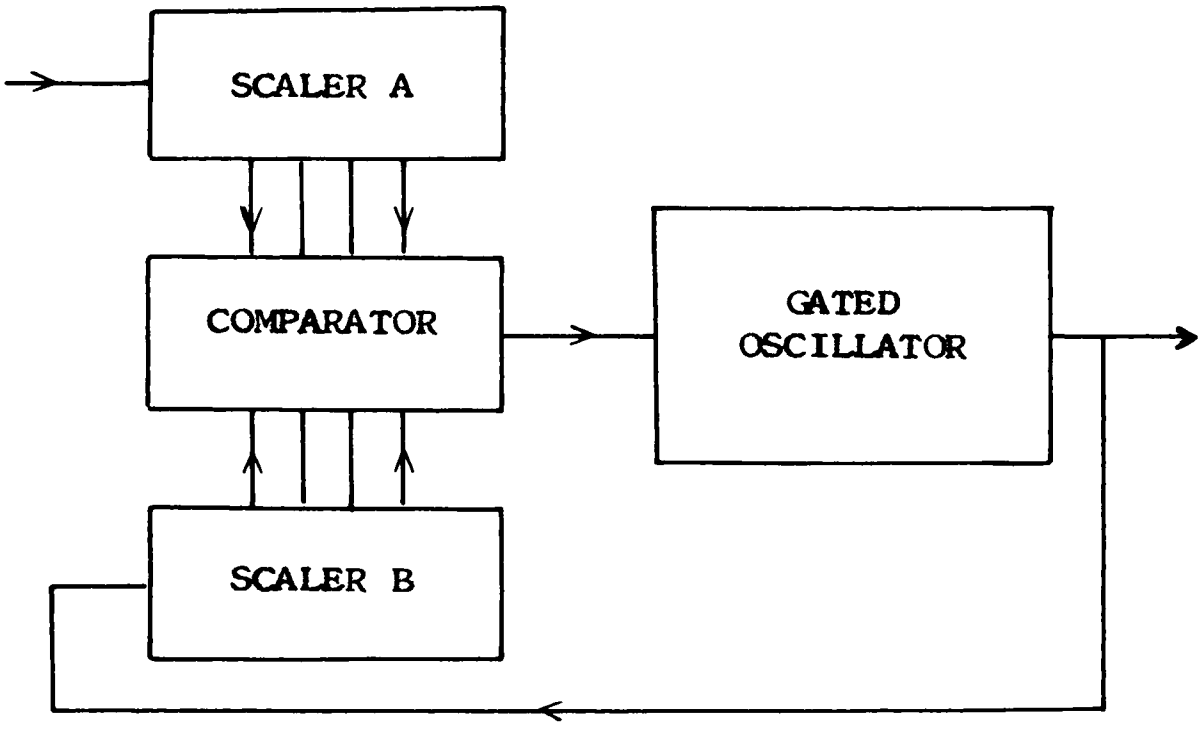
4.9. The Reduction of Dead Time Losses

The memory cycle time of the multiscaler was determined as

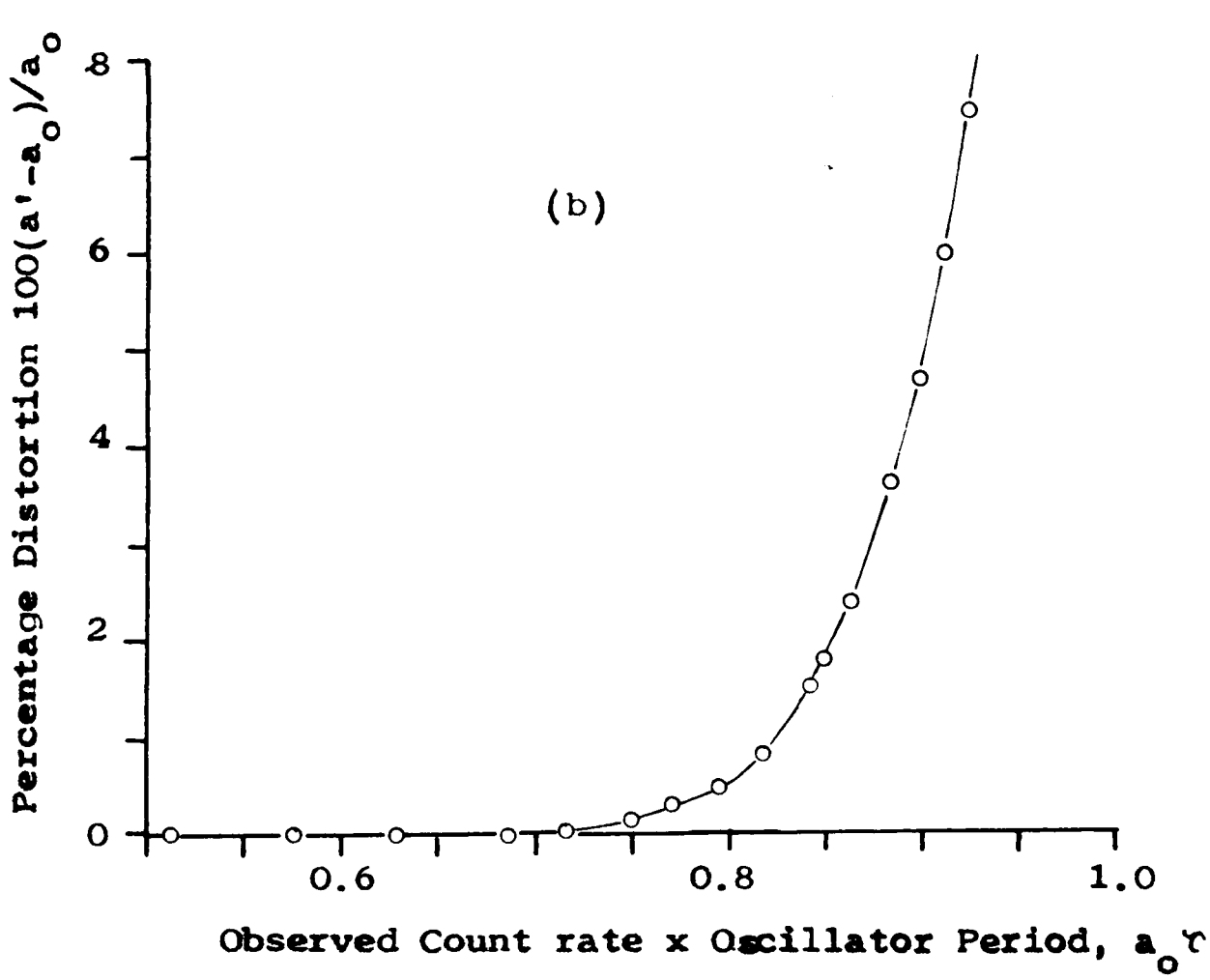
7.0 μs by a measurement of the minimum interval between two signal pulses that the instrument could resolve. As a result of this finite deadtime, the recorded count rate (a_0) is smaller than the real count rate (a) since no events are recorded during the deadtime d that follows the occurrence of an event accepted by the scaler. For a signal from a source of randomly spaced events, the scaler is then dead for a fraction $a_0 d$ of every second so that counts are lost at a rate $a(a_0 d)$. This leads directly to the well known result

$$a_0/a = 1 - a_0 d.$$

We see that for the multiscaler used, there is a loss of almost one percent for a count rate as low as 1 KHz and at higher signal levels the loss may become comparable with the recorded count rate. Although the real count rate may be evaluated accurately from the above relation, a better method of overcoming the effect is to restore the loss by using the delay generator described below to delay each event which would not normally be recorded, until the scaler is capable of accepting it. There is then no need to rely on the fact that the above relation holds strictly only for a random interval distribution. A block diagram of the "dead time loss restorer" developed for this purpose is shown in figure 14a. Full circuit details of the device are given by Williams et al[48].



(a)



(b)

THE DEAD TIME LOSS RESTORER

Figure 14

In the quiescent conditions the scalers hold equal numbers and the comparator output gates "off" the oscillator. If the scalers hold unequal numbers the comparator output gates "on" the oscillator which free runs giving pulses separated by a period τ to the scaler B and the multiscaler. Here τ is normally set to be slightly greater than the deadtime of the multiscaler.

If an input pulse arrives while the delay generator is quiescent the scaler counts become unequal so that the oscillator will start to generate pulses. If no further input pulses arrive before the end of the oscillator period, the first oscillator pulse rebalances the scalers and so restores the quiescent conditions. However, if more input pulses have arrived, further oscillator pulses will be generated, until after n input pulses, n oscillator pulses have been generated to restore the quiescent conditions. Each output pulse is then separated by at least τ from its neighbours.

The effective dead time of the delay generator is determined jointly by the real dead time of the scaler A and by the finite probability that the scalers A and B, which each have a capacity of 2^4 or 16 counts, will become out of step by sixteen counts. Whenever this occurs 16 counts will be lost. The dependence of this loss on the signal count rate has been investigated experimentally by recording the output count rates obtained over a range of signal count rates. The signals were obtained by illuminating the photo-

multiplier tube by different light intensities and the resulting pulses from the photon counting system were further shaped by a high frequency pulse generator to give standard pulses of 120 ns duration. These were coupled to the loss restorer and the ratio a'/a_0 of input to output count rates was measured by a 12 MHz digital counter for different values of input count rate. No real dead time losses were then recorded since the 120 ns deadtime of the standard pulses exceeded those of the input scaler A and the digital counter.

The measured percentage distortion is shown in figure 14b as a function of the dimensionless parameter $a_0\tau$, where τ is the oscillator period of the generator. For randomly spaced events, the form of the distortion curve is dependent only on the probability of losing 16 counts and has been determined for several different settings of oscillator period. The count rate a' is determined directly from the calibration curve for a particular observed count rate, and the real signal count rate thence obtained as $a'/(1 - a'd)$ where d is here the input system dead time, for these experiments being that of the discriminator circuit since the dead time of scaler A is only 25 ns. It can be seen immediately from figure 13 that the residual distortion after the loss restorer is incorporated in the multichannel scaling experiment is determined solely by the discriminator dead time for count rates as high as $0.7/\tau$. Losses of about 40% occur if a real signal rate of $0.7/\tau$

is fed directly into a multiscaler of dead time τ. This is reduced typically to a few tenths of a percent when the delay generator is used. It was found, in fact, that for the low count rates encountered here it was unnecessary to apply any correction to the recorded count rate.

Only when $a_0\tau$ approaches the limiting value of unity is there a significant probability that an event be delayed by several oscillator periods. Furthermore, for many multiscaling applications the dwell time per channel is at least an order of magnitude greater than the memory cycle time, so that the probability is low that a particular event be delayed by more than a single channel width. For such experiments there is little danger that use of the loss restorer introduces a significant channel distortion.

CHAPTER 5

TIME RESOLVED STUDIES OF THE AFTERGLOW

5.1. Decay Processes in the Afterglow

We examined in chapter 3 the processes by which oxygen metastable atoms were created and destroyed in an oxygen-neon or oxygen-argon discharge. We discuss here the decay of the charged species and of the metastable inert gas atom populations during the afterglow.

5.1a. Decay of the Charged Species

It is evident from the discussion of 3.4 concerning the spectral emissions from a low current oxygen-inert gas discharge that the excited states of both the atomic and molecular forms of the inert gas are populated during the discharge. Their emissions form the discrete line spectrum and the continuum background respectively. The ion current is shared between atomic and molecular ions, the latter species being formed by the three body conversion process

$$X^+ + 2X \longrightarrow X_2^+ + X \qquad (5.1)$$

and being destroyed by diffusion to the walls of the vessel and by the dissociative recombination

$$X_2^+ + e \longrightarrow X + X \; . \qquad (5.2)$$

The product atoms formed here are generally excited. Evidently, the importance of excited state molecules and molecular ions increases with increasing gas pressure.

Typical electron densities of the order of 10^8 cm^{-3} to 10^9 cm^{-3} are attained in the low current discharges employed in the experiments described here, and at these densities the diffusion of ions and electrons to the walls of the vessel is approximately ambipolar. The ambipolar diffusion coefficient D_a is connected to the free ionic diffusion coefficient D_i by the well-known relation

$$D_a = D_i (1 + T_e/T_i) \qquad (5.3)$$

(see, for example, von Engel[43], §5.3)

where T_e and T_i represent the electron and ion temperatures respectively.

After the discharge pulse is terminated, the importance of excitation and ionization by direct electron collisions decreases rapidly as the electrons in the volume thermalize. The rate of ambipolar diffusion is also severely diminished. Ambipolar diffusion coefficients at 300°K have been determined by Smith and Cromey[49] from measurements made in the afterglow of pulsed inert gas discharges. They determined the product $D_a p$ as 181 torr cm^2 s^{-1} for neon atomic ions and 67.6 torr cm^2 s^{-1} for argon atomic ions. They also measured the rate of the three body conversion process (5.1) as 99 $torr^{-2}$ s^{-1} and 313 $torr^{-2}$ s^{-1} for neon and argon

respectively. It is clear from their results that for the discharges employed in the experiments described in this thesis where a vessel of 2.2 cm diffusion length and pressures greater than a few torr were used, the atomic inert gas ions are rapidly converted into molecular ions during the early stages of the afterglow.

The rate constants for the dissociative recombination process (5.2) have been measured by a number of experimenters[36] as approximately 7×10^{-7} cm^3 s^{-1} and 2×10^{-7} cm^3 s^{-1} for argon and neon respectively. The importance of the recombination loss falls rapidly with electron density and during the late afterglow the loss rate is governed principally by diffusion. As the electron density falls, the wall loss process converts gradually from ambipolar diffusion to the free diffusion of ions and electrons. In general, the diffusion loss will be intermediate between the two extremes. In table 3 we have compared the rates of the loss processes which govern the populations of the ionic and metastable species in the late afterglow for the discharge vessel used throughout the experiments. Evidently, the ambipolar diffusion rate for molecular ions is smaller than the diffusion rate for the $O(^1S_0)$ metastable atom population. The consequences of this result are discussed in §5.2.

5.1b. Decay of the Inert Gas Metastable Populations

The inert gas metastable atom populations decay during the

Process	Ref.	Decay Rate (s^{-1})		
		1 torr	2 torr	5 torr
$O(^1S_0)$ diffusion through neon	(38)	84	42	16.8
Ne_2^+ ambipolar diffusion at 295°K	(50)	51.5	26	10.3
Neon metastable atom loss	(51)	135	225	540
$O(^1S_0)$ diffusion through argon	(38)	53	26.5	10.6
Ar_2^+ ambipolar diffusion at 295°K	(50)	15	7.5	3
Argon metastable atom loss	(52)	56	121	570

TABLE 3 Decay Rates in the Late Afterglow for Different Inert Gas Pressures.

afterglow by diffusion to the walls of the vessel, by three body collisions in which an excited inert gas molecule is formed, and by two body collisions in which the metastable atom is excited (or de-excited) to the nearest radiating state. This latter process is relatively unimportant during the discharge pulse when the radiation from the inert gas resonance levels is heavily trapped. Phelps[51] has studied the pressure dependence of the decay rates of the neon metastable atom populations by absorption measurements made in the afterglow of a pulsed discharge. Recently, Ellis and Twiddy[52] have made similar measurements in argon. In each study it was found that the singlet resonance level population decayed

considerably more rapidly than the triplet level populations. The decay rates for the populations of the latter species were found to be closely linked as a result of collisional mixing and were determined at 300°K as

$$\Gamma = \frac{145}{p\Lambda^2} + 105p + 0.5p^2 \text{ for neon}$$

and

$$\Gamma = \frac{48}{p\Lambda^2} + 29p + 17p^2 \text{ for argon}$$

to a good approximation. Here p is the pressure in torr at 300°K. The decay rates of the triplet level populations are compared in table 3 to the decay rates of $O(^1S_0)$ metastable atoms for diffusion through neon and argon. At pressures higher than 2 torr, the metastable inert gas populations decay at a considerably faster rate than the oxygen metastable atom population. However, at pressures of the order of 1 torr the decay rates are comparable and if there is significant coupling between the inert gas metastables and the oxygen metastable atoms during the afterglow, anomalies in the observed decay of the $O(^1S_0)$ population might occur. This point is discussed further in §6.4.

5.2. The Removal of Electrons from the Afterglow

The dissociative recombination process (5.2) leads to the formation of excited state inert gas atoms during the time that the molecular ion population is decaying. If the emissions from

these atoms lie within the wavelength region monitored by the light collection system there is a possibility that the observed afterglow intensity in the region of the 5577Å forbidden oxygen line will fall non-exponentially. The occurrence of such behaviour would increase considerably the uncertainty in the determination of the decay constant of the forbidden line component from the observed time-resolved afterglow curves. In practice, non-exponential decay curves were observed only in the oxygen-neon afterglows where several allowed NeI lines lie within the detected wavelength range centred about the forbidden line. (See the spectrum of figure 3, §3.4a.) No allowed spectral line of significant intensity lies close to the 5577Å line in the spectra of oxygen-argon discharges. (See figure 4, §3.4c.)

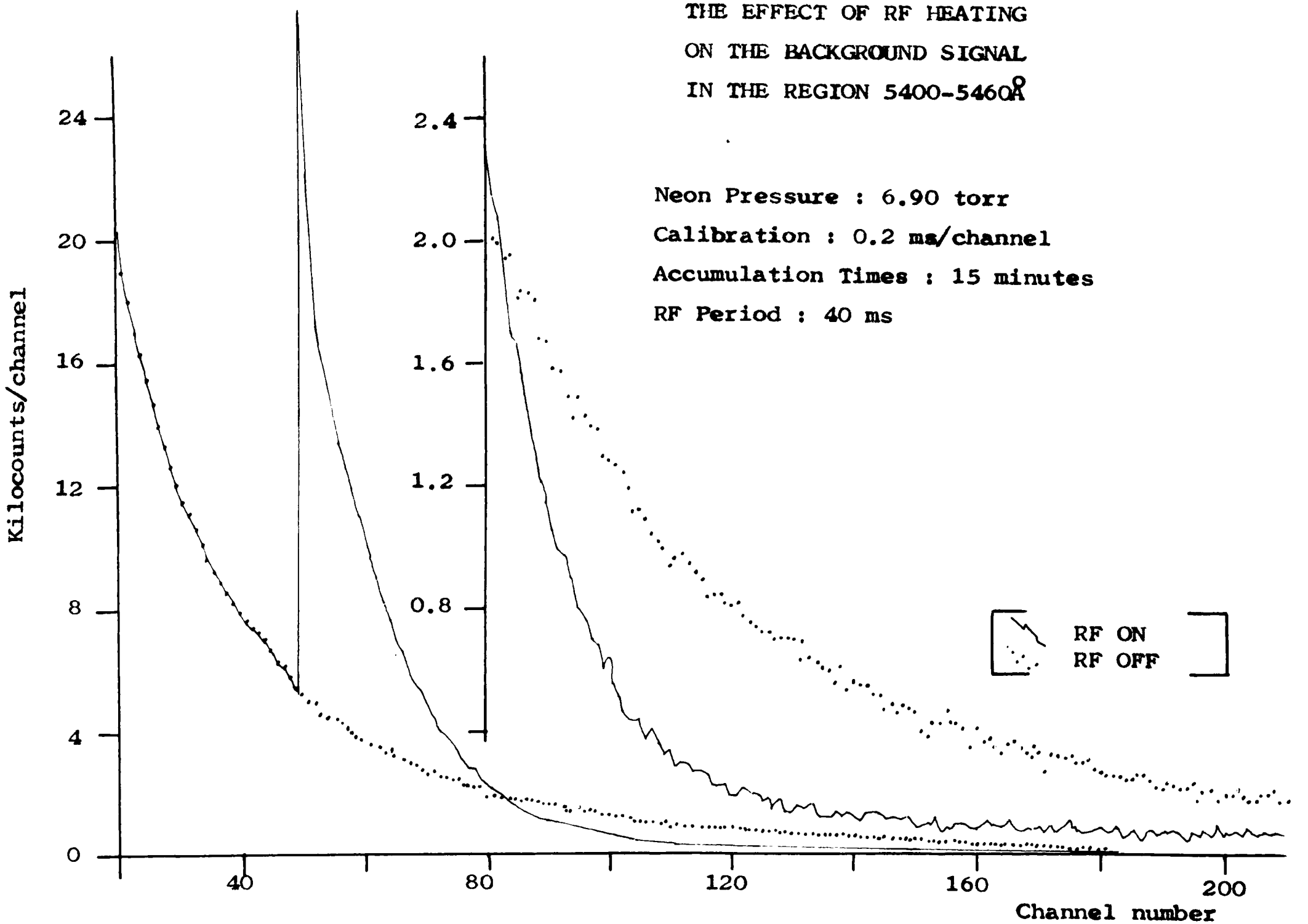
Rather than increase the resolution by closing the entrance and exit slits of the monochromator since this would considerably decrease the already small afterglow signal intensity, it was decided to attempt to reduce the dissociative recombination contribution to the recorded afterglow curves by artificially increasing the diffusion of the electrons to the walls of the vessel. It is clear from equation (5.3) that the ambipolar diffusion rate may be considerably increased if the electron temperature in the afterglow is raised. There would be a corresponding increase in the electron free diffusion rate, so that the dissociative recombination process would be of importance only in the vicinity

of the walls. The "electron heating" technique described here has been used in a number of experiments[53] as a convenient means for removing electrons from the volume of a vessel during an afterglow.

In the experiments described in this thesis, a Venner model TSA 628 pulse generator was triggered at the end of each discharge pulse and was used to generate a pulse of variable width delayed by a few milliseconds. This pulse was used to gate the output of a Heathkit model DX-100U transmitter. Radiofrequency power at approximately 20 MHz was coupled through an LC impedance matching network to a strip of aluminium foil wound about the circumference of the discharge tube. Care was taken to ensure that the power levels used were insufficient to generate new ionized species. The effects of the technique may be seen from the time-resolved afterglow curves plotted in figures 15 and 16. For completeness, afterglow curves from both the forbidden line region and the region of the strong NeI 5400Å line are shown, and in each case the afterglow observed when the electron heating technique is used is compared to the afterglow observed in the absence of applied radiofrequency power. This power was always removed before the end of the first decay lifetime of the metastable oxygen population. The abrupt increase in the detected intensity is caused by the renewed ability of the energetic electrons to excite the atoms within the volume. The intensity of this radiation decreases

Figure 15

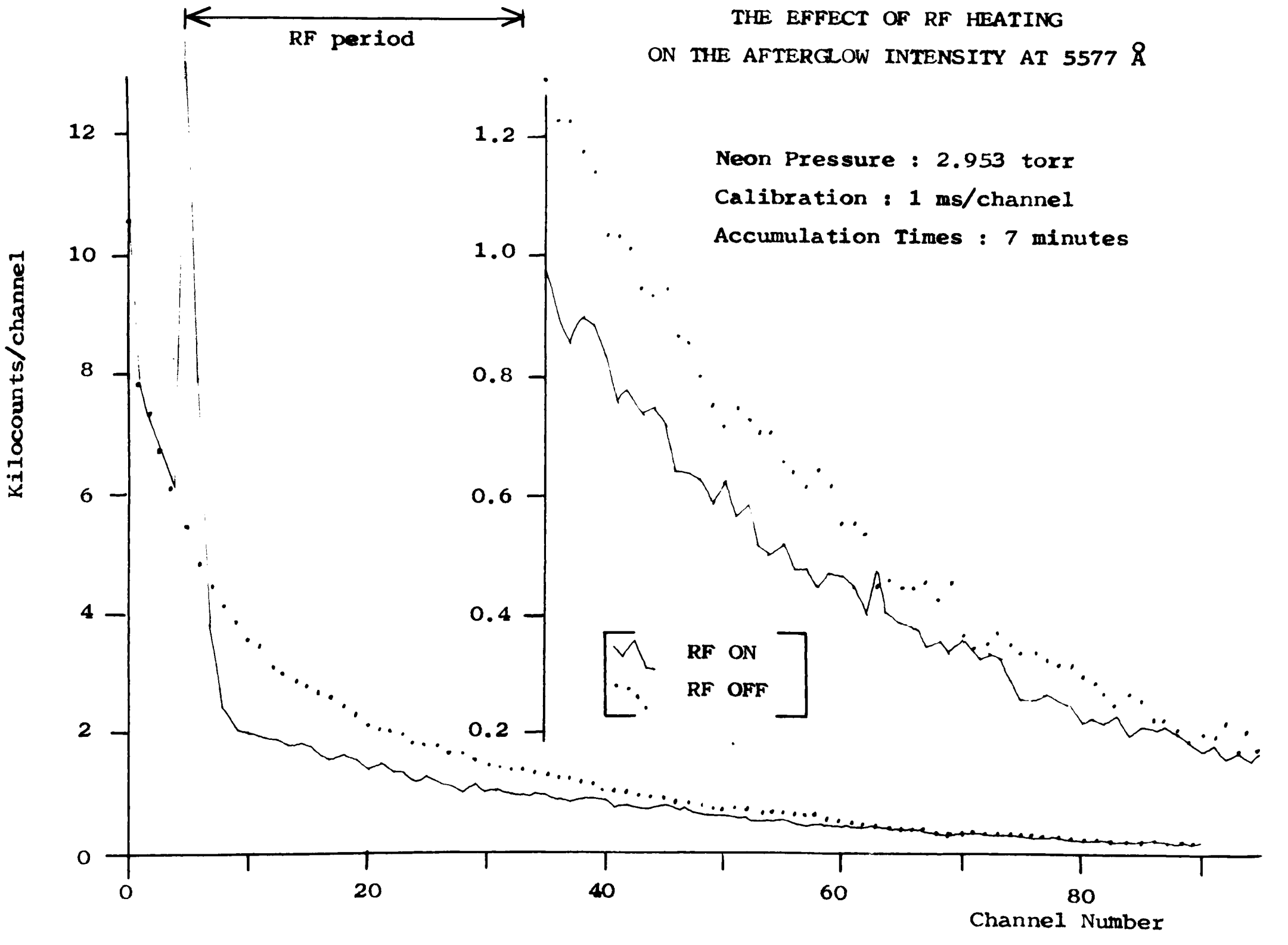
THE EFFECT OF RF HEATING
ON THE BACKGROUND SIGNAL
IN THE REGION 5400-5460Å



Neon Pressure : 6.90 torr
Calibration : 0.2 ms/channel
Accumulation Times : 15 minutes
RF Period : 40 ms

Figure 16

THE EFFECT OF RF HEATING
ON THE AFTERGLOW INTENSITY AT 5577 Å



rapidly as the electron density within the volume decreases and the observed intensity soon falls below that obtained under similar conditions in the absence of the applied radiofrequency power. The afterglow decay curve is generally analysed outside the region shown in figure 15. The efficiency of the electron heating technique was checked from the analysis of the observed decays. In no case was non-exponential behaviour detected when the technique was used.

5.3. The Forbidden Line Intensity Decay Rate

It was shown in §3.2c that the decay of the forbidden line intensity during the late afterglow is expected to be exponential with decay constant Γ given by

$$\Gamma = \frac{A'}{p} + \Gamma_o + \alpha' p + \beta' p^2 + \alpha'_o p_o \qquad (5.4)$$

where we have expressed here the number density dependence in terms of pressure at constant temperature. The decay time of the observed afterglow curve then depends on both the inert gas pressure p and the oxygen partial pressure p_o. Because of the adsorption of oxygen atoms on the walls of the vessel, the oxygen partial pressure cannot be measured directly but, as was shown in §3.7, is expected to be proportional to the product $I\Gamma$ of the intensity of the afterglow signal and the measured decay constant provided that the oxygen is fully dissociated and that the electron temperature does not change significantly as the oxygen is adsorbed. In order to evaluate the

effect of collisional deactivation of metastable oxygen atoms by ground state oxygen atoms, it is then necessary to record at each inert gas pressure investigated a number of afterglow decay curves accumulated during the time in which the oxygen partial pressure and hence the signal intensity are changing. It is readily seen from equation (5.4) and from the above discussion that the decay constant Γ'_0 which would be measured in the absence of atomic oxygen quenching may be determined as the zero intensity intercept of the linear plot of the measured decay constants Γ against the products $I\Gamma$. The reduced decay constant Γ'_0 then satisfies the relationship

$$p\,\Gamma'_0 = A' + \Gamma_0 p + \alpha' p^2 + \beta' p^3 \qquad (5.5)$$

so that the radiative decay constant Γ_0 may be determined as the linear coefficient of the cubic form obtained by plotting the values of the product $p\,\Gamma'_0$ measured at different inert gas pressures against the pressure p.

5.4. The Exponential Decay Curves

For each inert gas pressure investigated, a number of afterglow decay curves were recorded during the period in which the signal intensity was changing. Throughout this period, often lasting for eight hours or more, a 5 mA discharge was pulsed at a constant rate determined by the decay time of the afterglow. The discharge pulse lasted three to four decay periods, allowing sufficient time for

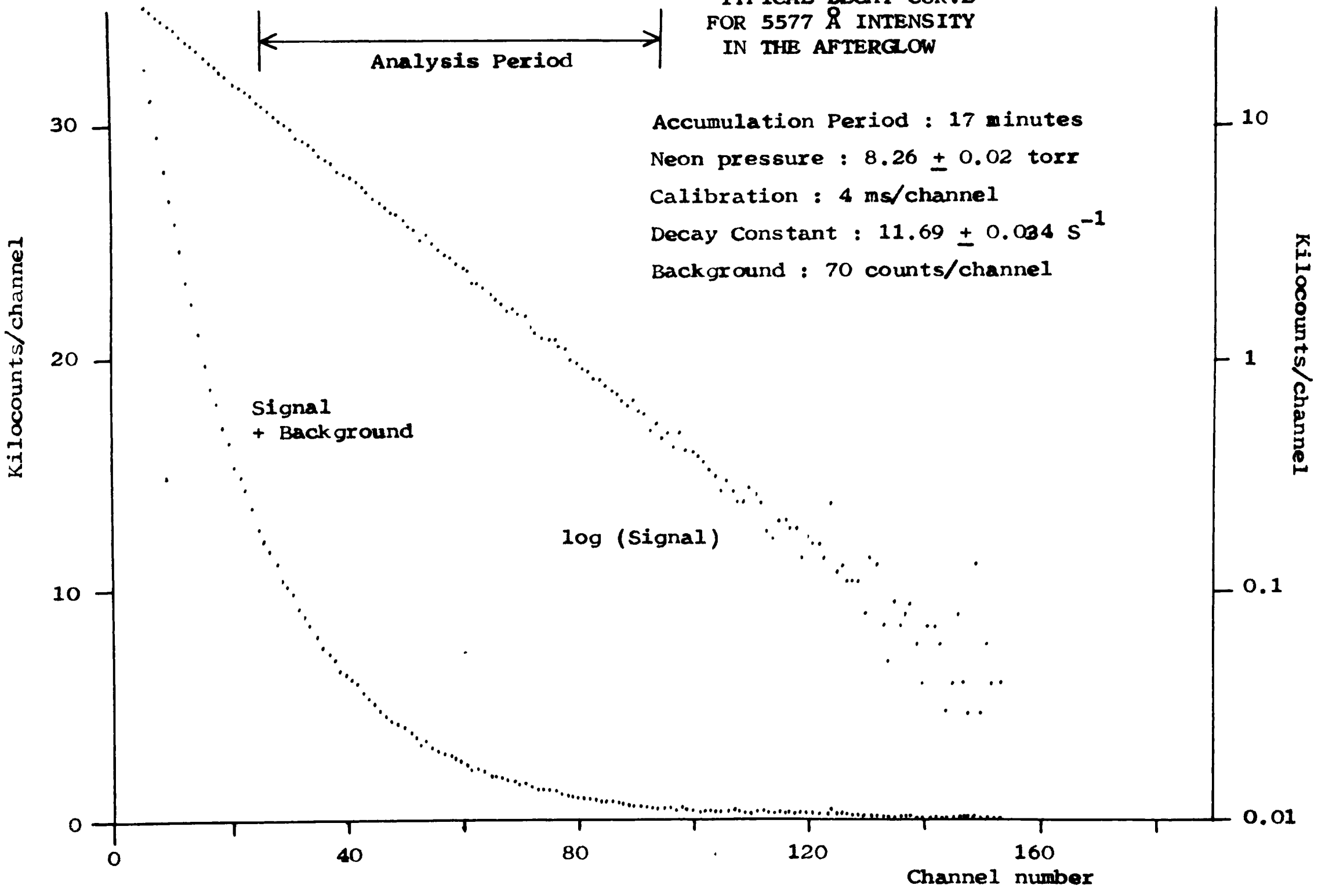
the metastable oxygen atom populations to approach their equilibrium values, and the afterglow was recorded over typically eight decay periods. It was then possible to accurately estimate the background signal due to dark current and stray light. The analyses of the exponential decay curves could then be considerably simplified.

The first afterglow curves recorded at each inert gas pressure were generally accumulated during the periods in which oxygen was being strongly adsorbed on the walls of the vessel. During these periods a limit was placed on the total accumulation time for each curve because of the rapidly changing value of decay constant. Typical count rates of 20 KHz to 40 KHz were recorded here at the start of each afterglow period and the accumulation time was limited to a few minutes. At later times the intensity decreased at a slower rate and longer accumulation periods were used in order that signals of similar magnitude could be recorded throughout the range of signal intensities. Ultimately, a dynamic equilibrium was established in the discharge vessel in which there was no net adsorption of oxygen. At this stage count rates of between 1KHz and 5 KHz were recorded at the start of each afterglow period and accumulation times of up to one hour were employed.

Figure 17 shows a typical decay curve recorded from an oxygen-neon afterglow over a period of 17 minutes at an initial count rate of about 12 KHz and a pulse rate of 50 per minute. It is evident that the ratio of signal to statistical scatter is large during

Figure 17

TYPICAL DECAY CURVE FOR 5577 Å INTENSITY IN THE AFTERGLOW



the early stages of the afterglow. The logarithmic plot of the signal shows clearly that the decay is of a single exponential component and it is particularly interesting to note that the linearity of this plot extends well into the early stages of the afterglow. Deviations from linear behaviour might be expected there because of the decay of higher order diffusion modes. Evidently the initial radial distribution of the metastable population must closely approximate that of the first order diffusion mode. The linearity of the logarithmic plot during the late afterglow gives a good indication of the accuracy of the estimate of the total background count.

5.5. Temperature Dependence of the Decay Constants

Since the values of the diffusion coefficient and the rate constants for deactivation are temperature dependent, it was necessary to record the ambient temperature in the vicinity of the discharge vessel. It was found possible to maintain a relatively constant temperature which normally varied over a range of $1^{o}C$ on each day. The diffusion coefficient is expected to vary as $T^{\frac{1}{2}}$ (see equation 3.12) and the temperature dependence of the two body rate constants is most conveniently evaluated if we express each constant as the product $\alpha = \bar{q}\,\bar{v}$ in the first order approximation. Here $\bar{q}$ is the velocity averaged cross-section and is not expected to have a strong temperature dependence. The two-body rate constants consequently vary as the average velocity $\bar{v}$ or as $T^{\frac{1}{2}}$. The

preliminary experimental measurements showed that the effect of three body deactivation on the value of the measured decay constant was small, so that the difference $\Gamma - \Gamma_0$ between the measured and radiative decay constants also should vary as $T^{\frac{1}{2}}$ in the first approximation. (See equation (5.4).) This result was used to calculate a temperature normalized decay constant from each measured value of decay constant. The theoretical estimate of 1.25 s^{-1} for the radiative decay constant was used here and the applied corrections never exceeded 0.3 percent.

5.6. Analysis of the Decay Curves

5.6a. The Logarithmic Fitting Procedure

Analysis of the afterglow intensity curves was considerably simplified by the pure exponential nature of the decay and by the accurate estimate of the background level which was measured from the late afterglow signal. The total number of signal counts in each channel was then evaluated simply as the difference

$$a - c = be^{-\Gamma t} \pm [\delta a^2 + \delta c^2]^{\frac{1}{2}} \qquad (5.6)$$

between the total count a and the background count c. If Poisson counting statistics are assumed, δa and δc may be replaced by $a^{\frac{1}{2}}$ and $c^{\frac{1}{2}}$ respectively. The unknown coefficients b and Γ may then be evaluated from the logarithmic form of equation (5.4):

$$\ln (a - c) = \ln b - \Gamma t \pm \frac{[a + c]^{\frac{1}{2}}}{a - c} . \qquad (5.7)$$

We have computed the standard deviation here to first order by using the assumption that the statistical scatter is small compared to the signal amplitude. The values of the linear coefficients ln b and Γ are evaluated by the well-known least squares fitting procedure in which the reciprocal of the square of the standard error is used to weight each experimental data point. (See, for example, Topping[54] p.86, pp 101.) The need for a weighting procedure is quite evident from the form of the logarithmic plot shown in figure 16 in which it is easily seen that the straight line is considerably better defined by the early afterglow signal than by the scatter of the late afterglow points. It may also be noted from this plot that the amplitude of the statistical scatter is close to that defined by Poisson statistics. Topping[54] gives full details of the least squares fitting procedure, including the formulae from which the standard errors of the evaluated coefficients may be determined.

Each decay curve was generally analysed over at least a decade change in intensity which typically occupied from sixty to eighty of the multiscaler channels. The curve was never analysed in the region of the first decay period as a precaution against the possible occurrence of higher order mode diffusion.

5.6b. Data Reduction

The decay curves were analysed with the aid of a Digital

model PDP8/L computer. Because of the small storage space and the rather slow data output system of this computer it was necessary initially to reduce the amount of curve data. This reduction was accomplished by use of the very convenient integration property of exponential curves, namely that

$$\int_{t-T}^{t+T} be^{-\Gamma t} dt = \frac{b}{\Gamma} \left(e^{\Gamma T} - e^{-\Gamma T} \right) e^{-\Gamma t} .$$

That is, the integrated curve has the same exponential time dependence as the original curve. The amplitude of the new curve depends only on the constants of the original curve and on the fixed range of integration. Analysis of the integrated curve then enables the required decay constant to be evaluated without any loss of information and with considerably less calculation. In practice, the integration was performed simply by the addition of the memory contents of neighbouring channels in sets of five across the range of the afterglow curve. The curve data was then reduced from between 60 and 80 points to between 12 and 16 equally spaced points which defined the integrated curve. The constants of this curve and their standard errors were then evaluated by computer by use of the weighted least squares method described above. The computed standard errors typically lay between 0.2% and 0.5% of the decay constant values.

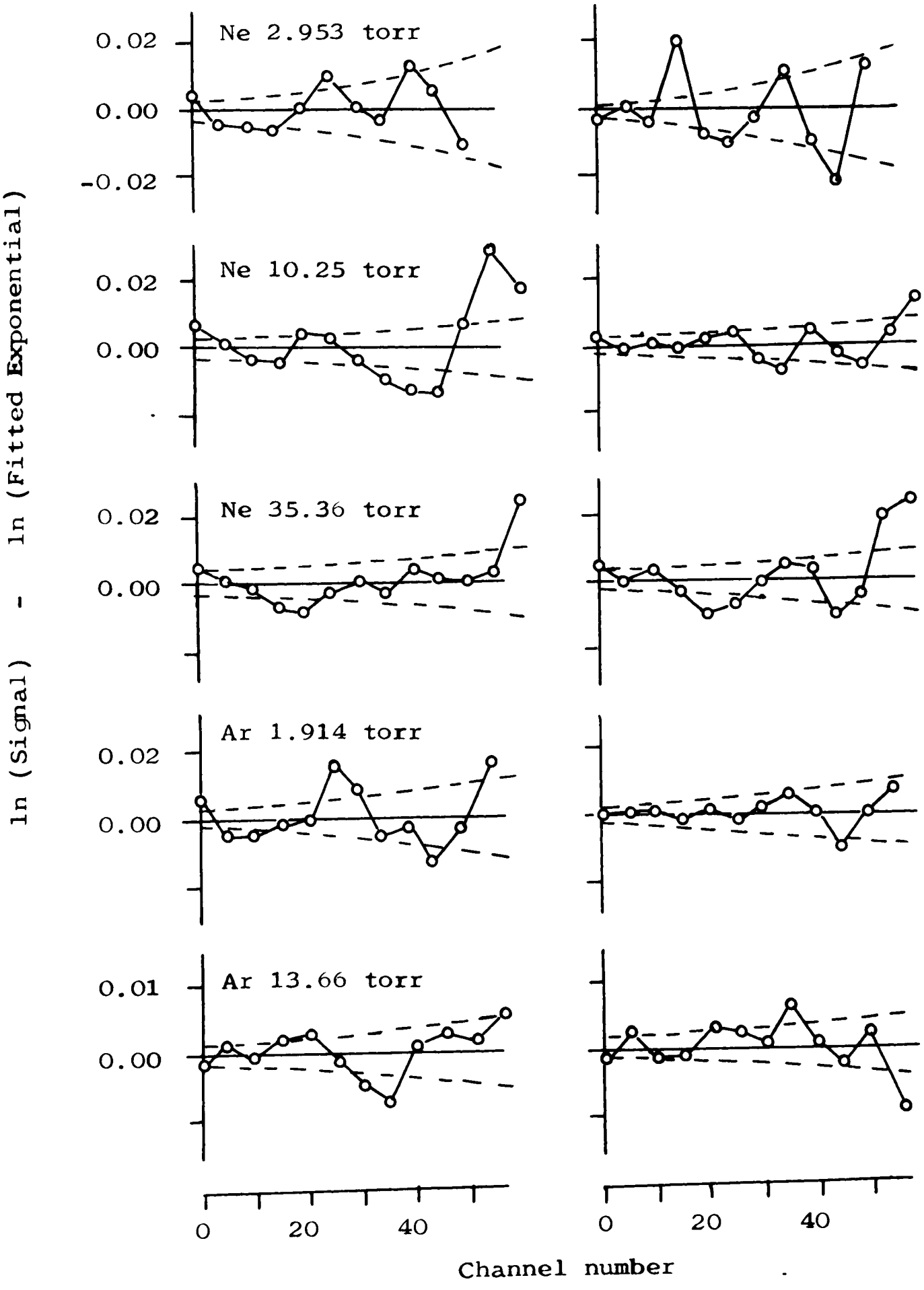


Figure 18 RESIDUALS BETWEEN THE EXPERIMENTAL AND FITTED EXPONENTIALS

5.6c. The Residuals Between Experiment and Fit

The residuals between the experimental data points of the logarithmic plot and the fitted straight line values are shown in figure 18 for a number of afterglow curves recorded at different pressures of neon and argon. The two sets of residuals shown at each pressure correspond to decay curves recorded at different signal intensities and the dotted lines correspond to a single standard deviation of the scatter from the computed best fit. These lines have been evaluated from the expected uncertainty of equation (5.7) under the assumption that Poisson statistics are obeyed, in which case 68 percent of the experimental points are expected to lie within the limits defined by the single standard deviation curves. Between 55% and 80% of the experimental points shown in figure 18 lie within these limits, in good accordance with the basic assumption of pure exponential behaviour. In fact, small deviations from pure exponential behaviour may be expected since the decay curves are accumulated during the periods in which the decay constant is changing slowly with time.

5.7. The Intensity-Decay Constant Correlation

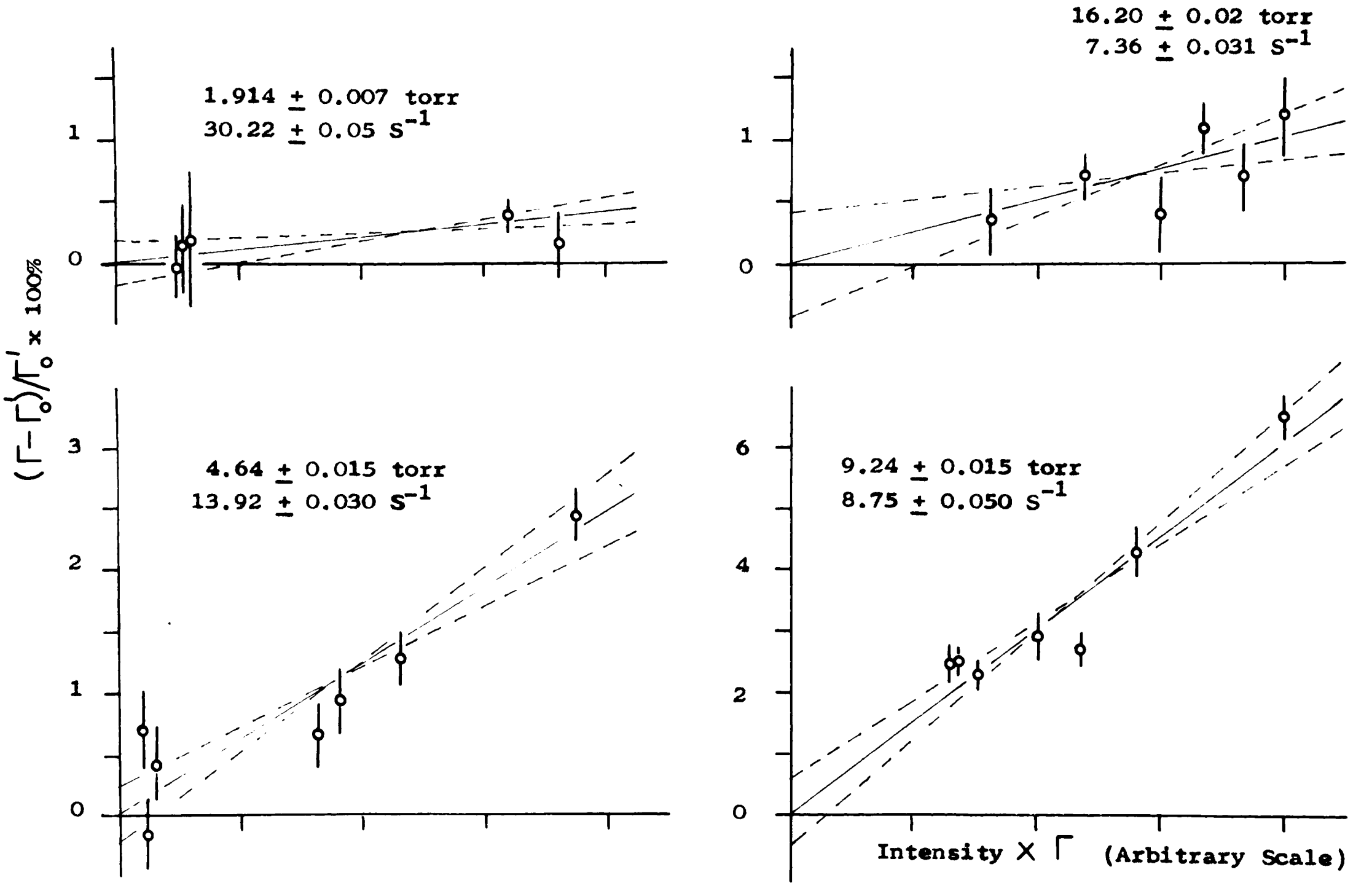
It was established in §3.5 that the effects of collisional deactivation of metastable atoms by ground state oxygen atoms could be evaluated indirectly by correlating the decay constants measured at different signal intensities. In particular, it was found that

the decay constant which would be measured in the absence of atomic oxygen quenching could be determined as the intercept of the linear plot of the measured decay constants Γ against the products $I\Gamma$ of the decay constant and intensity I at the start of the afterglow period. In figure 19 we show several of the intensity correlations obtained at different argon pressures. These results were recorded during the developmental stage of the experiments and in particular, before the full significance of the importance of the intensity correlation was realized. For this reason fewer experimental curves were recorded at each pressure than were recorded during the later studies of oxygen-neon discharges. However, there is sufficient information in the data of figure 19 to reveal that there is no significant deviation from the expected linear behaviour.

The values of the horizontal $I\Gamma$ scale of figure 19 have been determined as Γ times the intensity measured at a time $2/\Gamma$ into the afterglow period. For convenience we have plotted the percentage difference between the measured decay constant values and the computed value of the zero intensity intercept Γ'_0. This has been determined by use of the weighted linear least squares fitting procedure, although in this case there is rather more doubt as to whether there are sufficient data points to justify the use of statistical techniques, particularly for the evaluation of the standard error of the computed value of the intercept Γ'_0. It is clear that insufficient afterglow curves have been recorded for

Figure 19

INTENSITY CORRELATIONS IN ARGON

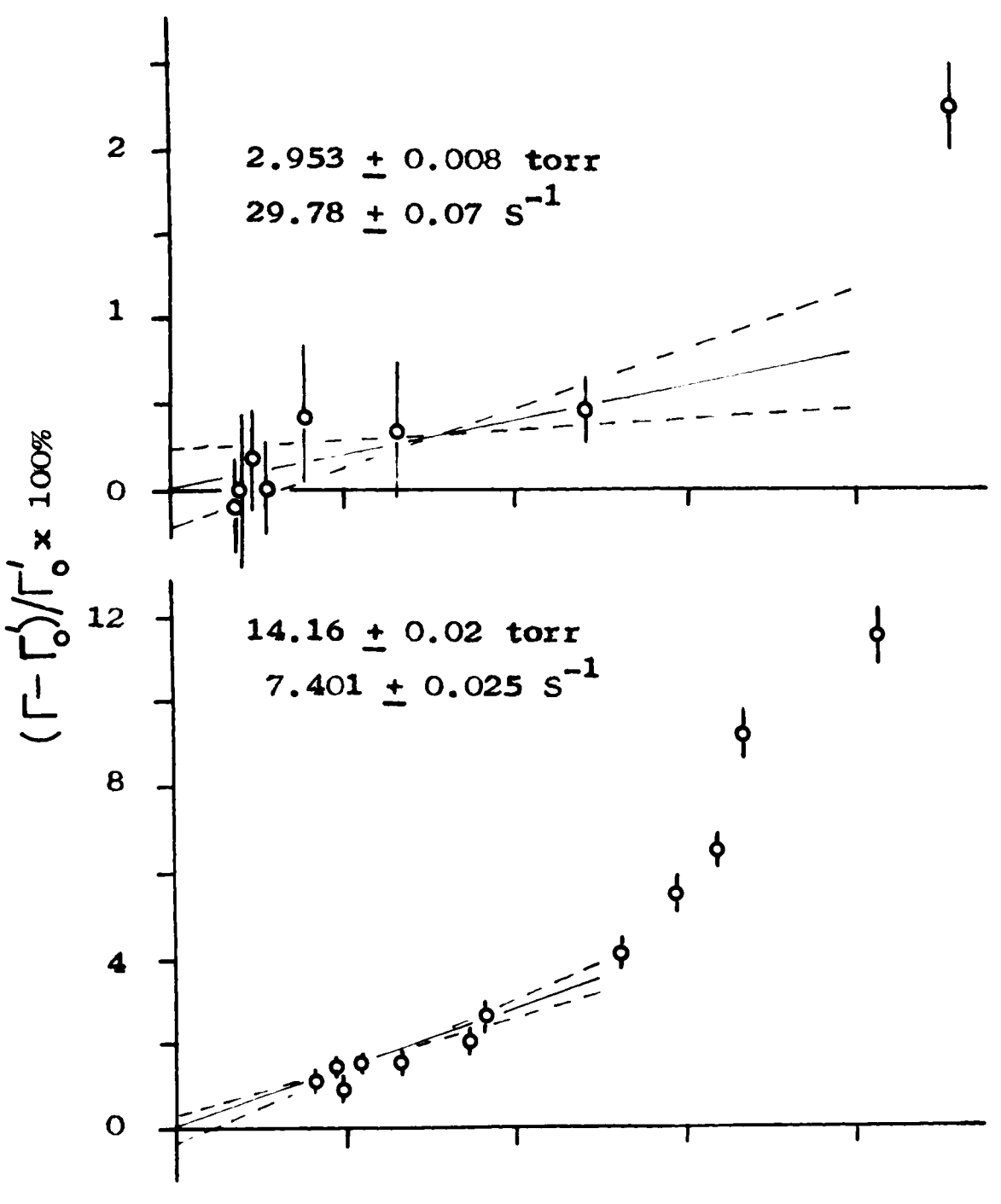


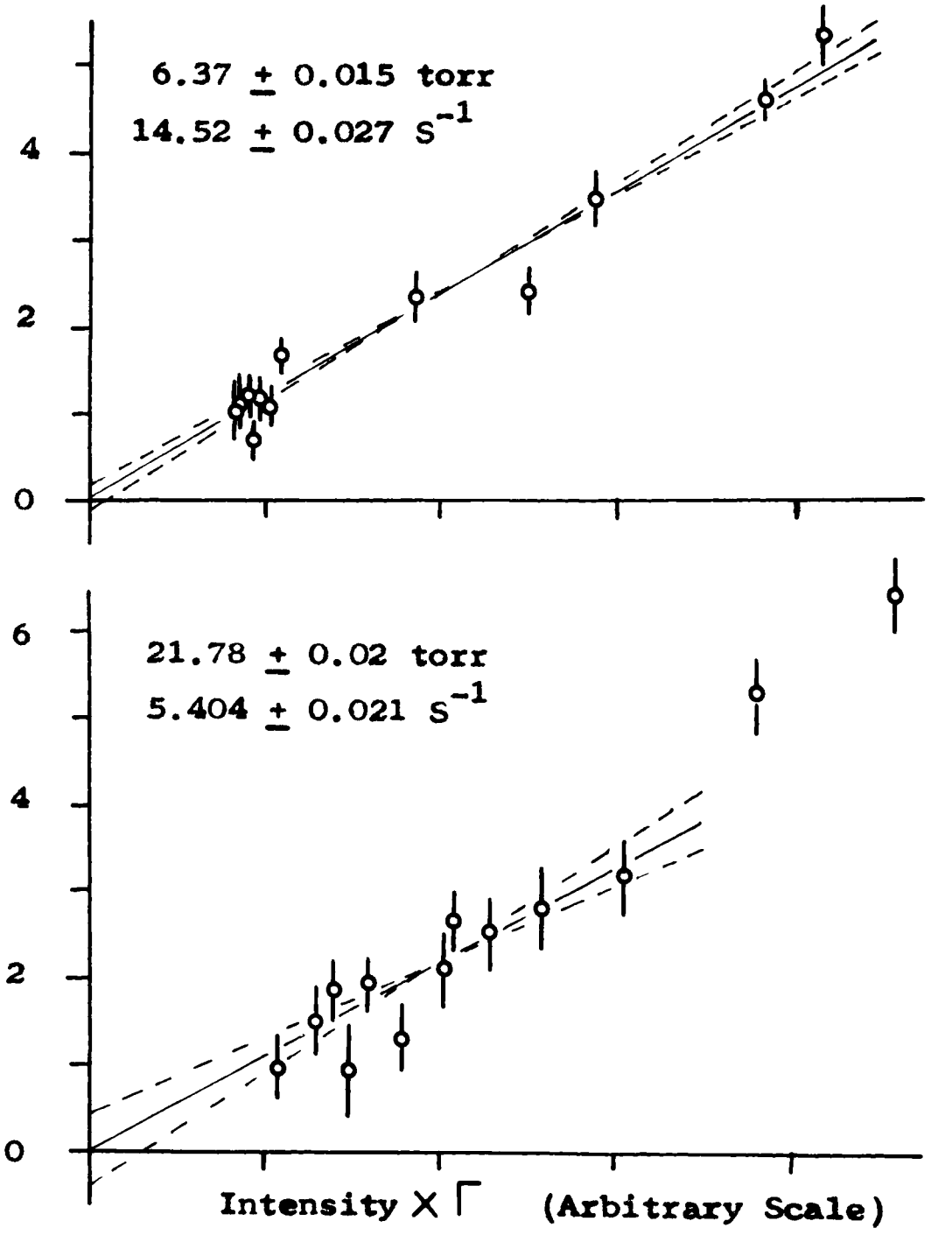
at least two of the intensity correlations shown in figure 19. However, the computed standard errors do give in most cases a reasonable indication of the real uncertainty in the evaluation of Γ'_0. These errors were used to define weights in the final decay constant - inert gas pressure correlation described below in §5.9. Only relative error estimates are required and the procedure is not critically dependent on the particular values used for the weights. The dotted straight lines of each intensity correlation shown in figure 19 are defined by the values of intercept and slope at a single standard deviation from the best fit values. These lines merely serve as an indication of the accuracy of the linear fit.

Several of the intensity correlations obtained at different neon pressures are shown in figure 20. More afterglow curves have been recorded at each pressure than for the argon correlations so that the use of a statistical analysis is more obviously valid. It is interesting to note that the correlations deviate from linear behaviour at the higher signal intensities, a feature which was not apparent from the measurements in argon. Evidently there is a breakdown in the assumptions of the correlation procedure, probably due to the presence of undissociated oxygen molecules within the discharge volume. Their presence would cause additional collisional deactivation of the metastable atoms and a consequent increase in the decay constant measured at a particular signal

Figure 20

INTENSITY CORRELATIONS IN NEON





intensity. As the intensity decreases because of wall adsorption of oxygen atoms the expected linear correlation is approached. At this time there are sufficient neon metastable atoms present during the discharge pulse to ensure that the lifetime of an oxygen molecule against dissociation is always short compared to the recombination lifetime of an oxygen atom.

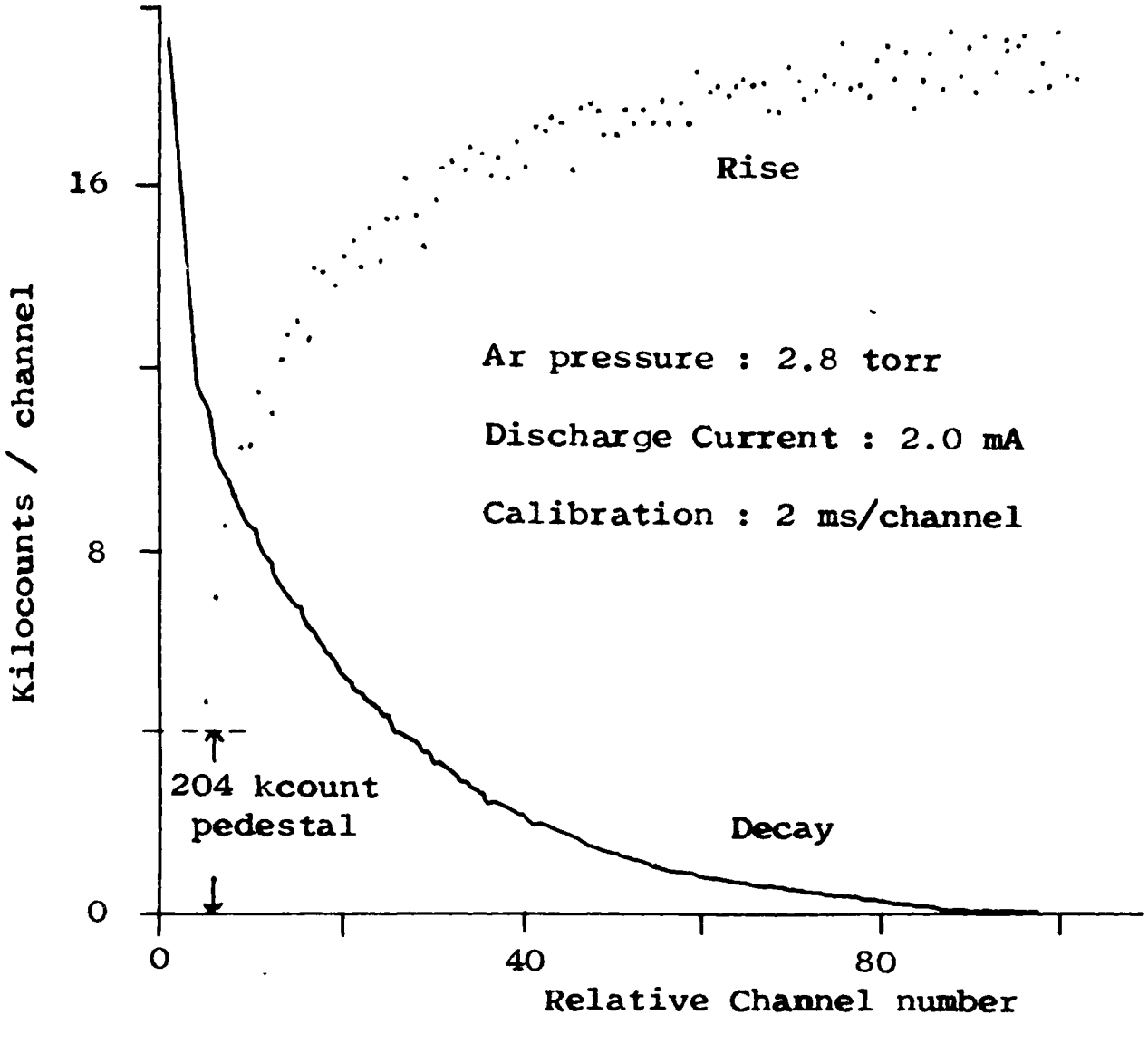
The values of the intercepts Γ'_0 were determined to an accuracy of typically between 0.2% and 0.5%, the uncertainty being governed principally by the extent of the linear region. Normally, oxygen at a pressure of a few tenths of a mtorr was added initially to the discharge volume. If there was insufficient change in the signal intensity to define the value of the intercept Γ'_0, further oxygen was added from the neighbouring calibration volume. The pressures were then corrected from the known ratio of volumes. On the other hand, if excess oxygen was initially added to the vessel, the decay constant reached a saturation value at an intensity higher than was desirable. The effects of saturation are particularly noticeable on the 0.37 torr plot shown in figure 20. Unfortunately, no remedy was found to enable lower intensities to be reached.

5.8. Deactivation by Electron Collisions

One of the assumptions upon which the theory of the intensity correlation is based is that the deactivation of metastable atoms by collisions with electrons is small compared to the other forms

of deactivation. The validity of this assumption for the experiments described here was established in §3.5 where it was shown that the observed forbidden line intensity increased linearly with discharge current. Further evidence of the validity of the assumption may be obtained from time-resolved intensity measurements at the start of the discharge pulse.

After the discharge is struck, the metastable oxygen atom population increases at a rate determined solely by the deactivation processes. If electron quenching is of importance, this rate is expected to be greater than the decay rate observed during the late afterglow when the electron density is significantly smaller. However, a detailed study of the rate of increase of the forbidden line intensity at different pressures of neon and of argon and at currents of up to 15 mA revealed no significant electron quenching. Furthermore, the decay constants measured from the afterglow data were found to be independent of discharge current up to 15 mA. A comparison between the rates of rise and decay of the metastable population is shown in figure 21. The large background signal increases the statistical scatter of the rising signal during the discharge pulse. The analysis of the curves reveals no significant difference between the two rates. It would be particularly interesting to repeat these experiments at discharge currents of the order of 100 mA at which significant electron quenching may occur. The combination of these observations with



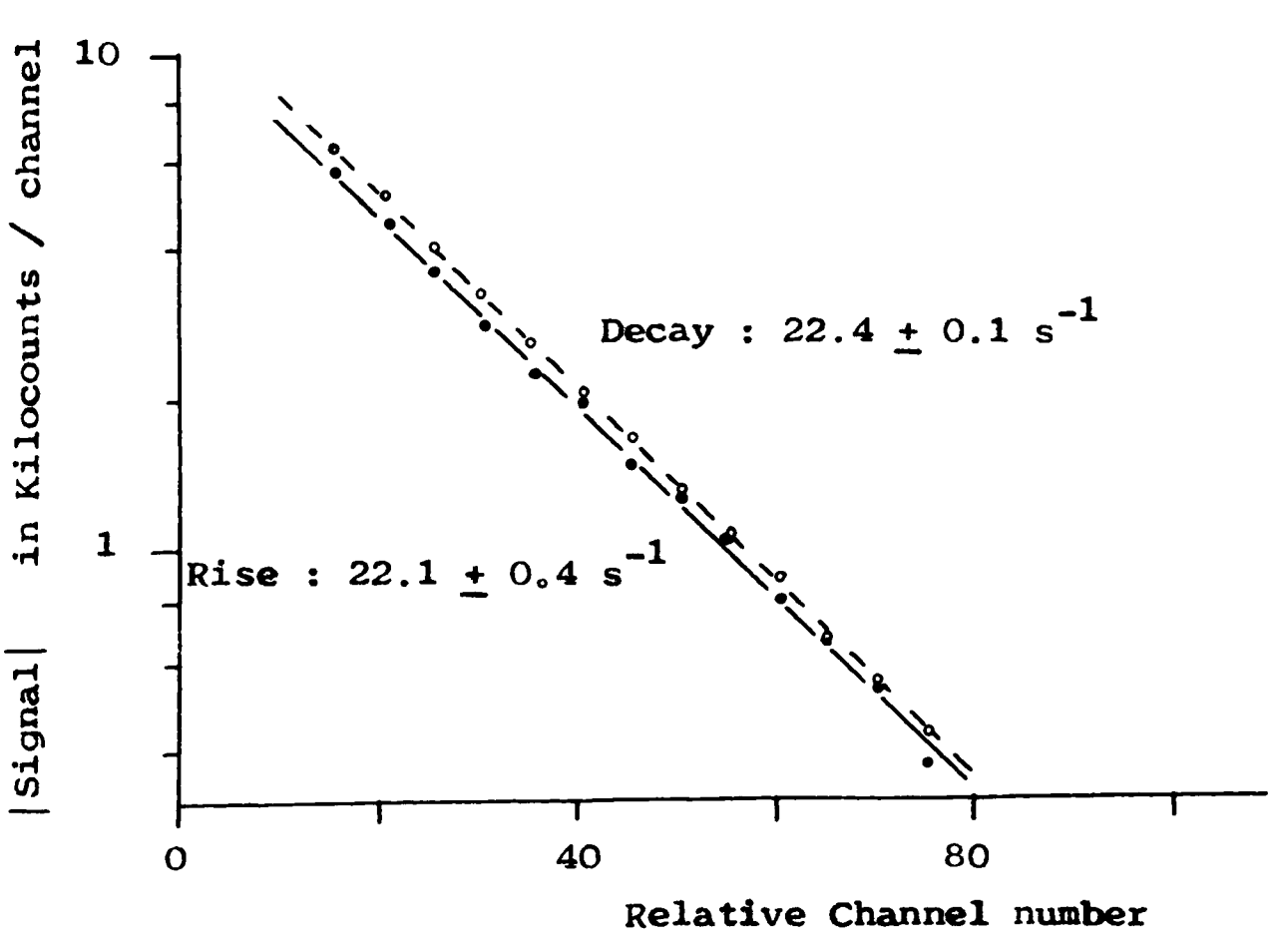


Figure 21 ELECTRON QUENCHING OF O(^{1}S) ATOMS IN AN ARGON-OXYGEN DISCHARGE

measurements of the electron density and electron temperature would then enable comparisons to be made with Seaton's theoretical rate constants[44] for electron deactivation of $O(^1S_0)$ metastable atoms. These rate constants determine directly the importance of the electron exchange collision process as a mechanism for producing $O(^1S_0)$ atoms in the aurorae.

5.9. The Decay Constant-Pressure Correlation

We have shown earlier in §5.3 that the reduced decay constants Γ_0' are expected to have a pressure dependence given by

$$\Gamma_0' = \frac{A'}{p} + \Gamma_0 + \alpha' p + \beta' p^2 \qquad (5.8)$$

so that the plot of the product $p\,\Gamma_0'$ against p is expected to be a cubic polynomial. The parameters of equation (5.8) are as defined in §5.3. Preliminary analyses of the data according to the cubic form by use of a standard computer program revealed that the contribution of three body deactivation to the values of the decay constants Γ_0' was small compared to the other contributions. Unfortunately, the standard fitting procedure was not weighted and the errors of the cubic coefficients were not computed. It was decided initially to neglect the cubic component and fit the plot of $p\,\Gamma_0'$ against p to a quadratic polynomial by a weighted least squares fitting procedure. It is shown later in §6.3 that the three body deactivation loss of metastablesis insignificant compared to the other forms of deactivation.

A simple computer program was written according to the weighted quadratic least squares fitting procedure of Topping[54]. In such a fit it is assumed that all the uncertainty occurs in only one of the measurable quantities. In order to use the statistical methods, it is necessary initially to compute the total uncertainty in Γ'_0 produced by the two contributions; namely, the direct uncertainty as determined from the intensity correlation, and the error in the value of Γ'_0 caused by the uncertainty of the pressure measurement. The latter contribution may be determined from the differential form of equation (5.8) as

$$(\Delta\Gamma'_0)_p = [-A'/p^2 + \alpha']\Delta p \ . \qquad (5.9)$$

At a pressure equal to $(A'/\alpha')^{\frac{1}{2}}$ there will be no increased uncertainty in the value of Γ'_0 due to uncertainty in the pressure measurement. At pressures other than $(A'/\alpha')^{\frac{1}{2}}$ the pressure contribution is nonzero and may be evaluated from equation (5.9) by use of approximate values for the unknown constants A' and α'. The total uncertainty in Γ'_0 is then determined from the standard error relationship

$$\Delta\Gamma'^{\,2}_0 = (\Delta\Gamma'_0)^2_{direct} + (\Delta\Gamma'_0)^2_p \ . \qquad (5.10)$$

The standard errors Γ'_0 are employed in the usual manner (Topping[54], p.86) to define the weights of the experimental data points $(p, p\,\Gamma'_0)$ used in the quadratic least squares fit.

CHAPTER 6

RESULTS AND DISCUSSION

6.1. The Pressure Correlation in Argon

The values of the reduced decay constants Γ_0' determined at different pressures of argon and neon are tabulated in appendix 1. In figure 22 the values of $p\,\Gamma_0'$ evaluated from the measurements in argon have been plotted against the argon pressure p. The full curve represents the computed best quadratic fit to the experimental data points and is defined by the coefficients

$$A' = 54.7 \pm 0.3 \text{ torr } s^{-1} \text{ at } 23^{\circ}C,$$

$$\Gamma_0 = 1.31 \pm 0.10 \; s^{-1}$$

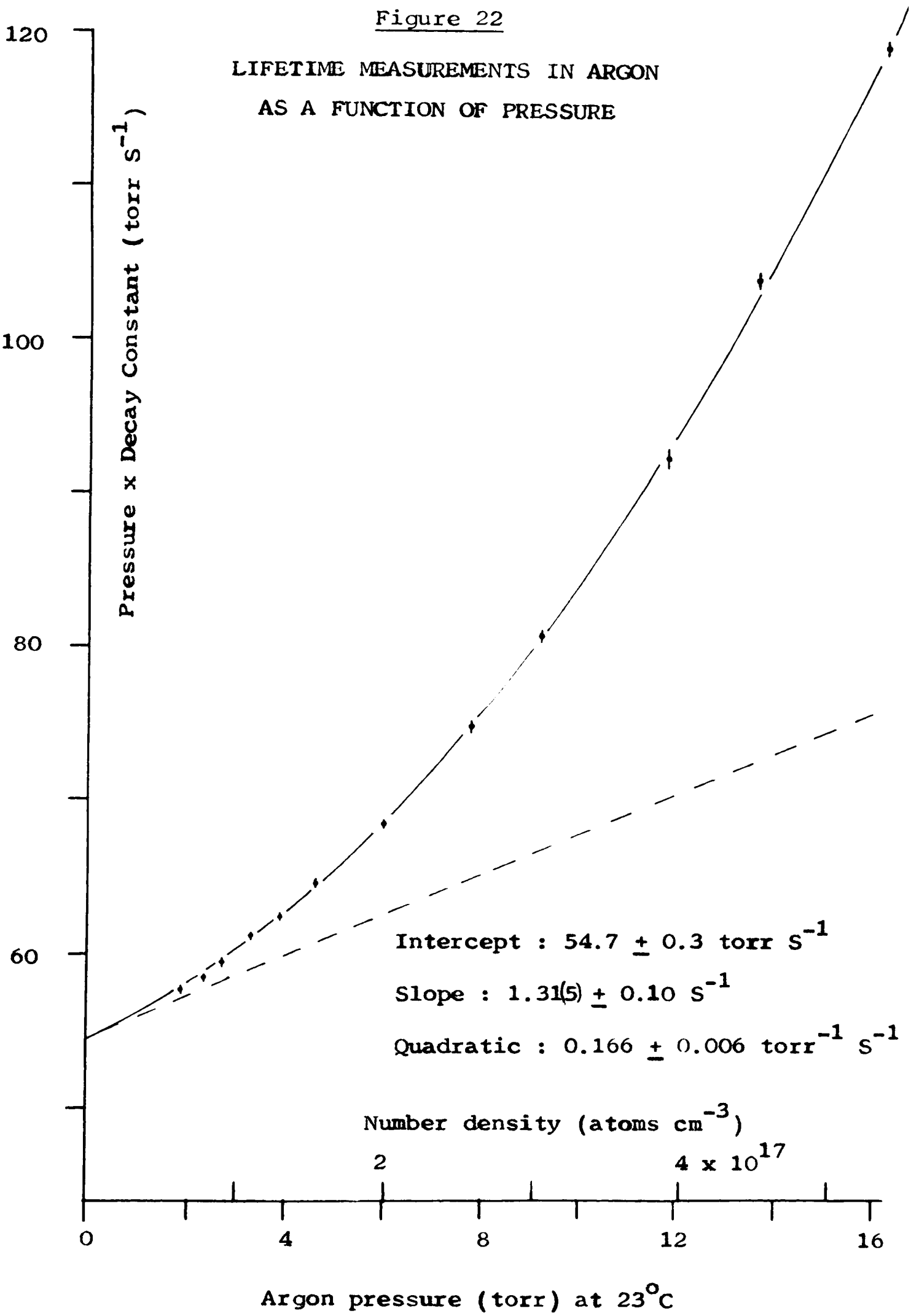
and $$\alpha' = 0.106 \pm 0.006 \text{ torr}^{-1}\; s^{-1} \text{ at } 23^{\circ}C .$$

Each uncertainty corresponds to a single standard deviation from the best fit value and has been calculated under the tacit assumption that there are sufficient experimental points to justify the use of statistical techniques. Twelve data points define the quadratic form of figure 22 and it is considered that the computed standard errors give a good indication of the real uncertainties in the calculated values of the coefficients. There is insufficient data, however, to statistically test the significance of the computed errors.

It is clear that the form of the quadratic fit is relatively insensitive to the value of the radiative decay constant Γ_0. At

Figure 22

LIFETIME MEASUREMENTS IN ARGON
AS A FUNCTION OF PRESSURE



low pressures, the main loss of the metastable oxygen atom population is by diffusion and at higher pressures, above 10 torr, the form of the quadratic fit is dominated by the value of the deactivation rate constant α'. There is no pressure region in which the form of the curve is dominated by the value of Γ_0.

The uncertainties of the computed values of the coefficients could be reduced if the pressure range were extended to both lower and higher pressures. However, non-exponential decay curves were observed at pressures below 1.5 torr. These were possibly due to the emission of allowed spectral lines during the afterglow since the significance of the dissociative recombination problem was realized only after the study of the oxygen-argon afterglow had been completed. (See the discussion of §5.2.) No deviation from the expected pure exponential behaviour was observed for argon pressures higher than 1.5 torr. The difficulties of low pressure measurements are discussed at greater length in appendix 2. The measurements were not extended to higher pressures since the only significant improvement to be expected would be a more accurate determination of the less interesting quadratic coefficient α'.

6.2. The Pressure Correlation in Neon

The pressure correlation of the decay constants determined from the oxygen-neon afterglow measurements is shown in figure 23. The four low pressure data points which clearly deviate from the

expected quadratic form were not used in the least squares fit to the experimental data. A detailed discussion of the possible causes of this deviation is given in appendix 2. Fortunately, the onset of the departure is very rapid so that the experimental data at the higher pressures is not greatly affected. A departure function was evaluated as the difference between the observed curve and the expected quadratic form and showed that only the lowest pressure experimental point used in the least squares fit was significantly affected by the deviation. The $p\,\Gamma_0'$ value there was corrected by 0.2 percent.

The quadratic least squares fit to the experimental data shown in figure 22 is defined by the coefficients

$$A' = 83.8 \pm 0.3 \text{ torr } s^{-1} \text{ at } 21^{\circ}C,$$

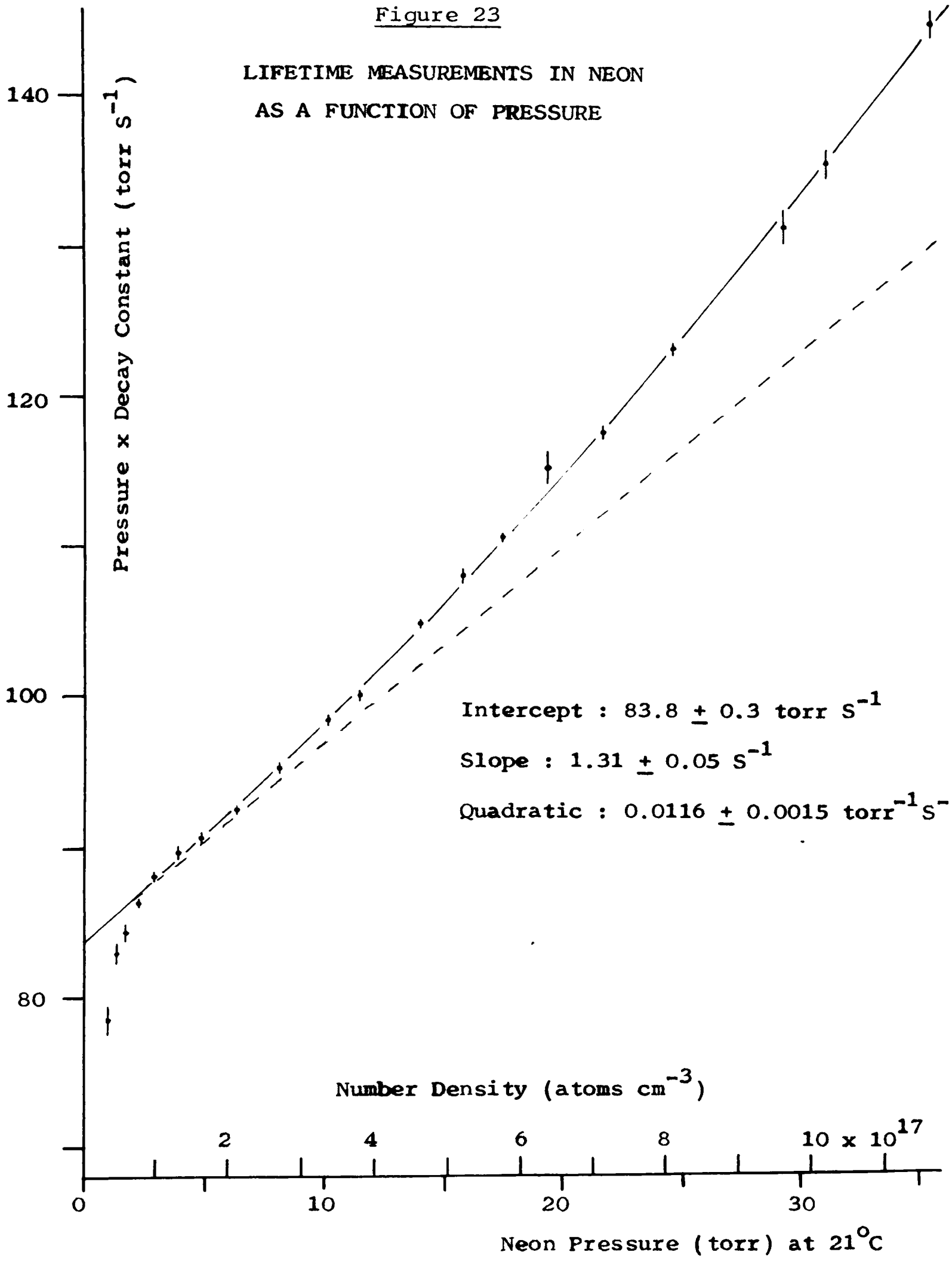
$$\Gamma_0 = 1.31 \pm 0.05 \; s^{-1}$$

and $$\alpha' = 0.0116 \pm 0.0015 \text{ torr}^{-1} \; s^{-1} \text{ at } 21^{\circ}C.$$

The exact agreement between the values of the radiative decay constant evaluated from the oxygen-argon and oxygen-neon afterglow studies is clearly fortuitous. As expected, neon is less effective than argon in preventing the diffusion of oxygen metastable atoms to the walls of the vessel. On the other hand, because of collision stimulated emission, argon atoms are more effective than neon atoms in deactivating oxygen metastable atoms. The values of the intercepts of figures 22 and 23 are used in §5.6 to evaluate the diffusion coefficients, and the rate constant measurements are discussed in

Figure 23

LIFETIME MEASUREMENTS IN NEON
AS A FUNCTION OF PRESSURE



detail in §6.7. The radiative decay constant measurement is discussed in §6.5.

The extent of the pressure range investigated in the oxygen-neon afterglow studies was determined by the decreasing accuracy of the decay constant measurements with increasing neon pressure. As the pressure is increased, the importance of the molecular ion and excited state molecule populations increases at the expense of the atomic ion and excited state populations. Fewer metastable neon atoms are produced so that the dissociation of oxygen molecules during the discharge pulse proceeds at a slower rate. At the same time, the importance of oxygen atom recombination is increased. As a result of these effects, the linear region of the intensity correlation extended over a much smaller range of intensities than that obtained at the lower pressures and the accuracy of the extrapolated decay constant Γ_0' was thereby reduced.

6.3. Three Body Collisional Deactivation

In §5.9 we assumed that three body collisional deactivation of $O(^1S_0)$ atoms was negligible. In order to justify this assumption, it is necessary to prove that the value of the rate constant for three body deactivation is not statistically significant. The most obvious way of evaluating this constant would be to least squares fit the experimental data to the cubic form

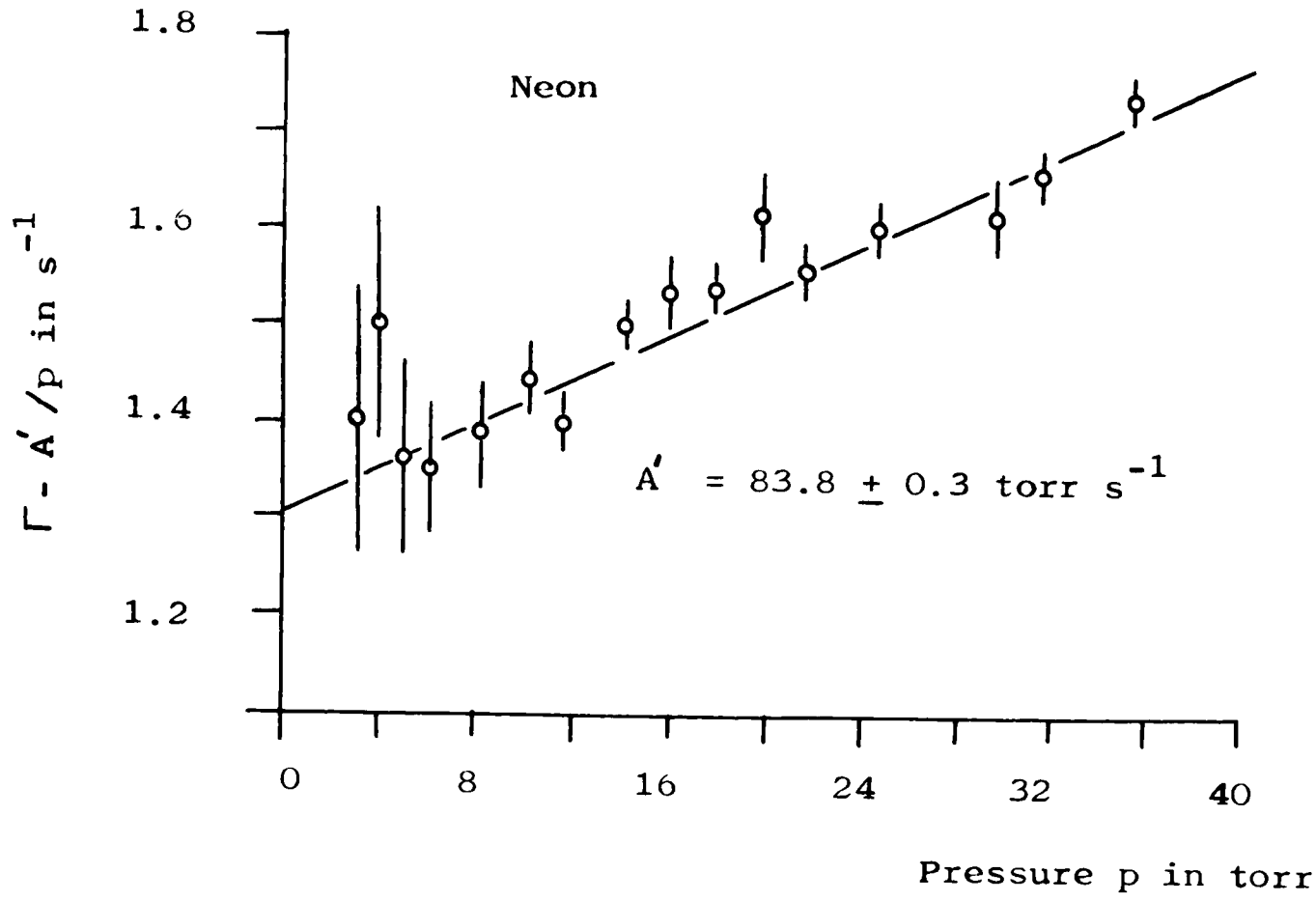
$$\Gamma_0' p = A' + \Gamma_0 p + \alpha' p^2 + \beta' p^3 . \qquad (6.1)$$

However, the algebra involved in a weighted cubic fit which includes the required evaluation of the standard errors of the coefficients is rather unwieldy. It is considerably easier to test the significance of the cubic coefficient if the value of the coefficient A' is known to reasonable accuracy. It is then possible to evaluate the coefficients of the quadratic form

$$\Gamma_0' - \frac{A'}{p} = \Gamma_0 + \alpha' p + \beta' p^2 \qquad (6.2)$$

by use of the weighted quadratic least squares procedure.

The value of A' may be determined by the quadratic method described in §5.9, or alternatively as the zero order coefficient evaluated from an unweighted least squares fit to the cubic form of equation (6.1). Values of 83.8 $\pm$ 0.3 torr s^{-1} and 83.5 torr s^{-1} were obtained for neon by these methods respectively, and values of 54.7 $\pm$ 0.3 torr s^{-1} and 54.5 torr s^{-1} respectively for argon. The other coefficients have been determined from the weighted quadratic fit to equation (6.2) for several chosen values of A'(table 4). The experimental data has been plotted in figure 24 according to the form of equation (6.2). It is quite evident from both the tabulated values of β' and the form of the curves of figure 24 that within the statistical scatter of the experimental data, three-body deactivation is not significant. Without introducing significant error, we may then set β' equal to zero and fit the experimental data to the quadratic form described in §5.9. We



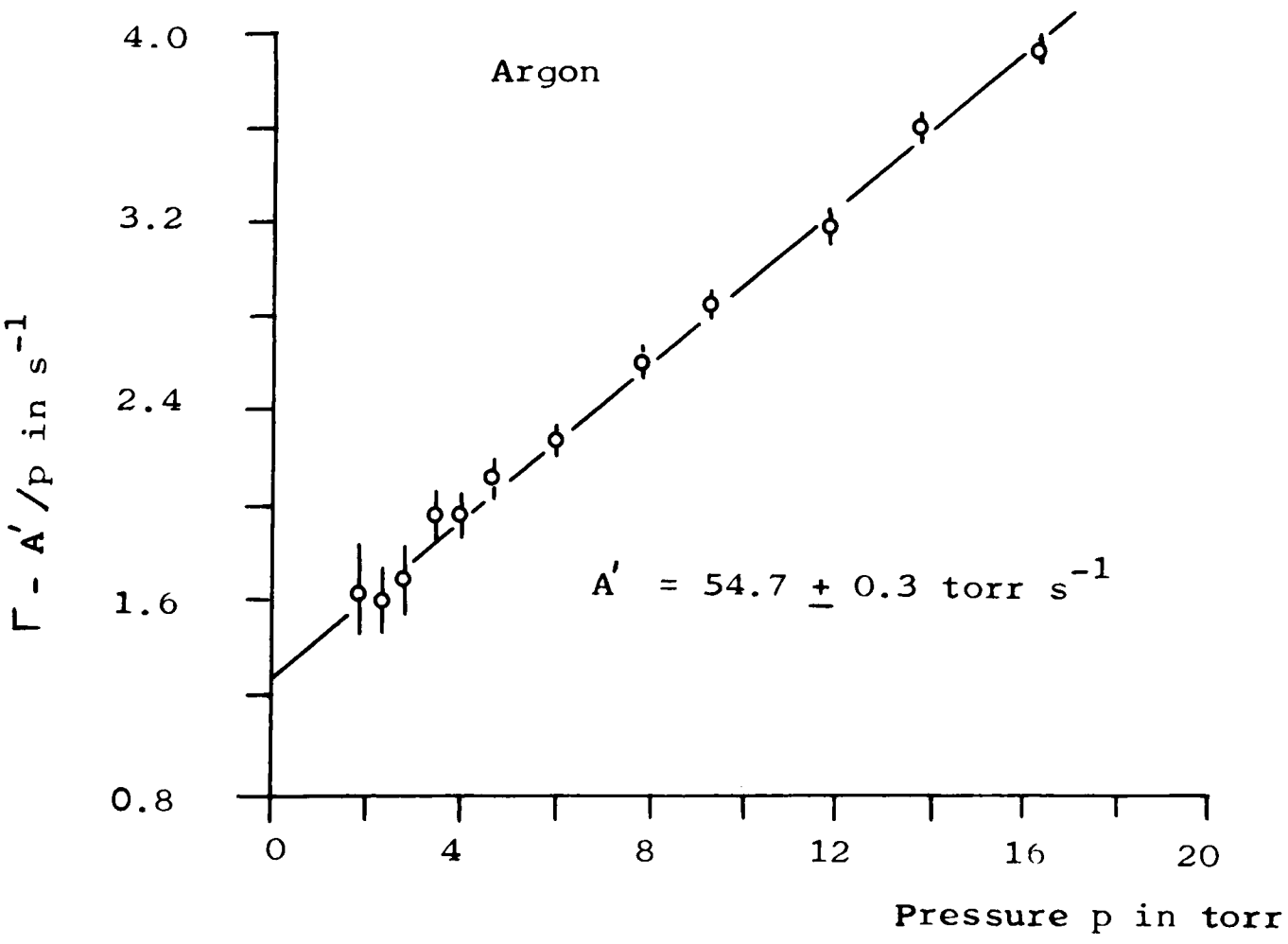


Figure 24 SIGNIFICANCE TESTS FOR THREE BODY DEACTIVATION

have used the data of table 4 to evaluate upper limits of the three-body deactivation rates as 2×10^{-38} cm^6 s^{-1} for neon and 2×10^{-37} cm^6 s^{-1} for argon.

	A' (chosen) torr s^{-1}	Γ_0 s^{-1}	$\beta' \times 10^5$ $torr^{-2}$ s^{-1}
Neon	83.5 ± 0.3	1.38 ± 0.05	5 ± 11
	83.8 ± 0.3	1.31 ± 0.05	-3 ± 11
	84.1 ± 0.3	1.24 ± 0.05	-10 ± 10
Argon	54.5 ± 0.3	1.41 ± 0.07	60 ± 80
	54.7 ± 0.3	1.30 ± 0.07	-10 ± 80
	54.9 ± 0.3	1.21 ± 0.07	-50 ± 80

TABLE 4 Coefficients Evaluated by the Cubic fitting procedure.

The fact that two-body deactivation of oxygen metastable atoms in neon dominates over three-body deactivation is possibly caused by the presence of residual impurity atoms in the gas. There is no a priori reason to believe that two body deactivation collisions involving a neon atom and a metastable oxygen atom should be more effective than three body collisions, although the latter type of impact occurs rather less frequently. For argon, however, the relatively large two-body deactivation coefficient is

certainly caused by collision stimulated emission of radiation. The two body rate constant values are discussed in detail in §6.7.

6.4. The Low Pressure Anomalies

The existence of deviations from quadratic behaviour in the low pressure region of the pressure correlation in neon unfortunately increases the uncertainty in the determination of the value of the intercept A'. A more accurate determination of this constant would place more severe constraints on the ranges of variation of the other coefficients and these would also be determined to a greater accuracy.

The cause of the longer decay lifetimes observed at lower pressures cannot at present be fully explained. A number of explanations have been proposed and are discussed in detail in appendix 2.

6.5. The $O(^1S_0)$ Radiative Decay Constant

We have listed in table 5 the theoretical transition probability estimates for the emissions from the $^1S_0$ state of atomic oxygen, and the experimental determinations of transition probability and of the $O(^1S_0)$ radiative decay constant. It is immediately clear that the experimental decay constant value presented here is much more accurate than either of the previous determinations. Each of the previous measurements represents the mean of a large number of separate determinations distributed over a wide range of values.

McConkey and Kernahan[22] regard their result as accurate to within only a factor of two and there is some doubt as to whether Omholt's measurements are completely free from the effects of collisional deactivation.

	Ref.	Year		$A(^1S_0-^1D_2)$	$A(^1S_0-^3P_1)$	Γ_0
Pasternack	55	1940	theory	1.92		
Garstang	56	1951	theory	1.25		0.078
Yamanouchi and Horie	18	1952	theory	2.04		0.067
Sinanoğlu	17	1970	theory	1.18		
McConkey and Kernahan	22	1970	expt.	$1.0^{+1.0}_{-0.5}$		
Omholt	24	1959	expt.			1.4 ± 0.2
Present work		1971	expt.			1.31 ± 0.05

TABLE 5 The $O(^1S_0)$ metastable state : theoretical estimates and experimental determinations of the transition probabilities and radiative decay constant in s^{-1}.

Great importance has been attached to the available theoretical estimates of forbidden transition probabilities because of the lack of reliable experimental measurements of the radiative lifetimes of metastable states. The relevant starting formulae for the calculations, given by Condon and Shortley[2] for the case of LS-coupling, are presented in §1.2. The oxygen atom is, however, more accurately

represented by the intermediate coupling scheme. The calculations are thereby more detailed than for the simple LS-coupling case, but are usually simplified by expressing the actual wavefunctions as linear combinations of the LS-coupling wavefunctions.

The value of the magnetic dipole $^1S_0$ - $^3P_1$ transition probability has been calculated independently by Garstang[56] and by Yamanouchi and Horie[18]. The calculations are independent of the radial overlap integral (see §1.2) and the principal uncertainty occurs in the evaluation of the transformation coefficients between the intermediate coupling and LS-coupling schemes. Garstang neglected the effects of spin-spin and spin-other-orbit interactions which were included in the Yamanouchi and Horie calculation. This latter calculation is generally considered to be the more reliable and is probably accurate to within 10 percent.

The calculations of electric quadrupole transition probabilities are not generally as accurate as the magnetic dipole calculations since they involve the evaluation of the square of the overlap integral

$$s_q(n1,n'1') = e\int_0^\infty r^2 R(n1)\, R(n'1')\, dr \qquad (6.3)$$

which is a very sensitive function of the form of the wavefunctions R(n1) of the individual electrons. Since the integral is essentially an average of r^2 over the extent of the atom, it is important that the charge density in the outermost parts of the atom is determined

accurately. Until recently, the most accurate estimates of s_q were evaluated by use of Hartree-Fock wavefunctions based on the self-consistent field with account taken of electron exchange. Neither Pasternack[55] nor Yamanouchi and Horie[18] included the effects of electron exchange in their calculations of the OI ($^1S_0$ - $^1D_2$) transition probability and their results are considered to be less reliable than those of Garstang[56] and of Sinanoglu[17].

Garstang used the wavefunctions of Hartree, Hartree and Swirles[57] which are based on the self consistent field with electron exchange. Deviation from a spherically symmetric charge distribution caused by the effects of correlation between the electrons was included in Garstang's calculation by an evaluation of the effect of configuration interaction. Unfortunately, there may be many interacting configurations and it is not always easy to identify the more important perturbers, let alone make an accurate estimate of their effects. Garstang[58] has discussed the problem with particular reference to the relative merits of using empirical parameters evaluated from experimental energy level data in the intermediate coupling part of the calculation, or of using purely theoretical parameters which do not give exact agreement with the experimental values of the energy levels. He has shown for the $1s^2\ 2s^2\ 2p^4$ configuration of interest here, that the major part of the effect of configuration interaction is included

indirectly if the empirical parameters are used. Garstang considers that the uncertainty caused by configuration interaction is then likely to be less than 5 percent. The major uncertainty in the transition probability calculation is, however, caused by inaccuracies in the wavefunctions used in the calculation of the overlap integral. Garstang[58] considers the uncertainty in his result to be at least 20 percent.

Recent advances[59] in the theories used to calculate more accurate wavefunctions for the complex atoms have enabled more precise estimates of transition probability to be made. Sinanoğlu has used an N-electron theory in which the wavefunction is expressed as the sum of a spherically symmetric Roothaan type[60] Hartree-Fock part and a perturbation wavefunction which includes the effects of electron correlations which result from short range "fluctuation potentials". He has shown that the dominant correlations are between pairs of electrons and has resolved the complicated N-electron correlation into $\frac{1}{2}N(N-1)$ separate 2-electron problems. The Roothaan type Hartree-Fock wavefunctions[60] are considerably more sophisticated than those used by Garstang and the results of the transition probability calculations are expected to be accurate to within about 5 percent. The effects of configuration interaction are included automatically in the calculations.

The best theoretical estimate of the radiative decay constant

of the $O(^1S_0)$ state is evaluated as 1.25 s^{-1} by addition of Yamanouchi and Horie's OI ($^1S_0$ - $^3P_1$) transition probability estimate to that of Sinanoğlu for the OI ($^1S_0$ - $^1D_2$) transition. This result compares well with the experimental determination of 1.31 $\pm$ 0.05 s^{-1} presented in this thesis. If Garstang's estimate for the OI ($^1S_0$ - $^1D_2$) transition probability were chosen, a theoretical decay constant estimate of 1.32 s^{-1} would be obtained. Although this result is closer to the experimental value, Sinanoğlu has indicated that Garstang would have obtained a value higher by some 20 percent had the Roothaan type Hartree-Fock wavefunctions been available at the time of calculation. The agreement between experiment and theory is sufficiently good to enable further calculations by the methods of Sinanoğlu to be regarded with increased confidence. This result is particularly important with regard to atomic metastable states which cannot be as readily investigated by experiment as the $O(^1S_0)$ state.

6.6. The Diffusion Coefficients

The coefficients for diffusion of $O(^1S_0)$ metastable atoms through neon and argon may be evaluated from the coefficient A' of the quadratic pressure correlations of §6.1 and §6.2 if the characteristic first order mode diffusion length of the vessel is known. This may be evaluated from equation (3.10). For the vessel used in the experiments described here (see figure 8), the value of the diffusion length is more critically dependent on the radius

than on the length so that little uncertainty is introduced in the calculation if a perfect cylinder of 5.50 ± 0.05 cm radius and 27 ± 2 cm length is assumed. The diffusion length is then determined from equation (3.10) as 2.21 ± 0.03 cm.

Source	$D_{12}p$ (Ne) torr cm^2 s^{-1}	$D_{12}p$ (Ar) torr cm^2 s^{-1}	$\frac{D_{12}p\ (Ne)}{D_{12}p\ (Ar)}$
Zipf[37]	405 ± 10	256 ± 5	1.57
Present Work	416 ± 12	268 ± 8	1.55 ± 0.01

TABLE 6 The measured diffusion coefficients for the flow of $O(^1S_0)$ atoms through neon and argon at 298°K.

Zipf[37] has previously made the same measurements in a similar pulsed afterglow experiment and it is of interest to compare his values of diffusion coefficient with the values obtained here. It is seen in table 6 that there is good agreement between the two sets of results. The diffusion coefficients measured here are slightly higher than the values measured by Zipf, a result which may be caused by the deactivation of oxygen metastable atoms on the surfaces of the internal electrodes. No account of this loss has been taken, other than to increase the value of the standard error of the diffusion length calculation. The ratio of the two diffusion coefficients is independent of the diffusion length and is thereby considerably more accurate than the absolute values of

the coefficients. Zipf does not quote the accuracy of his ratio but it is probably also in the region of one percent.

The classical collision diameters may be evaluated from the values of the diffusion coefficients by use of the Chapman-Enskog diffusion coefficient equation (3.12). These have been determined as 2.42 $\pm$ 0.04 Å and 2.84 $\pm$ 0.04 Å respectively for elastic sphere collisions between $O(^1S_0)$ metastable atoms and neon or argon ground state atoms. As expected, the collision diameter for oxygen-neon collisions is smaller than that corresponding to oxygen-argon collisions. It is of greater interest, however, to use the measured values of diffusion coefficient to evaluate the force constants for the more realistic Lennard-Jones interaction. The Lennard-Jones potential function for collisions between unlike atoms takes the form

$$V_{ij}(r) = 4\epsilon_{ij}\left[\left(\frac{\sigma_{ij}}{r}\right)^{12} - \left(\frac{\sigma_{ij}}{r}\right)^{6}\right] \qquad (6.4)$$

where ϵ_{ij} and σ_{ij} represent the well depth and Lennard-Jones collision diameter respectively. These constants are related empirically as

$$\epsilon_{ij} = [\epsilon_{ii}\,\epsilon_{jj}]^{\frac{1}{2}} \qquad (6.5)$$

and

$$\sigma_{ij} = \tfrac{1}{2}(\sigma_{ii} + \sigma_{jj}) \qquad (6.6)$$

to the corresponding force constants for elastic collisions between like atoms. (See, for example, Hirschfelder, Curtiss and Bird[61])

[HCB], §8.4.) The diameter σ_{ij} is related also in the first approximation of the Chapman-Enskog diffusion theory to the elastic sphere collision diameter d_{ij} by

$$d_{ij}^2 = \sigma_{ij}^2 \, \Omega^{*(1,1)}(T_{ij}^*) \tag{6.7}$$

where $$T_{ij}^* = kT/\epsilon_{ij} \tag{6.8}$$

is the reduced temperature. Here $\Omega^{*(1,1)}$ is a collision integral, the values of which depend on the form of the potential function. Such values have been tabulated in HCB for the Lennard-Jones interaction.

The force constants ϵ_{ii} and σ_{ii} have been determined by earlier experimenters for both neon and argon (see HCB[51], table 8.4-1) and may be used in the above relationships along with the measured values of the elastic sphere collision diameters presented here to determine the Lennard-Jones force constants for elastic collisions between two $O(^1S_0)$ atoms. The computed values are compared in table 7 with the corresponding values for neon and argon.

Gas	ϵ_{ii}/k (^oK)	σ_{ii} (Å)
Ne	35.7	2.789
Ar	124	3.418
$O(^1S_0)$	21.7	2.85

TABLE 7 Force Constants for the Lennard-Jones (6-12) Potential.

The well depth for $O(^1S_0)$ is smaller than that for either neon or argon, and consequently the van der Waals attractive forces between $O(^1S_0)$ atoms must be very weak.

The form of the potential function, assumed here to be of the Lennard-Jones type, may be tested experimentally by comparing the measured and predicted temperature dependence of the diffusion coefficients. The potential function governing the diffusion of He $(^3S_1)$ metastable atoms through helium has been tested in this way by Fitzsimmons et al[62] who found that the measured temperature dependence differed from that expected from theory.

6.7. The Rate Constants for Two Body Deactivation

The rate constants for deactivating collisions between $O(^1S_0)$ metastable atoms and argon or neon atoms may be evaluated directly from the coefficients α' of the quadratic pressure correlation of §6.1 and §6.2 as

$(5.2 \pm 0.2) \times 10^{-18}$ cm^3 s^{-1} for argon

and $(3.6 \pm 0.5) \times 10^{-19}$ cm^3 s^{-1} for neon.

The most interesting feature here lies in the fact that these values are respectively two and three orders of magnitude smaller than the rate constants measured by the flowing afterglow technique, as typified by the value of 3.6×10^{-16} cm^3 s^{-1} determined recently by Filseth et al[19] for deactivating collisions between $O(^1S_0)$ atoms and either argon or neon atoms. Evidently, considerably lower impurity levels have been obtained in the pulsed afterglow gas system

than in that of the flowing afterglow, so that the former experimental method is the more suitable for a determination of the $O(^1S_0)$ radiative lifetime.

Although the rate constant for deactivating collisions between $O(^1S_0)$ atoms and neon atoms corresponds to the extremely small velocity averaged cross-section of 5×10^{-24} cm^2, it is still sufficiently large to play an important role in determining the ultimate accuracy of the measured $O(^1S_0)$ radiative lifetime. It is not known whether the deactivation process is caused by neon atoms or by impurity atoms present in the neon.

The main part of the deactivation rate constant for collisions with argon atoms is expected to be caused by the collision stimulated emission process. The contribution caused by deactivation due to impurity atoms is not expected to be much greater than the deactivation rate constant for neon collisions. The spectra of figure 4, §3.4c, showed that the intensity of the diffuse structure which always accompanies the 5577Å line in the oxygen-argon discharges increases linearly with pressure relative to the line intensity. Furthermore, we have shown in §6.3 that the deactivating collisions are of a binary nature. It appears then that the diffuse radiation is emitted during a collision between an $O(^1S_0)$ atom and an argon ground state atom when there are weak van der Waals binding forces between the atoms. The binding forces between an argon atom and an $O(^1D_2)$ metastable atom are expected, however, to be stronger

than the forces between an argon atom and the spherically symmetric $O(^1S_0)$ atom. For this reason, the diffuse structure is expected to lie on the short wavelength side of the forbidden line.

6.8. Collisional Deactivation by Added Species

At the outset of the experimental work it was hoped that the pulsed afterglow technique would prove to be a useful method for determination of the rate constants for collisional deactivation of metastable oxygen atoms. Unfortunately, the ionization potentials of most of the atoms of atmospheric interest are considerably lower than the inert gas ionization potentials. When added to the discharge volume, these atoms not only seriously affect the decay rate of the metastable atom population, but tend also to supply the discharge positive ion current. The inert gas metastable atom population and hence the rate of dissociation of oxygen molecules are therefore considerably reduced.

Absolute measurements of the rate constants for deactivation by oxygen ground state atoms and molecules were attempted during the experimental work. Measured partial pressures of oxygen were added to the discharge volume but the observed signal intensities were too low to enable quantitative measurements to be made. This difficulty is not encountered in the flowing afterglow technique where the reactant gases are added downstream from the discharge region. We conclude that this is the more suitable technique for

the determination of deactivation coefficients.

6.9. The Red Forbidden Lines of Oxygen

Because of the close proximity of the allowed NeI 6304Å line to the 6300Å red forbidden line of OI, no serious attempt was made to detect the red oxygen lines during the discharge period. Both the 6300Å and the 6364Å lines were, however, easily detected during the afterglow period. The lines were respectively of the order of 30 and 100 times less intense than the 5577Å green line observed under the same conditions.

The ratio of the transition probabilities for the two red lines may be determined by the measurement of their relative intensities. Since both lines originate from the same $^1D_2$ upper level, the intensity ratio is given by equation (3.22) as

$$\frac{I(6364)}{I(6300)} = \frac{A(6364)}{A(6300)} \cdot \frac{S(6364)}{S(6300)} .$$

The sensitivity ratio here was measured as 0.95 ± 0.05 by determining the response of the light collection system at the two wavelengths to a tungsten lamp source. The colour temperature of the source was measured by an optical pyrometer as $2200 \pm 50^{\circ}K$ and the relative photon emission rates were evaluated from the theoretical Planckian relation. Afterglow decay curves at the two wavelengths were recorded at a time when there was no significant change in the oxygen partial pressure and the relative intensity ratio was determined as

0.31 ± 0.01. By combining these two results we obtain the ratio

$$\frac{A(6364)}{A(6300)} = 0.33 \pm 0.02$$

in good accordance with previous measurements[20] and with Yamanouchi and Horie's theoretical value[18] of 0.32.

6.10. Summary of Results

We have summarized here the results of this thesis.

$O(^1S_0)$ radiative decay constant	$1.31 \pm 0.05\ s^{-1}$
$O(^1S_0)$ radiative lifetime	0.76 ± 0.03 s
Diffusion coefficients at 298°K:	
$D_{12}p$ for $O(^1S_0)$ - Ne collisions	416 ± 12 torr $cm^2\ s^{-1}$
$D_{12}p$ for $O(^1S_0)$ - Ar collisions	268 ± 8 torr $cm^2\ s^{-1}$
$D_{12}p$ (Ne) / $D_{12}p$ (Ar)	1.55 ± 0.01
Elastic sphere collision diameters:	
$O(^1S_0)$ - Ne	2.42 ± 0.04 Å
$O(^1S_0)$ - Ar	2.84 ± 0.04 Å
Lennard-Jones Force Constants	
$O(^1S_0)$ - $O(^1S_0)$ collision diameter	2.85 Å
Well depth parameter ϵ/k	21.7°K
Two body deactivation rate constants:	
Neon	$\leq 4 \times 10^{-19}\ cm^3\ s^{-1}$
Argon	$\leq 5.5 \times 10^{-18}\ cm^3\ s^{-1}$

Three body deactivation rate constants	
Neon	$\leq 2 \times 10^{-38}$ cm^6 s^{-1}
Argon	$\leq 2 \times 10^{-37}$ cm^6 s^{-1}
Transition Probability Ratio	
A(6364) / A(6300)	0.33 ± 0.02

CHAPTER 7

CONCLUSIONS

7.1. The Pulsed Afterglow Method - Extension to Other Systems

We have presented in this thesis an experimental determination of the radiative lifetime of the $^1S_0$ state of atomic oxygen. It is interesting to examine the possible use of the techniques developed here to determine the radiative lifetimes of other long-lived metastable species.

It is evident that the pulsed afterglow method is not of general application in the sense that it cannot be applied immediately to determine the lifetimes of many different metastable systems. The excitation and deactivation properties of the metastable species of interest must be carefully considered in order that a satisfactory experimental approach may be devised for each particular problem. For example, it was found in the $O(^1S_0)$ lifetime determination that because of the relatively large rate constant for deactivating collisions between metastable oxygen atoms and ground state oxygen atoms or molecules, only trace concentrations of oxygen could be used in moderate pressures of an inert buffer gas.

A number of experimenters have determined the radiative lifetime of the $A\ ^3\Sigma_u^+$ metastable state of molecular nitrogen, both by absolute intensity measurements and by the pulsed afterglow

method applied to the forbidden $A\ ^3\Sigma_u^+ - X\ ^1\Sigma_g^-$ Vegard-Kaplan bands. The measurements have been collated recently by Shemansky[28] and indicate that the lifetime is in the region of one second. Shemansky[28] estimates his determination from absolute absorption measurements to be accurate to within 20 percent, but this estimate is based on agreement with previous measurements rather than on a systematic treatment of errors. It is considered that further measurements by the pulsed afterglow method could result in a new determination of the lifetime to within the same order of uncertainty as that obtained in the $O(^1S_0)$ lifetime measurement presented in this thesis. The $A\ ^3\Sigma_u^+$ metastable molecules are strongly deactivated by trace concentrations of both oxygen molecules and nitrogen atoms but are not deactivated to any great extent by nitrogen molecules. The experiment could therefore be performed in pure nitrogen which had been specially treated to remove residual oxygen impurities. Care would be required in order to reduce dissociation during the discharge pulse and the occurrence of significant concentrations of atomic nitrogen could possibly be tested by the variation of measured decay constant with discharge current. However, the true extent of the difficulties can only be gauged by extensive experimental investigation.

The ^2P state of atomic nitrogen from which the $^2P - ^4S$ 3446Å line is emitted presents a possible system for investigation by the pulsed afterglow techniques. Again, oxygen impurities

would have to be removed from the nitrogen since trace concentrations of nitric oxide formed during the discharge pulse may be very effective in deactivating the metastable nitrogen atoms. Perhaps the greatest difficulty would be the production of sufficient forbidden line intensities and it would be particularly interesting to test whether a similar dissociation and excitation mechanism occurs in nitrogen-neon discharges as has been shown to be important in oxygen-neon discharges. The radiative lifetime of the $N(^2P)$ state has been calculated by Garstang[58] as 12 seconds so that it would be unlikely that at the present stage of development an experimental determination would be very accurate.

7.2. The $O(^1D)$ Radiative Lifetime

It was mentioned in §3.6 that it may be possible to use relative measurements of the intensities and decay constants of the forbidden oxygen lines emitted from an oxygen-neon discharge to determine their relative transition probabilities. The experimental value of the $O(^1S_0)$ lifetime could then be used to determine the absolute radiative lifetime of the $O(^1D_2)$ metastable state provided that the rate constants for electron excitation to the metastable states of atomic oxygen were known. This lifetime has been calculated[18] as 135 seconds and it would be valuable to obtain a laboratory verification of the theoretical estimates.

It was shown in §3.6 (equation 3.28) that the intensities of the 5577Å and 6300Å forbidden oxygen lines from an oxygen-neon

discharge were related by

$$\frac{I(6300)}{I(5577)} = \frac{S(6300)}{S(5577)} \cdot \frac{A(6300)}{A(5577)} \cdot \frac{s_{01}}{s_{02}} \cdot \frac{\Gamma(^1S_0)}{\Gamma(^1D_2)}. \qquad (7.1)$$

That is, the observed intensity at each wavelength is directly proportional to the instrumental sensitivity, the transition probability and the rate constant for electron excitation to the emitting level, and is inversely proportional to the measured decay constant. It is assumed here that the $^1D_2$ level is not significantly repopulated during the afterglow by radiative cascade from the $^1S_0$ level. The assumption will generally hold since the principal $O(^1S_0)$ population loss is by the radiationless diffusion process, and in addition it is expected that the $^1D_2$ level will be more highly populated during the discharge by virtue of its higher statistical weight.

The determination of the intensity and decay constant ratios and of the instrumental sensitivity function is reasonably straight forward and preliminary measurements have been made to test the feasibility of the experiment. The relative intensities and decay constants have been determined by measurements from a 9 torr oxygen-neon afterglow as

$$\frac{I(5577)}{I(6300)} = 29 \pm 2 \quad \text{and} \quad \frac{\Gamma(^1S_0)}{\Gamma(^1D_2)} = 1.05 \pm 0.05 \text{ respectively.}$$

The sensitivity ratio was determined approximately as

$$\frac{S(5577)}{S(6300)} = 3.5 \pm 0.7$$

by a measurement of the combined response of the monochromator and photomultiplier tube to the radiation from a tungsten lamp of measured colour temperature equal to 2200 $\pm$ 50°K. The relative photon emission rates were calculated from the theoretical Planckian relation. De Vos[63] has shown that the emissivity of tungsten ribbon varies by only a few percent over the wavelength region of interest here.

By combining the above results, we obtain from equation (7.1) the relationship that

$$\frac{A(6300)}{A(5577)} = (0.12 \pm 0.03) \frac{s_{02}}{s_{01}} . \qquad (7.2)$$

The evaluation of the excitation rate constants, however, presents rather a more difficult problem. If a Maxwell distribution of electron energies is assumed, the electron excitation rate constants are related to the deactivation rate constants by equation (3.25). The average electron energy in a 9 torr discharge through an 11 cm diameter vessel may be evaluated for our present purposes as 2.0 eV from the theoretical relationship between electron temperature and the product of pressure and radius for the positive column of a gas discharge. (See, for example, von Engel[43], figure 124). This result is subject to a number of assumptions and it would be

considerably more desirable to perform an independent measurement of electron temperature. Since the 1.96 eV and 4.17 eV excitation energies of the oxygen metastable states do not greatly exceed the average electron energy, the excitation processes are not expected to depend critically on the form of the electron energy distribution at the higher energies The assumption of Maxwellian behaviour is not then expected to lead to large errors.

By use of the results of equation (3.25) we then have from equation (7.2) that

$$\frac{A(6300)}{A(5577)} = (0.007(3) \pm 0.003) \frac{s_{20}}{s_{10}} . \qquad (7.3)$$

It is expected that this result could be significantly improved if a detailed investigation were made. The result is particularly valuable since the deactivation rate constants have not been determined experimentally and there is no reliable experimental determination of the 6300Å transition probability. Theoretical estimates for these quantities have, however, been made and the above relationship provides an interesting experimental connection.

The radiative decay constant for the $O(^1D)$ level may be estimated by using the theoretical estimates of s_{20} and s_{10} made by Seaton[44]. The ratio s_{20}/s_{10} is given as 0.86 for an average electron energy of 2.0 eV. This value is not strongly dependent on the exact value of electron temperature and is probably accurate to within 10 percent. The 5577Å transition probability may be

evaluated as 1.24 ± 0.06 s^{-1} from the $O(^1S_0)$ decay constant measurement and from the determination by McConkey et al[20] of the relative transition probabilities of the oxygen 5577Å and 2972Å lines emitted from the $^1S_0$ state. By combining these results with the result of equation (7.3) and with the earlier determination of the 6300Å and 6364Å transition probability ratio, we obtain a radiative lifetime of 95 seconds for the $O(^1D_2)$ state. In view of the inherent inaccuracies of the test experiment, this result is in reasonable agreement with the theoretical estimate of 135 seconds and shows that the experiment is worthy of further investigation.

7.3. Improvements in the Lifetime Determination

The pulsed afterglow technique has been used to determine the radiative lifetime of the $O(^1S_0)$ metastable state to a higher degree of accuracy than has been obtained in previous lifetime measurements of long lived radiating species. It may be possible to use the method to measure the lifetimes of other radiating species and it is useful to examine whether the experimental techniques could be significantly improved.

Most of the uncertainty of the lifetime determination is at present caused by the relatively large diffusion loss of metastable population and the most obvious improvement would be a substantial increase in the size of the discharge vessel. Larger capacities of gas storage would then be required and care would be needed to

ensure that the present high vacuum conditions were achieved. The impurities present in the gases admitted to the discharge tube could be removed by cataphoretic cleaning. However, it is possible that the measured deactivation rate constant obtained from the neon-oxygen afterglow measurements is principally caused by binary collisions between oxygen metastable atoms and neon atoms. In that case, further cleaning of the admitted gases would produce little improvement in the accuracy of the lifetime determination. A further improvement would be to increase the collection efficiency of the optical system. Increased intensities could lead to decreased uncertainty in the correlation procedures.

It is considered that the accuracy of the $O(^1S_0)$ lifetime determination could be improved to 2 percent or possibly better. Such an improvement would then enable the technique to be used for the evaluation of lifetimes of an order of magnitude greater than that of the $O(^1S_0)$ metastable state.

APPENDIX 1

THE MEASURED REDUCED DECAY CONSTANTS

Argon at 23°C				Neon at 21°C			
p (torr)	Δp (torr)	Γ_0' (s^{-1})	$\Delta\Gamma_0'$ (s^{-1})	p (torr)	Δp (torr)	Γ_0' (s^{-1})	$\Delta\Gamma_0'$ (s^{-1})
1.914	0.007	30.22	0.050	1.022	0.003	76.6	0.7
2.347	0.009	24.92	0.039	1.403	0.004	59.0	0.4
2.751	0.011	21.57	0.045	1.802	0.005	46.7	0.3
3.372	0.014	18.17	0.020	2.300	0.006	37.5	0.07
3.917	0.013	15.91	0.050	2.953	0.008	29.78	0.07
4.64	0.016	13.92	0.030	3.926	0.015	22.84	0.05
6.02	0.016	11.36	0.030	4.935	0.020	18.34	0.035
7.82	0.016	9.58	0.045	6.37	0.014	14.51	0.027
9.24	0.016	8.75	0.050	8.20	0.020	11.53	0.010
11.83	0.027	7.82	0.060	10.25	0.025	9.611	0.030
13.66	0.022	7.62	0.028	11.66	0.020	8.583	0.014
16.20	0.022	7.36	0.031	14.16	0.014	7.413	0.025
				15.87	0.02	6.811	0.034
				17.58	0.02	6.301	0.020
				19.57	0.02	5.895	0.051
				21.78	0.02	5.404	0.021
				24.77	0.02	4.981	0.020
				29.55	0.02	4.447	0.034
				31.21	0.03	4.347	0.027
				35.36	0.03	4.102	0.030

APPENDIX 2

THE LOW PRESSURE ANOMALIES

Incomplete Wall Destruction

At neon pressures smaller than about 2.5 torr, the observed pressure dependence of the measured decay constants differs from that expected from the diffusion theory. (See §6.2). McCoubrey[64] has previously reported a similar departure from the expected behaviour for the diffusion of Hg_2 ($^3O_u^-$) metastable molecules through mercury vapour, and he successfully explained the deviation by assuming that not all the molecules which strike the walls of the vessel are destroyed. We examine here the extension of the diffusion theory to include incomplete wall destruction.

The appropriate boundary conditions for a cylindrical vessel may be evaluated from a consideration of the particle current density J_+ towards the walls

$$J_+ = \frac{n\bar{v}}{4} - \frac{D}{2}\frac{dn}{dr} \qquad (A1)$$

and the complementary current density J_- from the walls

$$J_- = \frac{n\bar{v}}{4} + \frac{D}{2}\frac{dn}{dr} \; . \qquad (A2)$$

(See, for example, McDaniel[36], §10.7). Here $\bar{v}$ is the mean particle speed and D is the diffusion coefficient. The first term in each of these equations represents the random contribution and

the second term is the contribution due to the gradient in the concentration of the diffusing particles. We note that the net current density towards the walls has the expected value $-D \frac{dn}{dr}$.

The boundary condition appropriate to a fraction β of the particles which strike the walls being destroyed is obtained by setting

$$J_- = (1-\beta) J_+ \qquad \text{(A3)}$$

which gives $$\left.\frac{n\bar{v}}{4}\right|_{r=r_0} = -\frac{2-\beta}{\beta} \left.\frac{D}{2}\frac{dn}{dr}\right|_{r=r_0} \qquad (\beta \neq 0) . \qquad \text{(A4)}$$

For simplicity, we have assumed here that the diffusion loss occurs only on the cylindrical surface of the vessel. For the vessel used in the experiments described in this thesis less than 6% of the wall destruction occurs on the end windows.

By using the condition (A4), the first order mode diffusion length is evaluated from

$$\frac{1}{\Lambda^2} = \left(\frac{x}{r_0}\right)^2 + \left(\frac{\pi}{H}\right)^2 \qquad \text{(A5)}$$

where x is the first root of the Bessel function equation

$$J_0(x) = \frac{2D}{\bar{v}r_0} \frac{2-\beta}{\beta} x J_1(x) . \qquad \text{(A6)}$$

Since the diffusion coefficient varies inversely with pressure, the right hand side of this equation approaches zero as the pressure is increased. The solution x then approaches the first zero of

$J_0(x)$ at $x = 2.405$. As the pressure is lowered, however, the value of x falls and the diffusion length is thereby increased. A nonzero particle number density will then exist at the walls. McCoubrey[64] obtained good agreement between the experimental and theoretical pressure dependence of the diffusion lifetime of Hg_2 ($^3O_u^-$) metastable molecules when a wall destruction probability of 0.11 was assumed. For the experiments here, equation (A6) reduces to

$$J_0(x) = \frac{1}{422p} \frac{2-\beta}{\beta} \times J_1(x) \qquad (A7)$$

and in figure 25 we show a comparison between the theoretical pressure dependence of the diffusion parameter D/Λ^2 evaluated for several different values of β, and the experimental values

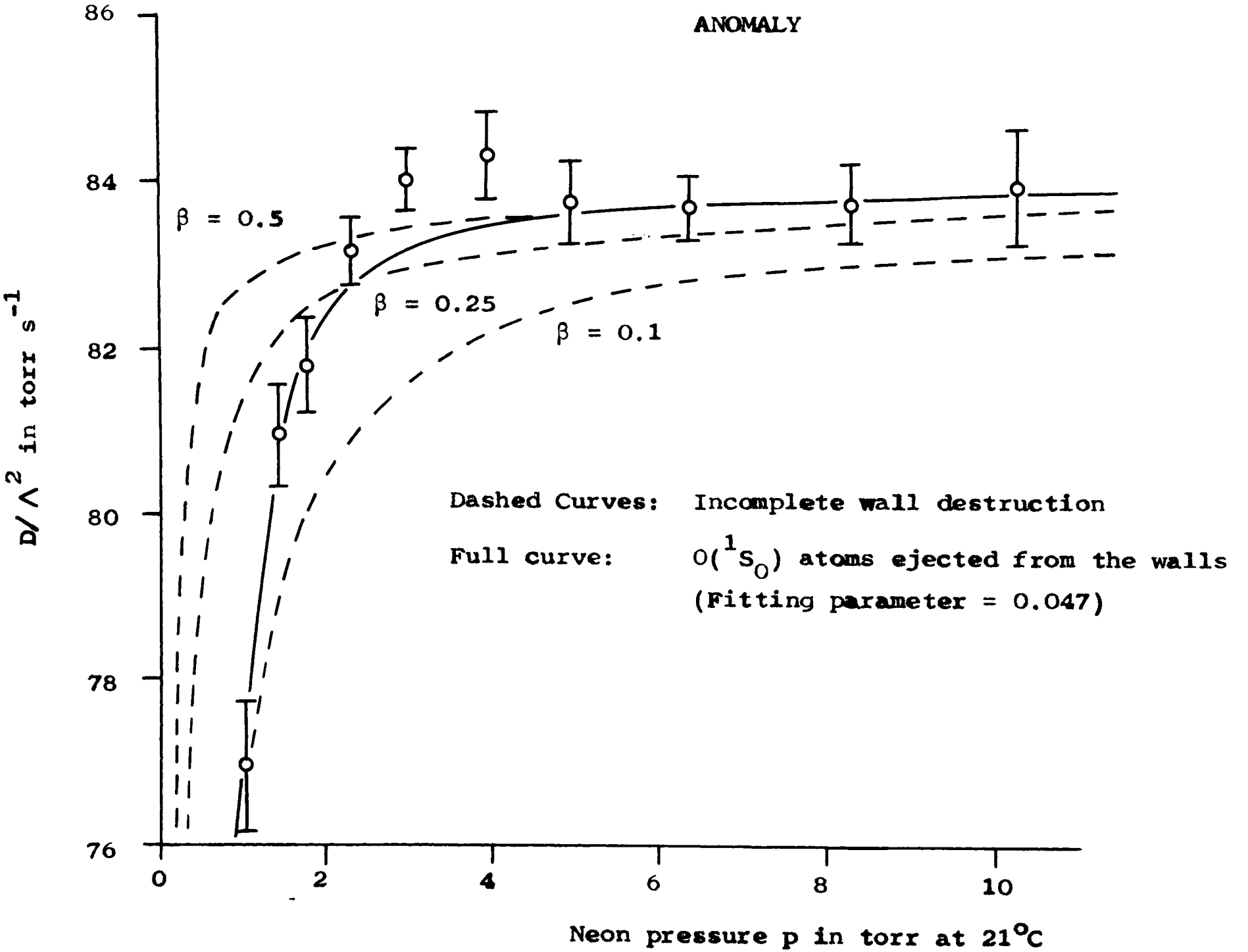
$$D/\Lambda^2 = \Gamma p - \Gamma_0 p - \alpha' p^2 . \qquad (A8)$$

It is clear that the theory does not fit well to the experimental values.

Ejection of $O(^1S_0)$ Atoms from the Walls

We are guided by the observation from figure 25 that a reasonable fit to the experimental data would possibly be obtained if the fraction of metastable atoms returned to the volume were dependent on the inert gas pressure. We recall from table 3, §5.1 that in the pressure region of interest, the diffusion lifetime of Ne_2^+ ions exceeds that of the $O(^1S_0)$ atoms. Although the electron

Figure 25 THEORETICAL FITS TO THE LOW PRESSURE ANOMALY



heating technique was used here to remove electrons from the volume, the radiofrequency field may not couple strongly with the ions and, particularly for the case of free diffusion, there is a possibility that $O(^1S_0)$ atoms may be ejected when Ne_2^+ ions strike the walls of the vessel. We assume here that the $O(^1S_0)$ current density leaving the walls is proportional to the flux of Ne_2^+ ions towards the walls. That is,

$$J_{1-} = k\, J_{2+} \tag{A9}$$

where we have labelled $O(^1S_0)$ as species 1 and Ne_2^+ as species 2. (We have considered the possibility of the effect being caused by neon metastable atoms, but it is clear from table 3, §5.1 that the metastable lifetime is considerably shorter than the $O(^1S_0)$ lifetime in the pressure region of interest between 1 torr and 2.5 torr. Neon metastable atoms are not expected to cause any effect during the late afterglow when the decay curves were recorded.)

Equation (A9) may be written as

$$\left(\frac{n_1 \bar{v}_1}{4} + \frac{D_1}{2}\frac{dn_1}{dr}\right)\Bigg|_{r=r_0} = -k\, D_2 \frac{dn_2}{dr}\Bigg|_{r=r_0} \tag{A10}$$

which leads to a first order mode diffusion length given by equation (A5) where x is now the first root of the equation

$$J_0(x) - \frac{2D_1}{\bar{v}_1 r_0}\, x\, J_1(x) = \frac{5.00\, kD_2}{r_0 \bar{v}_1} \cdot \frac{n_2}{n_1} . \tag{A11}$$

We have assumed here that the diffusion is by the first order mode and have evaluated the quantities $\frac{dn}{dr}$ by use of equation (3.9). We have assumed also that each $O(^1S_0)$ atom and Ne_2^+ ion which strikes the walls is destroyed. The number densities n_1 and n_2 are evaluated at the centre of symmetry.

It is to be expected that the ratio n_2/n_1 should show some time dependence since the decay rates of the $O(^1S_0)$ atoms and the Ne_2^+ ions are expected to differ. Examination of the decay rates of table 3, §5.1 shows that the difference is not large and we assume here that the ratio n_2/n_1 is time independent in the first approximation. The recorded afterglow curves were examined for non-exponential behaviour. Small deviations from pure exponential behaviour were noticed but could not definitely be ascribed to the above repopulating effect. At low pressures, there is a rapid adsorption of oxygen on the walls of the vessel, which causes the value of the $O(^1S_0)$ decay constant to change while a decay curve is being recorded. It is quite possible that this effect has lead to the observed deviations. However, the recorded decay curves were sufficiently close to pure exponentials to enable a definite decay constant to be determined without introducing large errors.

We now wish to examine the pressure dependence of the ratio n_2/n_1. The number density of Ne_2^+ ions is expected to be independent of the inert gas pressure. Conversely, we have from equation (3.27) that

$$n_1[O(^1S_0)] \propto 1/\Gamma \propto p$$

for a diffusion dominated metastable atom loss. We consequently expect that the ratio n_2/n_1 to vary inversely with pressure, so that for the experiments described here, equation (A11) reduces to

$$J_0(x) = \frac{1}{422p} \cdot x \cdot J_1(x) + \frac{\alpha}{p^2} \qquad \text{(A12)}$$

where α is a fitting parameter. It is clearly seen from figure 25 that a good fit to the experimental data is obtained if a value $\alpha = 0.047$ is assumed.

Although a good theoretical fit has been obtained to the observed pressure dependence of D/Λ^2, it is not claimed here that the explanation is complete. A more detailed experimental and theoretical investigation will, however, be undertaken in the near future in order that the above hypothesis may be tested. For example, the nature of the decay will be investigated more thoroughly in order to identify the source of the deviations from exponential behaviour.

REFERENCES

1. A. Corney, Adv. in Electronics and Electron Phys., Academic Press, New York, 29, 115 (1970).
2. E.U. Condon and G.H. Shortley, The Theory of Atomic Spectra, Cambridge University Press (1963).
3. R.H. Garstang, in Atomic and Molecular Processes (Ed. D.R. Bates), Academic Press, New York, Chapter 1 (1962).
4. S. Datta, Proc. Roy. Soc. A101, 539 (1922).
5. J.C. McLennan and G.M. Shrum, Proc. Roy. Soc. A108, 501 (1925).
6. J.C. McLennan and J.H. McLeod, Proc. Roy. Soc. A115, 515 (1927).
7. J.C. McLennan, J.H. McLeod and R. Ruedy, Phil. Mag. 6, 558 (1928).
8. J.C. McLennan, J.H. McLeod and W.C. McQuarrie, Proc. Roy. Soc. A114, 1 (1927).
9. R. Frerichs and J.S. Campbell, Phys. Rev. 36, 1460 (1930).
10. Lord Rayleigh, Proc. Roy. Soc. A117, 294 (1927).
11. M. Fukuda, Sci. Pap. Inst. Phys. Chem. Res. (Tokyo) 4, 171 (1926).
12. I.S. Bowen, Astrophys. J. 67, 1 (1928).
13. F. Paschen, Naturwiss 18, 752 (1930); Z. Phys 65, 1 (1930).
14. J.J. Hopfield, Phys. Rev. 37, 160 (1931).
15. E.C. Zipf, Can. J. Chem. 47, 1863 (1969).
16. E.E. Ferguson, F.C. Fehsenfeld and A.L. Schmeltekopf, Adv. in Atomic and Molec. Phys. 5, 1 (1969).
17. O. Sinanoğlu, Comments Atom. Molec. Phys. 2, 79 (1970).

18. T. Yamanouchi and H. Horie, J. Phys. Soc. Japan 7, 52 (1952).

19. S.V. Filseth, F. Stuhl and K.H. Welge, J. Chem. Phys. 52, 239 (1970).

20. J.W. McConkey, D.J. Burns, K.A. Moran and K.G. Emeleus, Physics Letters 22, 416 (1966).

21. F.J. Le Blanc, O. Oldenberg and N.P. Carleton, J. Chem. Phys. 45, 2200 (1966).

22. J.W. McConkey and J.A. Kernahan, Planet. Spa. Sci. 17, 1297 (1969).

23. A. Omholt and L. Harang, J. Atm. Terr. Phys. 7, 247 (1955).

24. A. Omholt, Geophys. Publ. 21, 1 (1959).

25. K.V. Paulson and G.G. Shepherd, J. Atm. Terr. Phys. 27, 831 (1965).

26. W. Stoffregen and H. Derblom, Nature 185, 28 (1960).

27. A. Omholt, Planet. Spa. Sci. 2, 246 (1960).

28. D. Shemansky, J. Chem. Phys. 51, 689 (1969).

29. J.F. Noxon, J. Chem. Phys. 36, 926 (1962).

30. L.F. Phillips, Can. J. Chem. 43, 369 (1965).

31. E.C. Zipf, J. Chem. Phys. 38, 2034 (1963).

32. H.H. Bromer and F. Spieweck, Planet. Spa. Sci. 15, 689 (1967).

33. L. Herman and R. Herman, Ann. Geophys. 1, 165 (1944).

34. R. Herman, C. Weniger and L. Herman, Phys. Rev. 82, 751 (1951).

35. N.D. Sayers and K.G. Emeleus, Proc. Phys. Soc. A65, 219 (1952).

36. E.W. McDaniel, Collision Phenomena in Ionized Gases, Wiley, New York (1964).

37. E.C. Zipf, Bull. Amer. Phys. Soc. 14, 264 (1969).

38. F.R. Gilmore, J. Quant. Spect. Rad. Transf. 5, 369 (1965).

39. S.V. Filseth and K.H. Welge, J. Chem. Phys. 51, 839 (1969).

40. H.I. Schiff, Can. J. Chem. 47, 1903 (1969).

41. W.R. Bennett Jr., W.L. Faust, R.A. McFarlane and C.K.N. Patel, Phys. Rev. Letts 8, 470 (1962).

42. W.R. Bennett Jr., App. Optics : Supp. on Optical Masers 1, 24 (1962).

43. A. von Engel, Ionized Gases, Clarendon Press, Oxford, 2nd edn. (1965).

44. M.J. Seaton, in The Airglow and the Aurorae (E.B. Armstrong and A. Dalgarno, eds), Pergamon, New York, 289 (1955).

45. J. Yarwood, High Vacuum Technique, 4th edn, Chapman and Hall, London (1967).

46. W.H. Kohl, Materials and Techniques for Electron Tubes, Reinhold, New York (1960).

47. C.E. Webb, D. Phil. thesis, University of Oxford (1964).

48. O.M. Williams, W.J. Siertsema and D.T. Smith, J. Phys. E: Sci. Instr. 4, 296 (1971).

49. D. Smith and P.R. Cromey, J. Phys B: Atom. Molec. Phys. 1, 638 (1968).

50. H.J. Oskam and V.R. Mittelstadt, Phys. Rev. 132, 1435 (1963).

51. A.V. Phelps, Phys. Rev. 114, 1011 (1959).

52. E. Ellis and N.D. Twiddy, J. Phys. B: Atom. Molec. Phys. 2, 1306 (1969).

53. C.E. Webb, A.R. Turner-Smith and J.M. Green, J. Phys B: Atom. Molec. Phys. 3, L134 (1970).

54. J. Topping, Errors of Observation and their Treatment, Chapman and Hall, London (1960).

55. S. Pasternack, Astrophys. J. 92, 129 (1940).

56. R.H. Garstang, Monthly Not. Roy. Ast. Soc. 111, 115 (1951).

57. D.R. Hartree, W. Hartree and B. Swirles, Phil. Trans. Roy. Soc. A238, 229 (1939).

58. R.H. Garstang, in The Airglow and the Aurorae (E.B. Armstrong and A. Dalgarno, eds), Pergamon, New York, 324 (1955).

59. O. Sinanoglu and K.A. Brueckner, Three Approaches to Electron Correlation in Atoms, Yale University Press (1970).

60. C.C.J. Roothaan and P.S. Kelly, Phys. Rev. 131, 1177 (1963).

61. J.O. Hirschfelder, C.F. Curtiss and R.B. Bird, Molecular Theory of Gases and Liquids, Wiley (1965).

62. W.A. Fitzsimmons, N.F. Lane and G.K. Walters, Phys. Rev.174, 193 (1968).

63. J.C. de Vos, Physica 20, 690 (1954).

64. A.O. McCoubrey, Phys. Rev. 93, 1249 (1954).